ON THE DEVELOPMENT AND APPLICATION OF INDICATORS TO CHARACTERIZE THE START OF SPRING ACROSS THE NORTHERN HEMISPHERE IN METEOROLOGICAL DATA, SATELLITE REMOTE SENSING, AND CLIMATE MODEL SIMULATIONS

A Dissertation

Presented to the Faculty of the Graduate School

of Cornell University

In Partial Fulfillment of the Requirements for the Degree of

Doctor of Philosophy

by

Xiaolu Li

August 2019

ON THE DEVELOPMENT AND APPLICATION OF INDICATORS TO CHARACTERIZE THE START OF SPRING ACROSS THE NORTHERN HEMISPHERE IN METEOROLOGICAL DATA, SATELLITE REMOTE SENSING, AND CLIMATE MODEL SIMULATIONS

Xiaolu Li, Ph. D.

Cornell University 2019

Large scale changes in the state of the land surface affect the circulation of the atmosphere, the structure and function of ecosystems, as well as health and economy of mankind. As global temperatures increase and regional climates change, the timing of plant phenological events will shift as well. Understanding and anticipating those changes require both observations of large-scale interannual phenological variability and global climate model simulations with realistic land surface phenology routines. Therefore, in my dissertation, I combined thermal-based indices, satellite remote sensing, and the Community Land Model (CLM) to characterize spring phenology variability and its linkage to the climate system and evaluate the skill of the CLM to represent spring onset and seasonal variations of plants.

I developed a new suite of thermal-based indicators to characterize the seasonal window of spring onset. Results showed that temperature dominates spring onset timing over the Northern Hemisphere and shifts the seasonal window of spring phenological changes as a whole. In addition, spring phenology has large interannual to decadal variation and its trends depend dramatically on the examined historical periods. Because of their long temporal depth and good spatial coverage, the newly-developed thermal-based indices can provide useful information in isolating the role of

the climate system in altering spring onset.

Evaluating how well state-of-the-art climate models can represent the above variabilities and trends are important for understanding and improving model performance. Therefore, I also evaluate a new suite of phenometrics designed to facilitate an “apples to apples” comparison between remote sensing products and climate model output. This systematic approach to comparing phenologically-relevant variables reveals broad consistency between the model and observations in large-scale spatial gradients of LAI amplitudes and mean spring onset dates. However, it exhibits fundamental difference between CLM and MODIS LAI seasonal cycle and spring onset timing. Therefore, any coupling between the land surface and the atmosphere that depends on vegetation state might not be fully captured by the existing generation of models. As a result, any future feedback of carbon, moisture, and energy that affect this coupling would be subject to sources of uncertainty originating in model phenology.

BIOGRAPHICAL SKETCH

Xiaolu Li was born in Jinan, Shandong, China. Growing up, she has always been a fan of science and won multiple prizes in math and chemistry competitions. She was pre-admitted into Peking University, China after receiving a gold medal at the 21st National Chemistry Competition and Winter Camp for High School Students in 2008. Xiaolu majored in Geography in the College of Urban and Environmental Sciences at Peking University. She also received a double-major in Economics from the National School of Development. Because she got interested into climate science during her undergraduate study, Xiaolu entered the master's program in Geography at the University of Minnesota, Twin Cities after she graduated from PKU. During her master's degree, Xiaolu adopted a forward model of tree-ring growth, the Vaganov-Shashkin model of tree-ring formation, applied it using daily meteorological records at all available Global Historical Climatology Network stations and evaluated the simulated climate sensitivity against climate signal in observed tree-ring chronology. After she finished her master's study, Xiaolu continued doing research and became a PhD student in the Field of Atmospheric Science at Cornell University. During her PhD, Xiaolu used a combination of ground phenological observations, indices models, satellite remote sensing, and earth system models to characterize spring onset variability over the Northern Hemisphere and interactions between the state of the climate system and phenophase changes on the ground.

[This dissertation is dedicated to my mom and dad who are always there to love and support me in my life.]

ACKNOWLEDGMENTS

This work is in part supported by USGS Grant/Cooperative Agreement Number G13AC00248 and National Science Foundation MSB-FRA EF-1702697. The author would also like to thank colleagues at Cornell University, the National Phenology Network, Boston University, Northern Arizona University, and the University Corporation for Atmospheric Research/National Center for Atmospheric Research for their comments and suggestions.

TABLE OF CONTENTS

CHAPTER 1

CHARACTERIZING INTERANNUAL TO MULTI-DECADAL VARIABILITY IN THE SEASONAL WINDOW OF SPRING ONSET ACROSS THE NORTHERN HEMISPHERE

Abstract

Spring onset variability shapes regional changes in both land-atmosphere coupling and ecosystem functioning. Yet, it is unclear how to define the seasonal window of spring onset using indicators that are both climatically and ecologically meaningful. Here we present a new suite of indicators to investigate spring onset variability and disentangle climatic and non-climatic influences on the start of spring over the Northern Hemisphere. It is shown that temperature shifts the window of spring phenological changes as a whole. Spring phenology has large interannual to decadal variation and its trends depend dramatically on the examined historical periods. At mid-to-high latitudes, spring arrives earlier by about 1 day/decade over 1950-2013, but this rate changes or even reverses sign in recent decades (1982-2013). Because of their long temporal depth and good spatial coverage, the newly-developed thermal-based indices can provide useful information in isolating the role of the climate system in altering spring onset.

Introduction

Understanding spring onset is critical for advancing research into the impacts of

climate change on ecology, hydrology, and agriculture, among many other disciplines. During springtime, plants flower and grow leaves, winter snowpack melts and fills reservoirs, and farmers plant crops and prepare for the coming growing season. Spring is therefore the phase of the annual cycle when the atmosphere transitions from a hostile winter regime into a state that supports activity in the terrestrial biosphere. At the same time, the terrestrial biosphere modifies the flow of energy, water, carbon, and other gasses through the atmosphere (e.g., *Fitzjarrald et al.*, 2001; *Richardson et al.*, 2013). Importantly, the timing of spring onset varies from one year to the next, as evidenced by interannual variability in observations of plant and animal phenophase changes (*Schwartz*, 1992; *Hogg et al.*, 2000; *Schwartz and Crawford*, 2001; *Cleland et al.*, 2007; *Forrest and Miller-Rushing*, 2010; *Visser et al.*, 2010; *Thackeray*, 2012; *Richardson et al.*, 2013; *Thackeray et al.*, 2016), indices of snow melt and streamflow (*Cayan et al.*, 2001; *Stewart et al.*, 2005; *Lundquist and Flint*, 2006), and remote sensing of land surface phenology (*de Beurs and Henebry*, 2005; *White et al.*, 2009; *Karkauskaite et al.*, 2017). Despite their importance to biology, hydrology, and food production, these year-to-year variations in the timing of spring are, at best, only poorly linked to climate fluctuations on similar timescales.

The gap in our understanding of spring onset and its relationship to climate has emerged, at least in part, from ambiguity in the concept of "spring" itself, which may have different definitions depending on application, discipline, or phenomena of interest. For example, a number of recent studies have proposed and utilized indicators of the growing season (*de Beurs and Henebry*, 2005; *Jolly et al.*, 2005; *Schwartz et al.*, 2006; *de Beurs and Henebry*, 2008; *White et al.*, 2009; *Melaas et al.*, 2016;

Karkauskaite et al., 2017; *Liu et al.*, 2017) with the goal of improving our understanding of phenology. Collectively, these studies show that "plant-based" indicators of spring onset exhibit considerable interannual variation because of climate variability on similar timescales. However, the indices themselves were not developed with the explicit goal of isolating climatic sources of interannual variability in spring onset. The "start of spring" in the climate system, by contrast, is typically characterized using state changes of atmospheric circulation (e.g., *Black and McDaniel*, 2007) or seasonal changes in hydrologic cycle. For example, the onset of monsoon (*Wu and Wang*, 2000; *Xu et al.*, 2004), the timing of spring snowmelt (*Cayan et al.*, 2001; *Lundquist and Flint*, 2006), or peak streamflow (*Stewart et al.*, 2005) have all received considerable attention in the literature.

Here, we are interested in the timing of the seasonal window of spring onset. In an ideal situation, we could estimate an empirical distribution of spring phenological events using many years of observations of thousands of species and comprise the seasonal window of spring onset. Recent studies have used a variety of ground observations to estimate the climate sensitivity of different species at varying locations (e.g., *Parmesan*, 2007; *Thackeray et al.*, 2016; *Prevéy et al.*, 2017). However, as spring phenology has large variability at interannual to decadal timescales, trends and sensitivities based on small-scale and short-term data may be altered from its long-term pattern by its limited temporal depth and the main state of its climate system during that time. Therefore, we need to rely on proxies for the seasonal windows at a hemispheric scale and over long historical periods, using both meteorological data and remote sensing to garner information about spring onset across large spatial scales and

over multiple decades.

We present a new suite of indicators designed to disentangle climatic and non-climatic characteristics of the start of spring. They are simple and easy-to-interpret as the day of year when heat accumulation reaches certain thresholds. By comparing these newly-developed indicators to existing model- and satellite-based phenological indices, we ask how well such a set of simple spring onset indicators can reproduce spring onset variability at a hemispheric scale, how spring onset has varied over the past few decades, and how meteorological-based indices can help isolate climate-induced changes in the start of spring.

Data preparation and methods

Phenological indicators

We developed a new set of thermal-based spring onset indicators to represent the timing of key seasonal windows that are both relevant to broad groups of species across space and through time, and indicative of near-surface temperature changes. Specific values of AGDD have been widely used to determine growing status and planting dates for various species (for instance, Robinson, 1971; Tollenaar et al., 1979; Snyder et al., 1999; Miller et al., 2001), but here we use percentile thresholds of local AGDD to diminish the influence of species and location-induced differences in heat accumulation. These new indicators identify the day of year (DOY) when AGDD reaches predefined percentile thresholds (i.e. 10% and 25% of early growing season, or day 212 AGDD) across the Northern Hemisphere. We used AGDD because of its

well-documented relevance to spring phenology (e.g., *Robinson*, 1971; *Tollenaar et al.*, 1979; *Snyder et al.*, 1999; *Miller et al.*, 2001; *Schwartz*, 2003), and because it is location-specific but insensitive to species and may better represent changes in ecosystem-level phenology under future climate changes. We stress, however, that our thresholds are based on local AGDD percentile thresholds and not tuned to any particular plant species or ecosystem types.

To calculate the AGDD-based indices, we first calculated the AGDD from day 1 to day 212 with a base temperature of 0°C at each grid point for each year as:

$$\mathrm{AGDD} = \sum_{t=t_0}^{t_N} \left[\frac{T_{max}+T_{min}}{2} - T_b\right], \quad \left(\frac{T_{max}+T_{min}}{2} \geq T_b\right) \qquad (1)$$

Where T_b is the base temperature, t_0 indicates the start day of aggregating period, and t_n represents the final day. On days when the mean of maximum (T_{max}) and minimum temperature (T_{min}) falls below T_b, the growing degree is counted as zero; at days when the mean of T_{max} and T_{min} is above or equal to base temperature but minimum temperature is below base temperature, minimum temperature is set to base temperature before calculating the growing degree (*McMaster and Wilhelm*, 1997). We used day 212 (July 31st in non-leap years) as the end date for calculating total climatological AGDD accumulations as we are interested in the spring accumulation of warm days. Next, we selected seven thresholds based on the mean 1981-2010 AGDD at each grid point: 10%, 25%, 33%, 50%, 66%, 75%, and 90% of mean AGDD values on day 212, respectively. For each year at each grid point during 1950-2013, we then calculated the day of year when annual AGDD reaches each threshold of the 1981-2010 mean. As most spring phenological events occur near the first two

thresholds ($AGDDI_{10\%}$ and $AGDDI_{25\%}$), it is likely that the first two indices are influenced by the same dominant factors with the phenological observations and therefore are better indicators of spring onset, so we focused on these for further analysis and comparisons. We noted, however, that spatial patterns and variation are similar among all seven indices.

We also used two other sets of spring onset indicators to evaluate the newly-developed AGDD-based indices. Firstly, we used the gridded extended spring indices (SI-x; or SIx_{leaf} for first leaf index and $SI\text{-}x_{bloom}$ for first bloom) because they are more directly tied to spring phenology of specific species and depend less on the overall heat accumulation during spring time than our pre-defined AGDD thresholds (*Schwartz et al.*, 2006; *Ault et al.*, 2015). The SI-x (and their predecessors, the original SI) were developed from historical records of lilac and honeysuckle phenology, and have been extensively used as proxies for certain groups of species, as well as for assessing the impact of abiotic changes on spring onset (*Schwartz and Marotz*, 1986; *Schwartz*, 1997; *Schwartz and Reiter*, 2000; *Schwartz et al.*, 2006; *Ault et al.*, 2011; *Schwartz et al.*, 2013; *Ault et al.*, 2015). SI-x uses daily minimum and maximum temperatures and latitude to estimate the timing of spring foliage (first leaf, hereafter $SI\text{-}x_{leaf}$) and blooms (first bloom, hereafter $SI\text{-}x_{bloom}$) for plants with temperature responsive phenology. It has also been extended to warmer locations that may not meet the chill requirements of the original SI (*Schwartz et al.*, 2013). Studies have demonstrated the reliability of SI-x and gridded SI-x to reproduce observed spring onset in the Northern Hemisphere (*Schwartz et al.*, 2006; *Ault et al.*, 2015).

As both AGDDIs and SI-x are calculated from daily temperature data, we refer to

them as the thermal-based indices. Data to calculate the thermal-based indices were obtained from the Berkeley Earth Surface Temperature – Gridded Land Daily Temperature dataset (available online at http://berkeleyearth. org/data/). This product includes daily maximum and minimum temperature at 1° × 1° latitude-longitude grid from 1880 to 2013. We only calculated the thermal-based indices from 1950 to 2013 as uncertainties in gridded temperature records at a hemispheric scale are higher before that due to decreasing data availability and spatial coverage of weather stations (*Rohde et al.*, 2013).

Secondly, following a similar procedure to the AGDDIs, we adopted the day of year when NDVI reaches pre-defined thresholds of its annual dynamical range (annual maximum minus annual minimum) to characterize the progression of land surface phenology. Consequently, NDVI values for each threshold at the same grid point vary from one year to another, and changes in maximum and minimum NDVI (e.g., from land use change or summer drought conditions unrelated to spring onset) are factored out. We selected 50% and 75% thresholds (hereafter referred to as $NDVI_{50\%}$ and $NDVI_{75\%}$, respectively, or combined as $NDVI_{\%}$) to represent spring phenophase changes triggered by both climatic and non-climatic factors (*White et al.*, 2009). We utilized data from the third generation of the Global Inventory Monitoring and Modeling System (GIMMS) NDVI (NDVI3g; *Tucker et al.*, 2005; *Pinzon and Tucker*, 2014) from NOAA's Advanced Very High-Resolution Radiometer (AVHRR) sensors. NDVI3g is developed by compositing cloud-free, high quality NDVI data using maximum value compositing. NDVI values are produced twice a month starting on the 1st and 16th day of the month and the results are then averaged to create a global

NDVI layer with a spatial resolution of 1/12 degree. As NDVI3g is resolved at 15-day timescales, whereas the thermal-based indices are based on calculations for each day of spring, to compare dates from these two sources, which differ in their temporal resolutions, we interpolated the original 15-day product to daily temporal scale using a cubic spline. We calculated the DOYs based on the original 1/12° × 1/12° resolution of NDVI3g and then averaged the results to 1° × 1° for comparisons against the thermal-based indices. For consistency with the other two types of indices, we only calculated $NDVI_{\%}$ spring onset dates during 1982-2013. While AGDD thresholds are based on climatological heat accumulation (i.e. mean day 212 AGDD), NDVI thresholds are tuned to its annual dynamical range and therefore the changes in their maximum and minimum values (e.g., from land use change or summer drought conditions unrelated to spring onset) are factored out.

Methods

The indices record year-to-year variations in spring onset during different "seasonal windows", on average (e.g., as shown by *Ault et al.*, 2015, for the SI-x). By seasonal window, we refer to the period of time comprised by different indicators surrounding similar phenological events, which will not be the same DOY each year (by definition). Despite their interannual variations, the sequence in which our indices cross key thresholds will remain fixed for any given grid point. That is, $AGDDI_{10\%}$ will always be sensitive to early-spring variations, whereas $NDVI_{75\%}$ may tend to respond to conditions later in the season. We therefore divided the indices into two groups based on their characteristic seasonal window. The first group contains $AGDDI_{10\%}$, $SI\text{-}x_{leaf}$, and $NDVI_{50\%}$ and yields dates that are similar, on average, to

those of the emergence of first leaf in the observational lilac dataset (e.g., *Rosemartin et al.*, 2015), as demonstrated in Figure 1a for one grid point. The second group consists of $AGDDI_{25\%}$, SI-x_{bloom} and $NDVI_{75\%}$, and the mean dates occur close to the bloom dates from lilac observations (e.g., late spring phenological changes; Figure 2a).

As the sequence of indices varies between regions, we characterize these regional differences using simple (Pearson) correlation coefficients between indices at each grid point. For all simple correlation analyses, we used a 5% significance level and adjusted for false discovery (*Benjamini and Hochberg*, 1995). We also used pattern correlation to assess how similar the spatial patterns are between different indices pairs. Specifically, we calculated DOY anomalies of the three datasets from their 1982-2013 mean and correlated the anomalies of each indices pair.

To examine the interannual variability and consistency between the three sets of indicators, we also calculated standard deviations of each indicator and root mean square errors (RMSE) between indices pairs. RMSE measures the difference between onset dates from varying indicators at the same grid point. To calculate the mean RMSE, we averaged the three RMSEs of different indices pairs within each group, i.e. averaging RMSEs between $AGDDI_{10\%}$ and SI-x_{leaf}, $AGDDI_{10\%}$ and $NDVI_{50\%}$, and SI-x_{leaf} and $NDVI_{50\%}$ for group 1 indicators.

We used Principal Component Analysis (PCA) to evaluate whether different sets of indices are *significantly similar* to each other at a given grid point on interannual timescales. Specifically, we conducted PCA at each grid point based on time series of

all six indices. Under this application, the total variance accommodated by the leading PC (PC1) shows the fraction of variance shared between the three sets of indicators at that grid point. We evaluated the significance of this metric using a bootstrapping. That is, we then bootstrapped the thermaland NDVI-based indices separately as two groups for 1000 times each. In other words, at each grid point, we bootstrapped 1) $AGDDI_{10\%}$, $AGDDI_{25\%}$, $SI\text{-}x_{leaf}$, and $SI\text{-}x_{bloom}$, and 2) $NDVI_{50\%}$ and $NDVI_{75\%}$ for 1000 times, respectively, combined them into six-index groups, and conducted PCA analysis on the combined six-index data to assess the significance of each grid point's PC1.

We also calculated linear trends of the thermal- and NDVI-based indices over different time windows during 1950-2013 and 1982-2013, respectively. We used a one-tailed 5% significance level to evaluate the importance of all analyzed trends, and adjusted for false discovery (*Benjamini and Hochberg*, 1995). Because most of the indices have only nonsignificant and negative autocorrelation, we did not adjust the degrees of freedom for calculating significance.

Uncertainties may emerge from the remote sensing data product we adopted as well as the pre-defined thresholds we selected. However, studies suggested that NDVI3g is applicable for detecting NDVI variation and ecosystem-level changes at large spatial scales (for instance, *Tucker et al.*, 2005; *Fensholt and Proud*, 2012; *Fensholt et al.*, 2015). We also tested the sensitivity of spatial patterns, variability, and correlation to indices determined by different thresholds against our pre-defined thresholds. We found similar spatial and temporal patterns, which is also present when comparing Group I with Group II indices.

Results

Gridded spring onset datasets of the Northern Hemisphere

Both thermal- and NDVI-based indicators exhibit later spring onset dates at high-latitude and high-altitude locations than at other places (Figure 1bcd). For AGDDIs and SI-x, day of the year (DOY) values increase gradually from south to north in the Northern Hemisphere, or from low to high elevations as in the Rocky Mountains and on the Tibetan Plateau. Spring onset dates are also earlier along the western margins of the continents than on the eastern edges, causing onset dates to angle along northwestern trajectories. This pattern is altered in North America due to the later onset dates on the Colorado Plateau. $NDVI_{\%}$ exhibit similar spatial pattern but experience more abrupt changes in the timing of spring onset. Like the thermal-based indices, the NDVI-based indices generally increase along northward transects and along northwestern sloping lines of constant dates, but the latest spring onset occurs mostly in high-latitude regions. Desert regions in sub-tropical area experience exceptionally early "spring" (DOY<20), though indices of spring onset are probably not particularly meaningful in such arid climates. Compared to thermal-based indices, $NDVI_{\%}$ exhibit more abrupt changes between grid points.

Standard deviations computed from the thermal-based indices are more similar to each other, and of a lower magnitude, than those from $NDVI_{\%}$ (Figure 3). For AGDDI and SI-x, variability is larger in early spring phenology ($SI\text{-}x_{leaf}$ and $AGDDI_{10\%}$) and the largest temporal variations occur along the Pacific coast of Canada, in the

Mediterranean, and over high-elevation regions in the Rocky Mountains and on the Tibetan Plateau (Figure 3a-d). Phenological events in the later part of the growing season are more consistent from year to year and show smaller temporal variability, with a few exceptions. Over 1982-2013, standard deviations of AGDDIs and SI-x are generally smaller than 10 days, while $NDVI_{\%}$ exhibits similar spatial pattern but much greater variation over the same period (more than 15 days at mid-latitudes). In arid regions like the Sahara and extratropical regions in North America and Asia, temporal variations are large in the NDVI-based indices (10-15 days) and much smaller in the two thermal-based indices (less than 10 days, mostly less than 5 days). NDVI-based indices exhibit largest standard deviation around the Great Lakes region, in western North America, in Western Europe, in Central Asia, and on the Tibetan Plateau.

Relationship between the three sets of indicators shifts as latitude changes. Compared to $SI\text{-}x_{leaf}$, $AGGDI_{10\%}$ occurs earlier in mid-to-high latitude (north of 40°N) and high-elevation regions. Except for several high-latitude or high-elevation locations, $SI\text{-}x_{leaf}$ generally happens around 10% threshold in AGDD accumulation (Figure 4), though the percentage of annual AGDD increases when moving further north. For $NDVI_{50\%}$, larger percentage of annual AGDD is required at selected locations in the south and northeast part of North America and South Asia (Figure 4b) and smaller percentage is found over dessert regions, at high elevations, and at high latitudes. $SI\text{-}x_{leaf}$ has large disagreement (over 10 days) with $NDVI_{50\%}$ in the low-to-mid latitude regions in Asia and over North America (Figure 4c). Difference in standard deviations between $SI\text{-}x_{leaf}$ and $AGDDI_{10\%}$ is generally small (Figure 5b) except over the Rocky Mountains and in the Mediterranean. $NDVI_{50\%}$ exhibits large

variance in low-latitude regions and lower variance at some locations at high latitudes than the thermal-based indices (Figure 5ac).

Mean onset dates also show consistent timing and variability between the three sets of indicators, but their relative timing may change from one year to another. Root mean square error (RMSE) among the three DOY pairs suggests that spring onset timing from different indicators are more consistent at higher latitudes (Figure 6b). Particularly, in Europe, North Asia, and near the Great Lakes region in North America, RMSE among indices is close to or even lower than their individual standard deviation (Figures 6b and 3a-c). For instance, even though standard deviations of Group I indices are large in Western Europe (more than 15 days), RMSE between indices is relatively small (10-15 days) in that region. For Group I indices, $NDVI_{50\%}$ usually happens the earliest over subtropical desserts and in high-latitude and high-altitude regions, as opposed to latest in low-to-mid latitude regions with lower elevations (Figure 6a).

Indices within each group exhibit relatively high agreement in their average onset dates and variability at all time scales. Group I indices generally have high temporal correlation across the Northern Hemisphere. SI-x_{leaf} and $AGDDI_{10\%}$ are highly correlated ($r>0.8$, p-value<0.05) in the Northern Hemisphere, except for a few high-elevation grid points over the Tibetan Plateau and the Rocky Mountains (Figure 7a). $NDVI_{50\%}$ correlates well with both $AGDDI_{10\%}$ and SI-x_{leaf} in East Asia and in the mid-to-high latitude regions in North America, Eastern Europe, central part of Asia and Siberia, but negative correlation is present in subtropical regions in both North America and Asia and in the high-elevation regions in Asia (Figure 7bc). Pattern

correlations also show high agreement between thermal-based indices in their spatial patterns through time, while spatial patterns of $NDVI_{50\%}$ and thermal-based indices are still positively correlated but with lower coefficients (Figure 8a). PCA at each grid point also shows high and significant shared variance across the analyzed region (Figure 9). Across the Northern Hemisphere, the first PC from each grid point generally explains more than 50% of the total variance. In northeastern North America, Western Europe, and Siberia, more than 75% of the total variance is shared among the three sets of indices. Although lower latitudes exhibit negative and nonsignificant correlations between the indices, the first PC at each grid point in these regions still accounts for more than 50% of the total variance and is significant.

Relationship between AGDDI and NDVI% differs across space and time. Although the seasonal window, or the period covered by AGDDI and $NDVI_{\%}$ generally centers around the same time, changes in land-surface phenology between thermal thresholds vary as location changes (Figure 10). As AGDD accumulates, NDVI changes most dramatically at mid-latitudes. Overall, at mid-to-high latitude regions, changes from $AGDDI_{10\%}$ to $AGDDI_{25\%}$ correspond to approximately 25% changes in NDVI, agreeing with the changes from $NDVI_{50\%}$ to $NDVI_{75\%}$ (Figure 11).

Trends

The magnitudes of short- and long-term trends in the thermal-based indices vary substantially across space and over different time horizons (Figure 12). Over longer time periods (1950-2013; Figure 12), AGDDIs exhibit significant long-term trends along the Pacific coast of North America, in western United States, throughout the

Mediterranean, and across mid-latitude regions in Asia. In SI-x, relatively large trends are also observed throughout the Mediterranean and across mid-to-high latitudes in North America and Asia, but non-significant negative trends are present in the mountain regions in western North America. Compared to more recent historical periods, AGDDIs and SI-x only exhibit weak trends of spring advancement (around 1 day/decade), and positive trends (delay of spring) are observed only in the coastal region around the Gulf of Mexico and over the Tibetan Plateau.

During the satellite era (1982-2013), thermal-based indices exhibit much larger amplitude changes in spring onset timing and some reverse in the signal of their trends. These shorter-term trends are of nearly twice the magnitude of the longer-term ones (1950-2013) in most regions over the Northern Hemisphere. In both AGDDIs and SI-x, the largest spring advancement rates are found near the Great Lakes, in the Mediterranean, and in central and east part of Siberia and Asia, with a magnitude of more than 2 days/decade. Non-significant trends of later spring onset are present at western and central Canada and some locations in Europe and East Asia, with a magnitude of up to 3 days/decade. When only examining the most recent decades (2001-2013), many of the long-term trends are altered or even reversed. Large amplitude trends towards earlier spring are still present in Siberia, northern Canada, eastern US, and Central Asia. However, locations where significant earlier spring are present over 1950-2013, such as the Pacific coast of North America, western United States, the Mediterranean, and East Asia, exhibit nonsignificant rates of spring onset delay. The magnitude of the trends also increases dramatically as thermal-based indices suggest spring occurs more than 3 days earlier during 2001-2013.

Trends in $NDVI_{\%}$ exhibit similar spatial patterns over the satellite era (Figure 12). The NDVI-based indices show stronger trends across all periods than the thermal-based indices, but the magnitude of the trends is still larger in the 2001-2013 interval. The reversed trends between the 1982-2013 and 2001-2013 periods in western North America, Europe, central and south part of Asia are also present.

Although the spatial patterns are similar, when examining mid-to-high latitudes of the Northern Hemisphere (north of 40°N), magnitude of the trends varies across time and indicators (Figure 13). $AGDDI_{10\%}$ suggests that spring becomes earlier at a rate of 1.3 day/decade during 1950-2013, which increases to 1.6 day/decade for 1982-2013 but changes to 0.1 day/decade for 2001-2013. $SI\text{-}x_{leaf}$ advances by 1.0 day/decade during 1950-2013, and the rate is 0.8 day/decade during 1982-2013 and -0.2 day/decade for 2001-2013. $NDVI_{50\%}$ has an earlier trend of 0.6 day/decade during 1982-2013 and 1.8 day/decade for 2001-2013. Overall, the direction of changes matches for both 1950-2013 and 1982-2013 periods, but the magnitude varies for different indicators. Although there is large disagreement during 2001-2013, none of the trends are significant.

Spatial patterns of onset dates, temporal variability, and relationships of Group II indices are similar to those of Group I indices. As Group II indices represent late spring phenological changes, onset dates are later than those in Group I indices, but the spatial patterns are similar among indices. We also observed smaller magnitude of both interannual variability and trends in Group II indices than Group I over most regions. In addition, the agreements between $NDVI_{75\%}$ and corresponding AGDDI and SI-x are better than that in Group I (not shown). Across all time ranges, compared to

events happening earlier in the spring (SI-x_{leaf} and $AGGDI_{10\%}$), late spring phenological events (SI-x_{bloom} and $AGGDI_{25\%}$) exhibit smaller trends.

Previous studies showed that the NDVI3g dataset may have consistency and data quality uncertainties and issues due to changes in sensors and different calibration procedures, especially at regional scales (for example, *Beck et al.*, 2011; *Pinzon and Tucker*, 2014; *Kern et al.*, 2016). So we also tested indicators developed from GIMMS NDVI3g against those from the Moderate Resolution Imaging Spectroradiometer (MODIS) NDVI from both Terra (MOD13C1.006) and Aqua (MYD13C1.006) to assess their consistency and uncertainties. We found considerable good agreement in the spatial patterns of the DOYs from different remote sensing products (not shown). We also note that, despite changes in the absolute dates of spring onset, changing the pre-defined thresholds of AGDD or NDVI will not modify the major spatial and temporal patterns of the indices.

Trends in springtime temperature also change with different examined historical periods (Figure 14). Over 1950-2013, terrestrial temperature in both February, March, and April (FMA) and March, April, and May (MAM) window increases significantly over the Northern Hemisphere, except for a few locations in East Asia, around the Hudson Bay, and in Greenland. These increasing trends persist and intensify in low-to-mid latitude regions in Eurasia and in Greenland during 1982-2013, while the Pacific coast of North America, central Canada, Northern Europe, and East Asia experience non-significant decreasing trends in springtime temperature. During 2001-2013, Siberia and the northeastern part of North America still exhibit increasing temperature, while decreasing trends are present in Alaska, western US, Europe, and

across mid-latitude regions in Asia. Compared with trends of the spring onset indicators (Figure 12), trends in springtime temperature share some similarities in their spatial patterns with the trends of the indices over the same historical periods, but trends in the spring onset indicators are not exact mimics of the temperature trends.

Discussion and conclusion

Climate variability and change play an important role in altering the timing of spring onset, and thermal-based indices can provide useful information in isolating that role. Here, we adopted both thermal- and NDVI-based indices to characterize Northern Hemisphere spring phenology and how temperature paces spring onset on interannual to multidecadal timescales. For almost all characteristics we examined, though SI-x are more tuned to specific plant species, AGDDIs and SI-x are similar in their spatial patterns and magnitude of variability. Even though NDVI-based indices exhibit influences of both climatic and non-climatic factors, at mid-to-high latitudes, their onset dates, interannual variability, trends, and spatial variation are still consistent with those of AGDDIs and SI-x. Overall, because AGDDIs are able to reproduce the major spatial and temporal patterns of spring onset, we argue that AGDDIs are good proxies for spring phenological events in temperate and cold climates. In addition, as AGDDIs only require daily temperature as input and are not tuned to specific species or location, they may be seen as benchmarks of climate impacts on the start of spring and used to assess climate induced changes at large spatial or long temporal scales. They may also be well suited to further climate

analysis to trace the dynamic and thermodynamic origins of the interannual to multi-decadal variations in spring onset.

Temperature dominates the large-scale patterns of spring onset and shifts the seasonal window of spring onset as a whole. Even though different phenological indicators may differ in their magnitude of interannual variability, they have high agreement in their temporal variation, or how early or late spring occur at a certain grid point. Although the magnitude of interannual and long-term changes of thermal- and NDVI-based indicators can vary at the site level and regional scale (Figures 1a, 2a, 5, and 12), they remain in the same seasonal window and have high temporal correlation (Figures 6b, 7, and 9). This suggests that temperature variability from one year to another modifies the seasonal window of spring phenological changes as a whole, causing all the indicators to shift in the same direction from their mean onset dates. In other words, there is a seasonal window of spring onset that is determined mainly by climatic factors. Although relative timing of plant phenophase changes and other seasonal transitions such as circulation pattern change and snow melt may vary, these events still center in the same seasonal window (as illustrated in Figure 10). Therefore, threshold-based indicators of spring onset can be used to estimate the seasonal window of spring and provide insights into spring onset variations in broad groups of seasonal transitions across space and through time, as well as into specific species.

Other climate and non-climate factors may modify the timing and order of phenological changes in the seasonal window. Even though thermal- and NDVI-based indicators are similar in their mean onset dates and trends and highly correlated at

north of 40°N, their order of occurrence also changes at mid-latitudes. Difference in the order between SI-x_{leaf} and $AGDDI_{10\%}$ is present approximately along 40°N while shifts between $NDVI_{50\%}$ and thermal-based indices occur at a higher latitude (roughly along 60°N) and angled along northwestern trajectories (Figure 6a). This variation in their ordering suggests that though temperature is the dominant factor at a hemispheric scale, at regional and local scales, relative importance of temperature, moisture, and synoptic events in altering spring onset may change. In addition, at high-altitude and high-latitude locations, changes in snow-cover may also influence NDVI-based indices (e.g. *Dye and Tucker*, 2003; *Buus-Hinkler et al.*, 2006). The varying influences of different climatic factors are also present in comparisons between temporal correlations and pattern correlations among the indices. Compared to their overall spatial patterns, the three indicators exhibit larger similarity in their temporal variability at each grid point (Figures 7 and 8).

We also provide a new way to isolate the role of climate change in altering the timing of spring onset. As shown by different spring onset indicators, trends of spring phenological events are consistent across metrics but depend dramatically on the examined historical period (Figure 12). Researchers have discovered different changing rates of spring phenology across the Northern Hemisphere from observational data, satellite remote sensing, and phenological models and suggested that these differences may result from limitation of the data source, species, spatial distribution, and examined periods (for example, *Dose and Menzel*, 2006; *Parmesan*, 2006; *Schwartz et al.*, 2006; *Cleland et al.*, 2007; *Wu et al.*, 2016). In particular, *Schwartz et al.* (2006) adopted station-based spring index precursors to the SI-x and

emphasized the potential application of spring indices to assess trends over standard periods and locations. Here, with three different sets of gridded spring onset indicators, we further argue that these differences in variability and trends of spring phenology may be due to the different investigating period and spatial coverage, both of which can result in a misrepresentation of the long-term trends. When the temporal coverage of the spring onset data changes, the magnitude and significance of its trend change significantly, sometimes the signal even reverses. However, trends in spring onset dates are relatively small compared to their interannual variability at all spatial and temporal scales, so trends in small-scale and/or short-term data may be altered by its limited temporal depth and the main state of its climate system during that time. Any conclusions about the role of climate change in driving spring onset trends within short observational periods should therefore be interpreted with caution. These considerations also apply to the satellite era because its temporal coverage spans only a few decades, and this timescale is not necessarily long enough to isolate long-term changes (e.g., Figure 12). We also argue that, thermal-based indices may provide a historical baseline of large-scale or long-term trends.

Among many other topics, future work should examine causes of the above heterogeneity of trends and climate impacts over the Northern Hemisphere. These differences in climate-phenology relationships may result from significant and yet different impacts of various atmospheric modes. For instance, processes like the North Atlantic Oscillation (NAO) and El Niño-Southern Oscillation (ENSO) have consistent large-scale influence on spring onset over North America (*Ault et al.*, 2011; *McCabe et al.*, 2012). As spring onset timing is an important indicator of changes in both

natural and managed ecosystems, disentangling influences of the climate system on spring phenology is critical to understand and predict future changes in both ecosystems and the climate system. This study is a first step to isolate the role of climate factors in modulating the timing of spring onset and therefore may have important implications in understanding climate-phenology relationships and predicting future changes in spring phenology at various spatial and temporal scales.

REFERENCES

Ault, T. R., A. K. Macalady, G. T. Pederson, J. L. Betancourt, and M. D. Schwartz (2011), Northern Hemisphere Modes of Variability and the Timing of Spring in Western North America, *Journal of Climate*, *24*(15), 4003–4014, doi:10.1175/2011JCLI4069.1.

Ault, T. R., M. D. Schwartz, R. Zurita-Milla, J. F. Weltzin, and J. L. Betancourt (2015), Trends and natural variability of spring onset in the coterminous united states as evaluated by a new gridded dataset of spring indices, *Journal of Climate*, *28*(21), 8363–8378.

Beck, H. E., T. R. McVicar, A. I. van Dijk, J. Schellekens, R. A. de Jeu, and L. A. Bruijnzeel (2011), Global evaluation of four avhrr–ndvi data sets: Intercomparison and assessment against landsat imagery, *Remote Sensing of Environment*, *115*(10), 2547–2563.

Benjamini, Y., and Y. Hochberg (1995), Controlling the False Discovery Rate: A Practical and Powerful Approach to Multiple Testing, *Journal of the Royal Statistical Society. Series B (Methodological)*, *57*(1), 289–300, doi:10.2307/2346101.

Black, R. X., and B. A. McDaniel (2007), The dynamics of northern hemisphere stratospheric final warming events, *Journal of the atmospheric sciences*, *64*(8), 2932–2946.

Buus-Hinkler, J., B. U. Hansen, M. P. Tamstorf, and S. B. Pedersen (2006), Snowvegetation relations in a high arctic ecosystem: Inter-annual variability inferred from new monitoring and modeling concepts, *Remote Sensing of Environment*, *105*(3), 237– 247.

Cayan, D. R., M. D. Dettinger, S. A. Kammerdiener, J. M. Caprio, and D. H. Peterson (2001), Changes in the onset of spring in the western united states, *Bulletin of the American Meteorological Society*, *82*(3), 399–415.

Cleland, E. E., I. Chuine, A. Menzel, H. A. Mooney, and M. D. Schwartz (2007), Shifting plant phenology in response to global change., *Trends in ecology & evolution*, *22*(7), 357–65, doi:10.1016/j.tree.2007.04.003. de Beurs, K., and G. Henebry (2005), A statistical framework for the analysis of long image time series, *International Journal of Remote Sensing*, *26*(8), 1551–1573.

de Beurs, K. M., and G. M. Henebry (2008), Northern annular mode effects on the land surface phenologies of northern eurasia, *Journal of Climate*, *21*(17), 4257–4279.

Dose, V., and A. Menzel (2006), Bayesian correlation between temperature and blossom onset data, *Global Change Biology*, *12*(8), 1451–1459, doi:10.1111/j.1365-2486.2006. 01160.x.

Dye, D. G., and C. J. Tucker (2003), Seasonality and trends of snow-cover, vegetation

index, and temperature in northern eurasia, *Geophysical Research Letters*, *30*(7).

Fensholt, R., and S. R. Proud (2012), Evaluation of earth observation based global long term vegetation trends—comparing gimms and modis global ndvi time series, *Remote sensing of Environment*, *119*, 131–147.

Fensholt, R., S. Horion, T. Tagesson, A. Ehammer, E. Ivits, and K. Rasmussen (2015), Global-scale mapping of changes in ecosystem functioning from earth observation-based trends in total and recurrent vegetation, *Global Ecology and Biogeography*, *24*(9), 1003– 1017.

Fitzjarrald, D. R., O. C. Acevedo, and K. E. Moore (2001), Climatic consequences of leaf presence in the eastern united states, *Journal of Climate*, *14*(4), 598–614.

Forrest, J., and A. J. Miller-Rushing (2010), Toward a synthetic understanding of the role of phenology in ecology and evolution, *Philosophical Transactions of the Royal Society of London B: Biological Sciences*, *365*(1555), 3101–3112.

Hogg, E. H., D. T. Price, and T. A. Black (2000), Postulated Feedbacks of Deciduous Forest Phenology on Seasonal Climate Patterns in the Western Canadian Interior, *Journal of Climate*, *13*(24), 4229–4243, doi:10.1175/1520-0442(2000)013<4229:PFODFP>2.0. CO;2.

Jolly, W. M., R. Nemani, and S. W. Running (2005), A generalized, bioclimatic index to predict foliar phenology in response to climate, *Global Change Biology*, *11*(4), 619–632, doi:10.1111/j.1365-2486.2005.00930.x.

Karkauskaite, P., T. Tagesson, and R. Fensholt (2017), Evaluation of the plant phenology index (ppi), ndvi and evi for start-of-season trend analysis of the northern hemisphere boreal zone, *Remote Sensing*, *9*(5), 485.

Kern, A., H. Marjanović, and Z. Barcza (2016), Evaluation of the quality of ndvi3g dataset against collection 6 modis ndvi in central europe between 2000 and 2013, *Remote Sensing*, *8*(11), 955.

Liu, Q., Y. H. Fu, Y. Liu, I. A. Janssens, and S. Piao (2017), Simulating the onset of spring vegetation growth across the northern hemisphere, *Global change biology*.

Lundquist, J. D., and A. L. Flint (2006), Onset of Snowmelt and Streamflow in 2004 in the Western United States: How Shading May Affect Spring Streamflow Timing in a Warmer World, *Journal of Hydrometeorology*, *7*(6), 1199–1217, doi:10.1175/JHM539.1.

McCabe, G. J., T. R. Ault, B. I. Cook, J. L. Betancourt, and M. D. Schwartz (2012), Influences of the El Niño Southern Oscillation and the Pacific Decadal Oscillation on the timing of the North American spring, *International Journal of Climatology*, *32*(15), 2301–2310, doi:10.1002/joc.3400.

McMaster, G. S., and W. Wilhelm (1997), Growing degree-days: one equation, two interpretations, *Agricultural and Forest Meteorology*, *87*(4), 291–300.

Melaas, E. K., M. A. Friedl, and A. D. Richardson (2016), Multiscale modeling of spring phenology across deciduous forests in the eastern united states, *Global change biology*, *22*(2), 792–805.

Miller, P., W. Lanier, and S. Brandt (2001), Using growing degree days to predict plant stages, *Ag/Extension Communications Coordinator, Communications Services, Montana State University-Bozeman, Bozeman, MO*.

Parmesan, C. (2006), Ecological and Evolutionary Responses to Recent Climate Change, *Annual Review of Ecology, Evolution, and Systematics*, *37*, 637–669, doi:10.2307/ 30033846.

Parmesan, C. (2007), Influences of species, latitudes and methodologies on estimates of phenological response to global warming, *Global Change Biology*, *13*(9), 1860–1872.

Pinzon, J. E., and C. J. Tucker (2014), A non-stationary 1981–2012 AVHRR ndvi3g time series, *Remote Sensing*, *6*(8), 6929–6960.

Prevéy, J., M. Vellend, N. Rüger, R. D. Hollister, A. D. Bjorkman, I. H. Myers-Smith, S. C. Elmendorf, K. Clark, E. J. Cooper, B. Elberling, et al. (2017), Greater temperature sensitivity of plant phenology at colder sites: implications for convergence across northern latitudes, *Global change biology*, *23*(7), 2660–2671.

Richardson, A. D., T. F. Keenan, M. Migliavacca, Y. Ryu, O. Sonnentag, and M. Toomey (2013), Climate change, phenology, and phenological control of vegetation feedbacks to the climate system, *Agricultural and Forest Meteorology*, *169*, 156–173.

Robinson, R. G. (1971), Sunflower phenology—year, variety, and date of planting effects on day and growing degree-day summations, *Crop Science*, *11*(5), 635–638.

Rohde, R., R. Muller, R. Jacobsen, S. Perlmutter, A. Rosenfeld, J. Wurtele, J. Curry, C. Wickham, and S. Mosher (2013), Berkeley earth temperature averaging process, *Geoinformatics & Geostatistics: An Overview*.

Rosemartin, A. H., E. G. Denny, J. F. Weltzin, R. L. Marsh, B. E. Wilson, H. Mehdipoor, R. Zurita-Milla, and M. D. Schwartz (2015), Lilac and honeysuckle phenology data 1956–2014, *Scientific data*, *2*.

Schwartz, M. D., and G. A. Marotz (1986), An Approach to Examining Regional

Atmosphere-Plant Interactions with Phenological Data, *Journal of Biogeography*, *13*(6), 551–560, doi:10.2307/2844818.

Schwartz, M. D. (1992), Phenology and Springtime Surface-Layer Change, *Monthly Weather Review*, *120*(11), 2570–2578, doi:10.1175/1520-0493(1992)120<2570: PASSLC>2.0.CO;2.

Schwartz, M. D. (1997), Spring index models: an approach to connecting satellite and surface phenology, *Phenology in seasonal climates I*, pp. 23–38.

Schwartz, M. D., and B. E. Reiter (2000), Changes in North American spring, *International Journal of Climatology*, *20*(8), 929–932, doi:10.1002/1097-0088(20000630)20: 8<929::AID-JOC557>3.0.CO;2-5.

Schwartz, M. D., and T. M. Crawford (2001), Detecting energy-balance modifications at the onset of spring, *Physical Geography*, *22*(5), 394–409, doi:10.1080/02723646.2001. 10642751.

Schwartz, M. (2003), Phenoclimatic measures, in *Phenology: An Integrative Environmental Science*, edited by M. Schwartz, pp. 331–343, Kluwer Academic Publishers, Dordrecht, The Netherlands, doi:10.1163/_q3_SIM_00374.

Schwartz, M. D., R. Ahas, and A. Aasa (2006), Onset of spring starting earlier across the Northern Hemisphere, *Global Change Biology*, *12*(2), 343–351, doi:10.1111/j. 1365-2486.2005.01097.x.

Schwartz, M. D., T. R. Ault, and J. L. Betancourt (2013), Spring onset variations and trends in the continental United States: past and regional assessment using temperaturebased indices, *International Journal of Climatology*, *33*(13), 2917–2922, doi:10.1002/ joc.3625.

Snyder, R. L., D. Spano, C. Cesaraccio, and P. Duce (1999), Determining degree-day thresholds from field observations, *International Journal of Biometeorology*, *42*(4), 177– 182, doi:10.1007/s004840050102.

Stewart, I. T., D. R. Cayan, and M. D. Dettinger (2005), Changes toward earlier streamflow timing across western north america, *Journal of climate*, *18*(8), 1136–1155.

Thackeray, S. J. (2012), Mismatch revisited: what is trophic mismatching from the perspective of the plankton?, *Journal of plankton research*, *34*(12), 1001–1010.

Thackeray, S. J., P. A. Henrys, D. Hemming, J. R. Bell, M. S. Botham, S. Burthe, P. Helaouet, D. G. Johns, I. D. Jones, D. I. Leech, et al. (2016), Phenological sensitivity to climate across taxa and trophic levels, *Nature*, *535*(7611), 241.

Tollenaar, M., T. B. Daynard, and R. B. Hunter (1979), Effect of temperature on rate of leaf appearance and flowering date in maize, *Crop Science*, *19*(3), 363–366.

Tucker, C. J., J. E. Pinzon, M. E. Brown, D. A. Slayback, E. W. Pak, R. Mahoney, E. F. Vermote, and N. El Saleous (2005), An extended avhrr 8-km ndvi dataset compatible with modis and spot vegetation ndvi data, *International Journal of Remote Sensing*, *26*(20), 4485–4498.

Visser, M. E., S. P. Caro, K. Van Oers, S. V. Schaper, and B. Helm (2010), Phenology, seasonal timing and circannual rhythms: towards a unified framework, *Philosophical Transactions of the Royal Society of London B: Biological Sciences*, *365*(1555), 3113– 3127.

White, M. A., K. M. De Beurs, K. Didan, D. W. Inouye, A. D. Richardson, O. P.

Jensen, J. O'keefe, G. Zhang, R. R. Nemani, W. J. D. Van Leeuwen, J. F. Brown, A. De Wit, M. Schaepman, X. Lin, M. Dettinger, A. S. Bailey, J. Kimball, M. D. Schwartz, D. D. Baldocchi, J. T. Lee, and W. K. Lauenroth (2009), Intercomparison, interpretation, and assessment of spring phenology in North America estimated from remote sensing for 1982–2006, *Global Change Biology*, *15*(10), 2335–2359, doi:10.1111/j.1365-2486.2009. 01910.x.

Wu, R., and B. Wang (2000), Interannual variability of summer monsoon onset over the western north pacific and the underlying processes, *Journal of climate*, *13*(14), 2483– 2501.

Wu, X., R. Zurita-Milla, and M.-J. Kraak (2016), A novel analysis of spring phenological patterns over europe based on co-clustering, *Journal of Geophysical Research: Biogeosciences*, *121*(6), 1434–1448.

Xu, J., X. Gao, J. Shuttleworth, S. Sorooshian, and E. Small (2004), Model climatology of the north american monsoon onset period during 1980–2001, *Journal of climate*, *17*(20), 3892–3906.

FIGURES

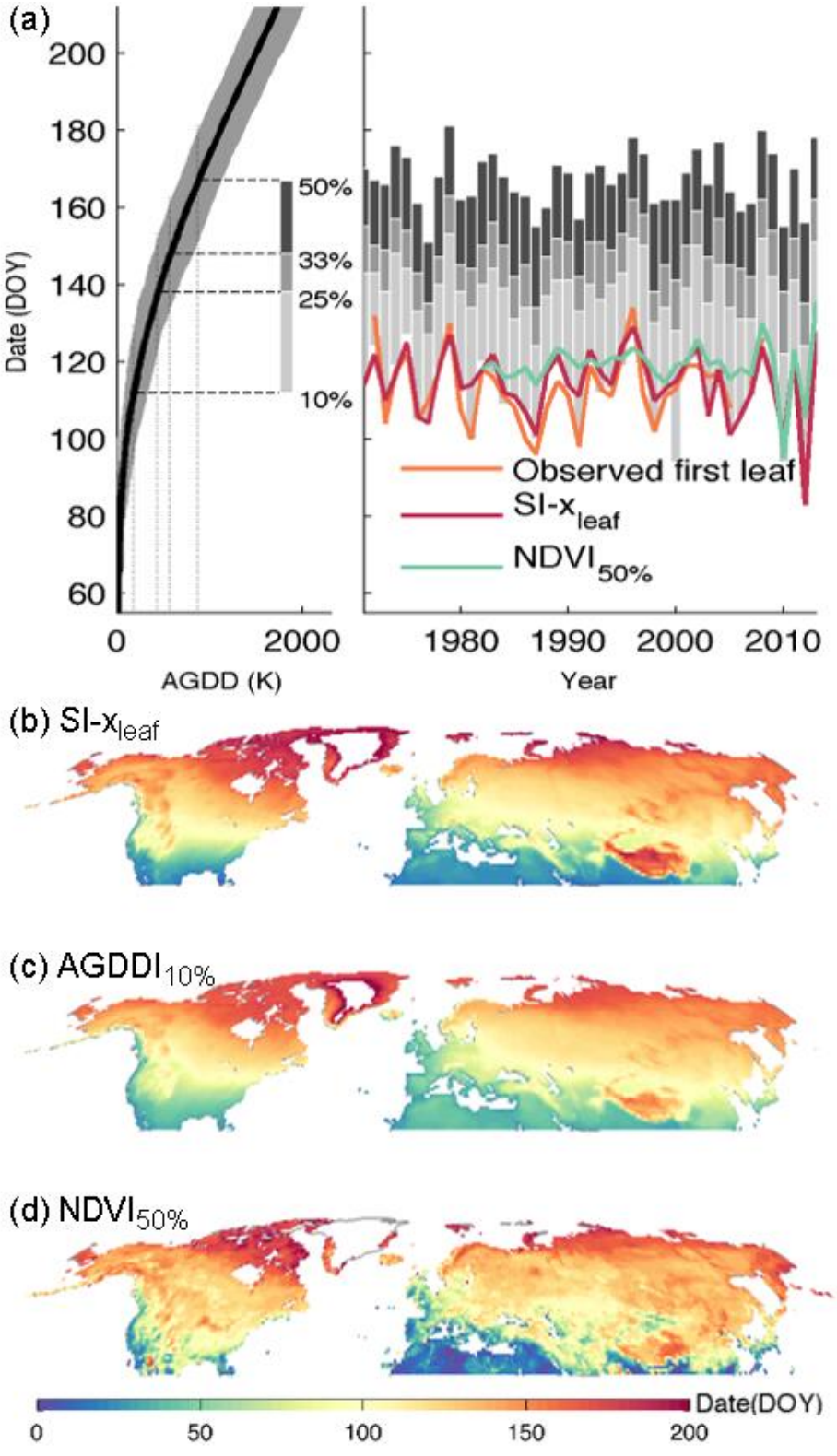
(a)
Date (DOY)
200
180
160
140
120
100
80
60
50%
33%
25%
10%
0
2000
AGDD (K)
1980
1990
2000
2010
Year
Observed first leaf
SI-x leaf
NDVI 50%
(b) SI-x leaf
(c) AGDDI 10%
(d) NDVI 50%
Date(DOY)
0
50
100
150
200

Figure 1. An example of AGDD thresholds and temporal variability of the three types of indices and the time-averaged onset dates. (a) An example of AGDD thresholds, the order of events, and temporal variability of the three types of indices along with observed phenology, at the nearest grid point (47.5°N, 93.5°W) to one of the longest available phenological observations at Grand Rapids Forestry Lab [47.23°N, 93.5°W; data is from *Rosemartin et al.*, 2015]. (Left) An example of AGDD thresholds and how the AGDDIs are derived. The black curve represents mean AGDD from January 1st (day 1) to any specific date until day 212 averaged over 1981-2010. Gray areas surrounding the black curve indicate the range of AGDD achieved by a given day (horizontal or dashed line), which can also be interpreted as the seasonal window when different years reach a given AGDD threshold at the same location (vertical or dotted line) between 1981 and 2010. Dashed lines indicate the pre-defined values used to determine each threshold and their corresponding symbols. (Right) An example of the order of events and variability of the three types of indices and observed phenology. Grey symbols indicate the distributions of AGDDIs each year as shown in left. Solid lines exhibit time series of observed first leaf dates (dark orange), SI-x leaf index (SI-x_{leaf}, dark red), and the day of year when NDVI cross the 50% threshold ($NDVI_{50\%}$, green); (b) time-averaged (1982-2013) onset dates of mean SI-x_{leaf}; (c) mean day of year when AGDD crosses the threshold of 10% climatology ($AGDDI_{10\%}$, see text); (d) mean day of year when NDVI crosses 50% threshold of the dynamical range of annual NDVI ($NDVI_{50\%}$, see text).

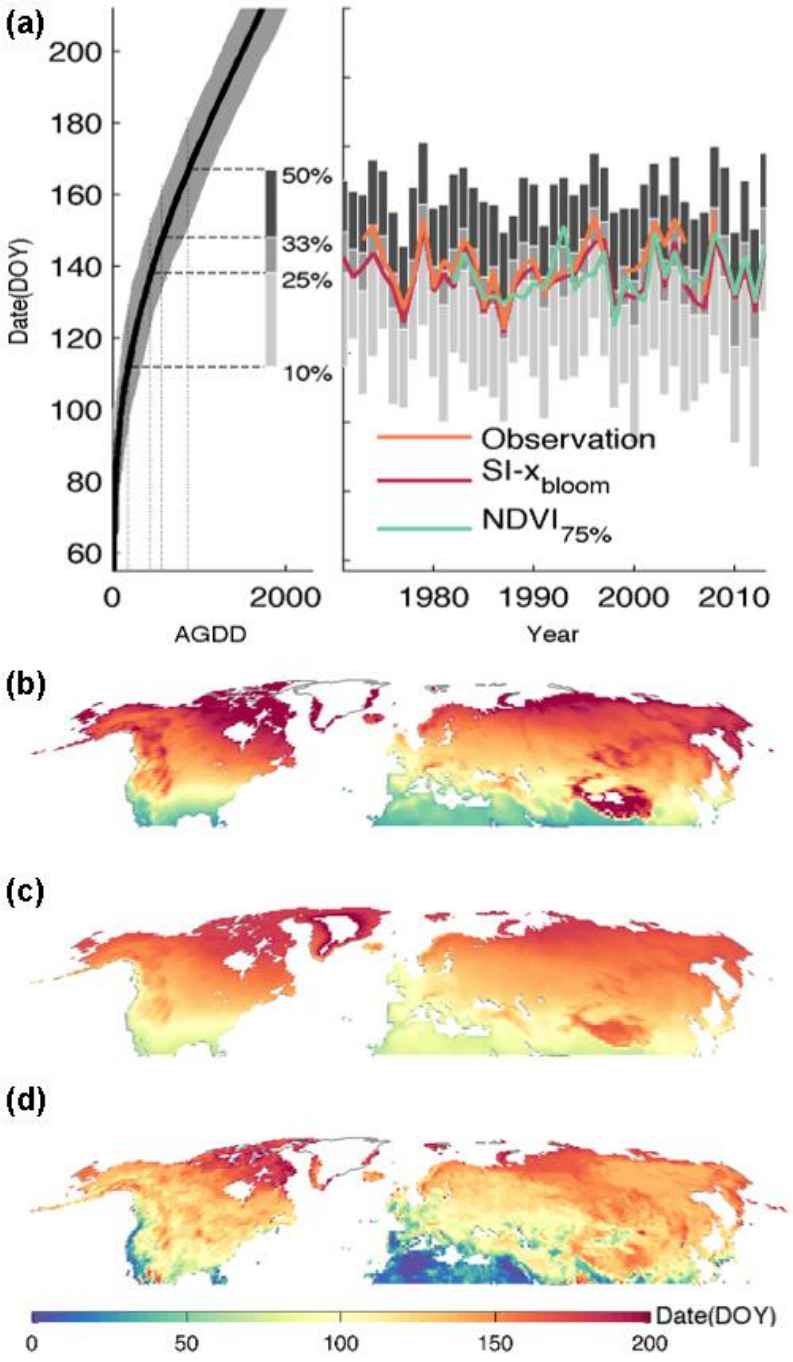

Figure 2. An example of AGDD thresholds and temporal variability of the three types of indices and the time-averaged onset dates for indices in Group II. (a) An example of AGDD thresholds, the order of events, and temporal variability of the three types of indices along with observed phenology, at the nearest grid point (47.5°N, 93.5°W) to one of the longest available phenological observations at Grand Rapids Forestry Lab [47.23°N, 93.5°W; data is from *Rosemartin et al.*, 2015]. (Left) An example of AGDD thresholds and how the AGDDIs are derived. The black curve represents mean AGDD

from January 1st (day 1) to any specific date until day 212 averaged over 1981-2010. Gray areas surrounding the black curve indicate the range of AGDD achieved by a given day (horizontal or dashed line), which can also be interpreted as the seasonal window when different years reach a given AGDD threshold at the same location (vertical or dotted line) between 1981 and 2010. Dashed lines indicate the pre-defined values used to determine each threshold and their corresponding symbols. (Right) An example of the order of events and variability of the three types of indices and observed phenology. Grey symbols indicate the distributions of AGDDIs each year as shown in left. Solid lines exhibit time series of observed first leaf dates (dark orange), SI-x bloom index (SI-x_{bloom}, dark red), and the day of year when NDVI cross the 75% threshold ($NDVI_{75\%}$, green); (b) time-averaged (1982-2013) onset dates of mean SI-x_{bloom}; (c) mean day of year when AGDD crosses the threshold of 25% climatology ($AGDDI_{25\%}$, see text); (d) mean day of year when NDVI crosses 75% threshold of the dynamical range of annual NDVI ($NDVI_{75\%}$, see text).

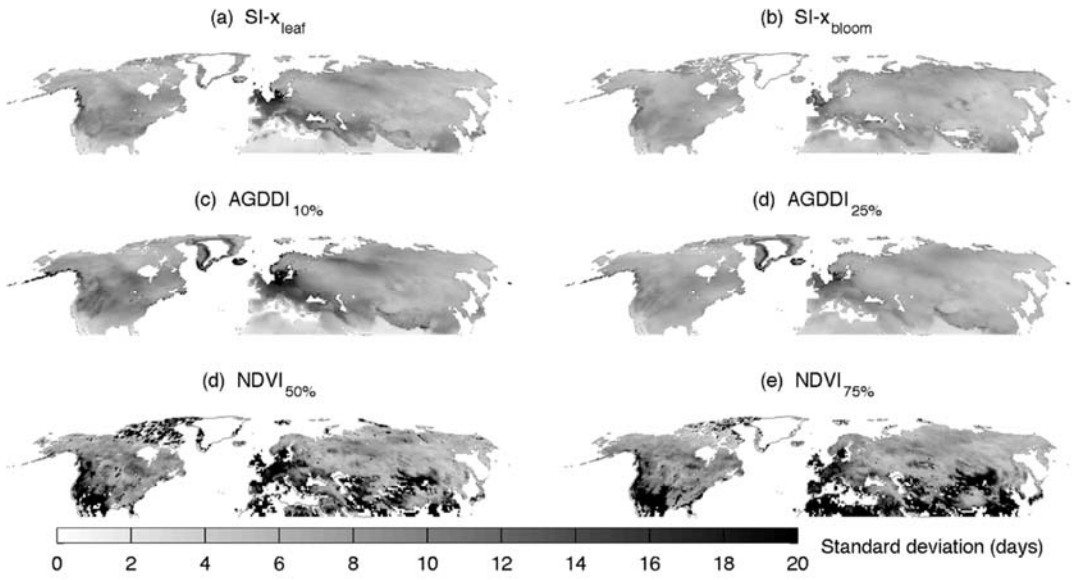

Figure 3. Maps showing the standard deviation of the three metrics calculated over 1982-2013: (a) SI-x_{leaf}; (b) SI-x_{bloom}; (c)-(d) day of the year when AGDD crosses thresholds of 10% (c) and 25% (d) of climatology; (e)-(f) day of the year when NDVI crosses 50% (f) and 75% (g) thresholds of the dynamical range of annual NDVI.

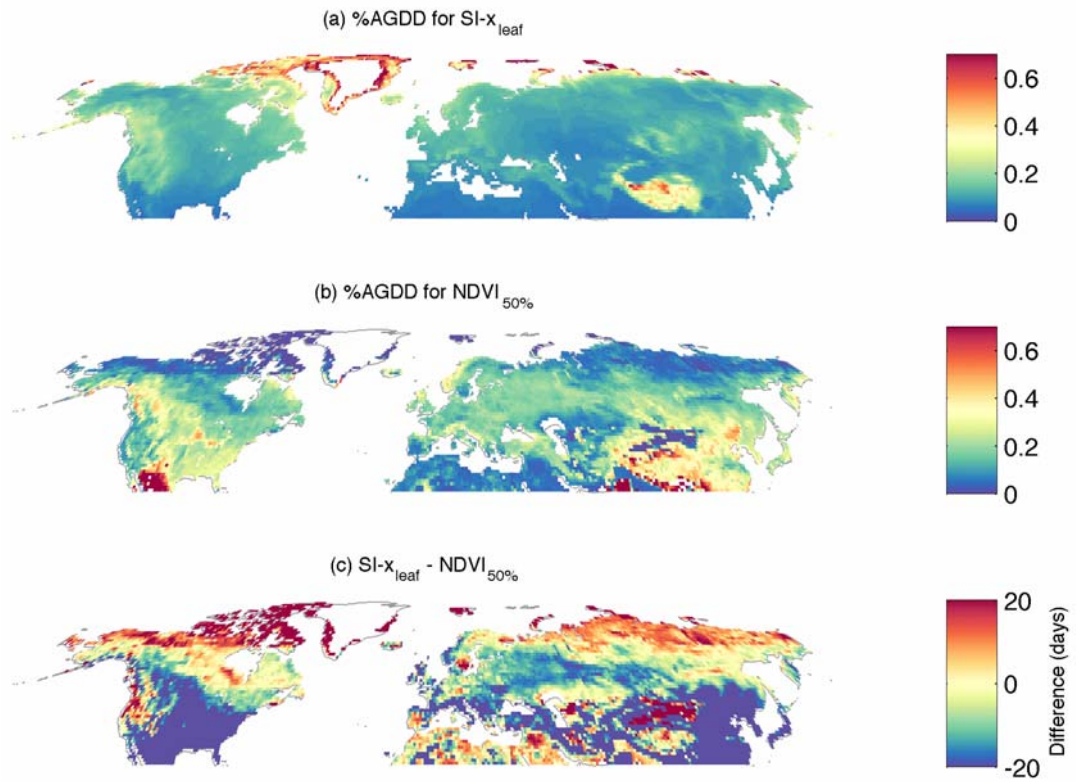

Figure 4. Maps showing the relationships between Group I indices ($AGGDI_{10\%}$, $SI\text{-}x_{leaf}$, and $NDVI_{50\%}$): (a)-(b) the percentage of mean day 212 AGDD reached at the mean $SI\text{-}x_{leaf}$ dates (a) and mean $NDVI_{50\%}$ dates (b). Mean daily AGDD were calculated over the climate reference period (1981-2010) and mean $SI\text{-}x_{leaf}$ and $NDVI_{50\%}$ were calculated over the longest overlapping period (1982-2013). Panel (c) maps the difference between $SI\text{-}x_{leaf}$ and $NDVI_{50\%}$ DOYs averaged between 1982 and 2013.

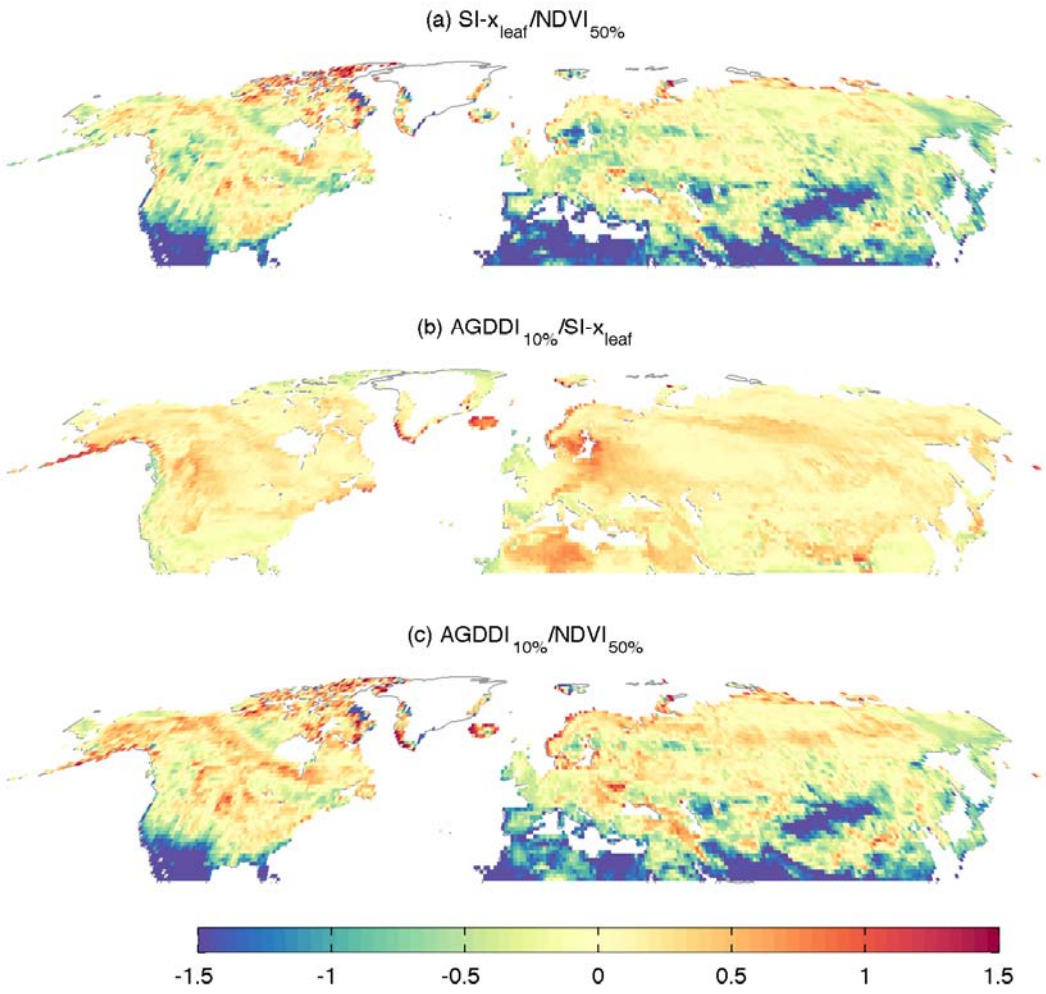

Figure 5. Maps showing the relative temporal variations of Group I indices ($AGGDI_{10\%}$, $SI\text{-}x_{leaf}$, and $NDVI_{50\%}$): (a)-(c) the log value of ratios of standard deviations of each indices pairs over 1982-2013.

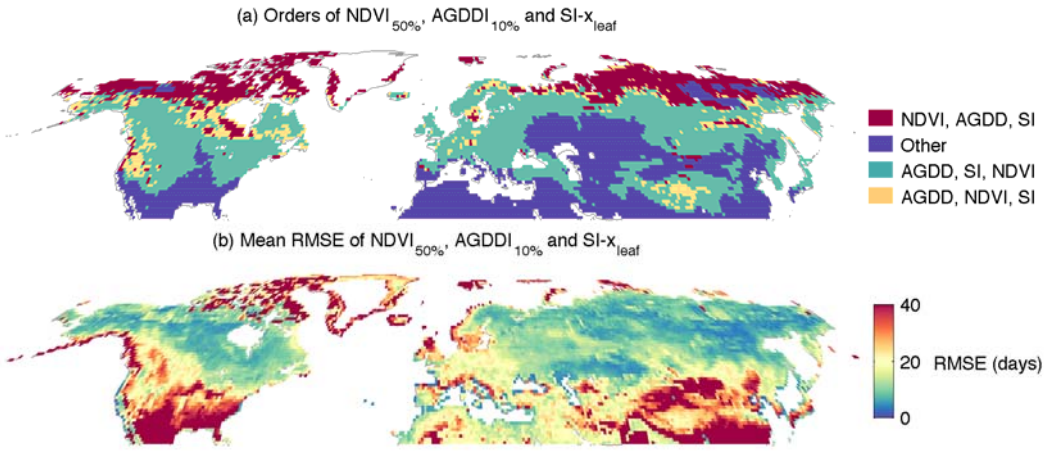

Figure 6. Maps showing the order of events and difference in onset dates of Group I indices ($AGGDI_{10\%}$, $SI\text{-}x_{leaf}$, and $NDVI_{50\%}$). (a) order of indices within the group at each grid point. Index indicates earliest spring is in the front of the order in which they occur. (b) mean RMSE averaged using RMSEs of indices pairs over 1982-2013.

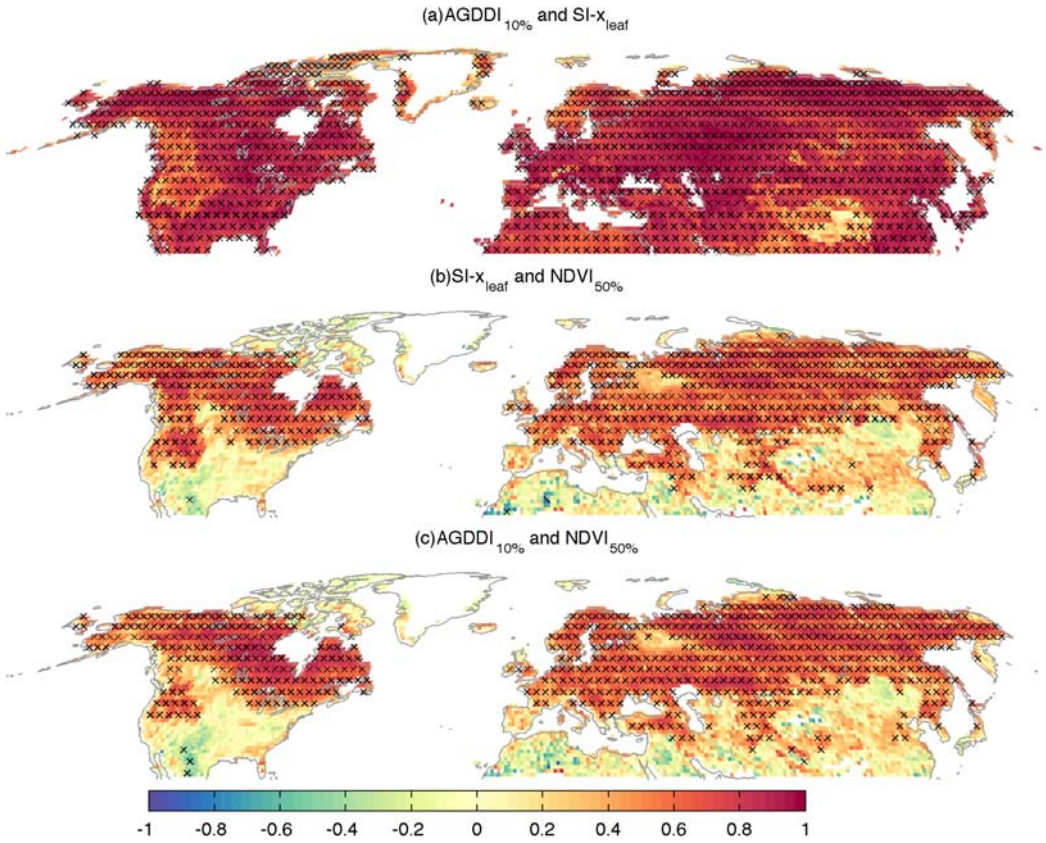

Figure 7. Maps showing correlation coefficients among Group I indices ($AGDDI_{10\%}$, $SI\text{-}x_{leaf}$, and $NDVI_{50\%}$). Correlation coefficients were calculated over 1982-2013 between $AGDDI_{10\%}$ and $SI\text{-}x_{leaf}$ (a), $NDVI_{50\%}$ and $SI\text{-}x_{leaf}$ (b), and $AGDDI_{10\%}$ and $NDVI_{50\%}$ (c), respectively. Grid points with significant correlations after adjusted for false positive are marked with a black "x".

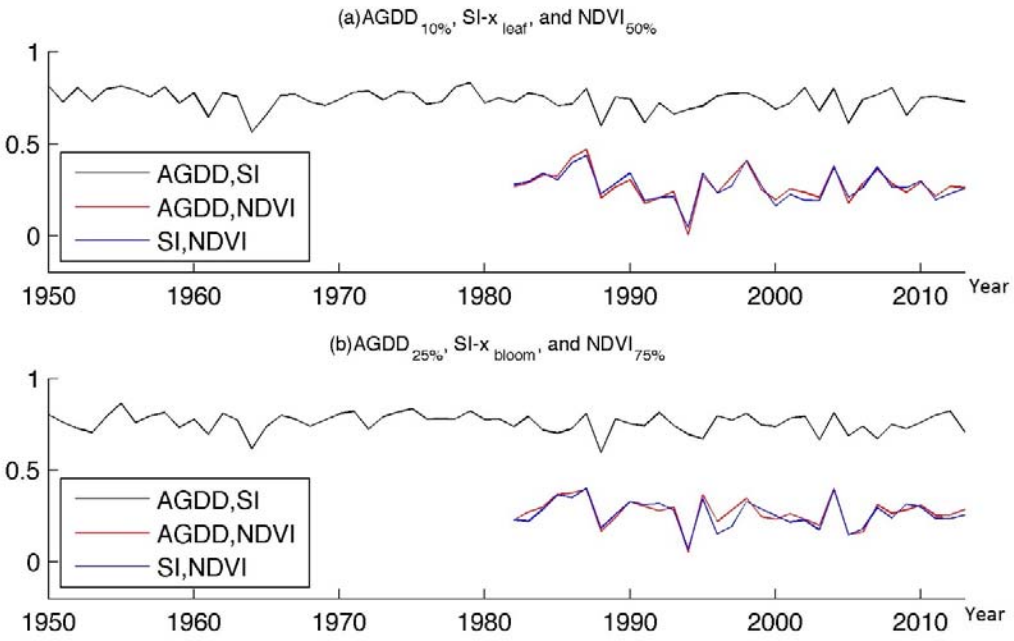

Figure 8. Pattern correlation among indices pairs in Group I ($AGGDI_{10\%}$, $SI\text{-}x_{leaf}$, and $NDVI_{50\%}$; panel a) and Group II ($AGDDI_{25\%}$, $SI\text{-}x_{bloom}$, and $NDVI_{75\%}$; panel b) for all available years. Correlation coefficients were calculated using pattern correlations between temporal anomalies of each indices pair at each grid point.

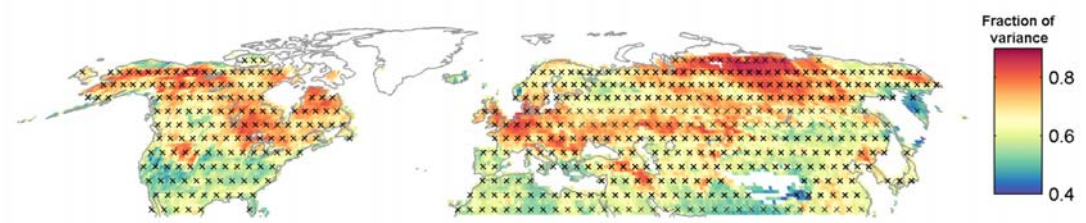

Figure 9. Explained total variance by pointwise first PC at each grid point. Grid points with significant PC1 are marked with a black "x".

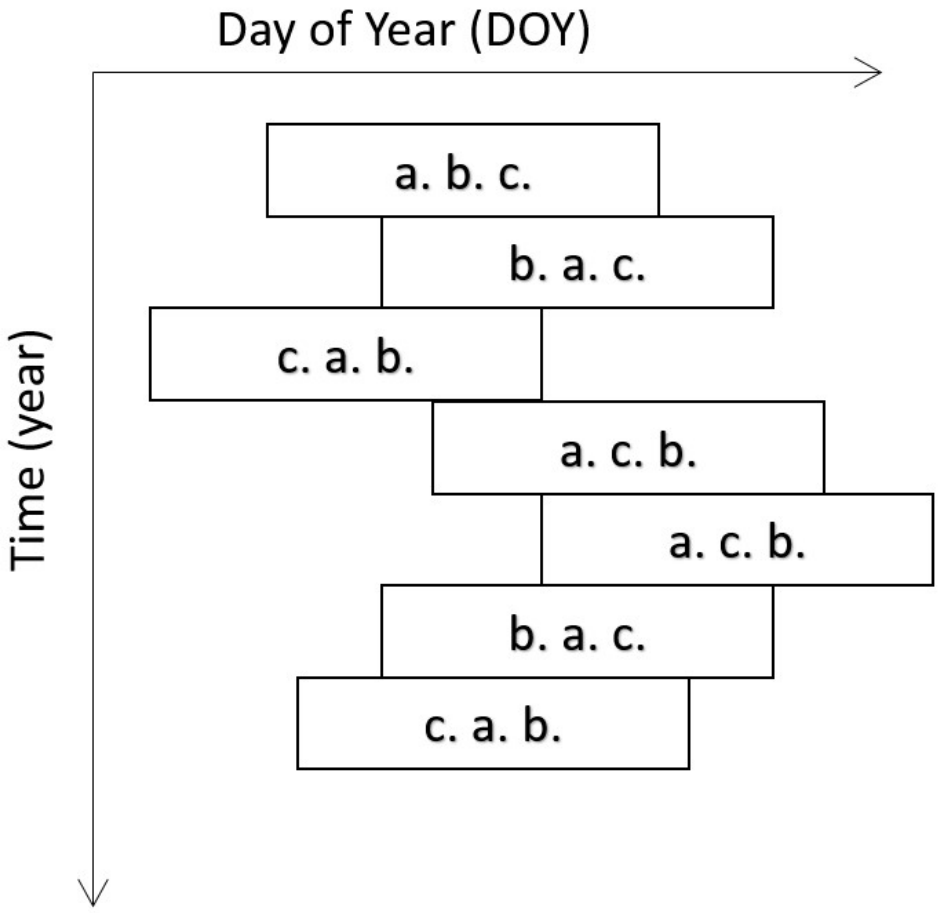

Figure 10. Schematic diagram of how the "seasonal window" of spring onset varies because of interannual climate variability. Species or indicators that respond to this seasonal window (marked a. b. and c.) will necessarily also exhibit interannual variability, although the order of each individual event during any given year may vary from one year to the next.

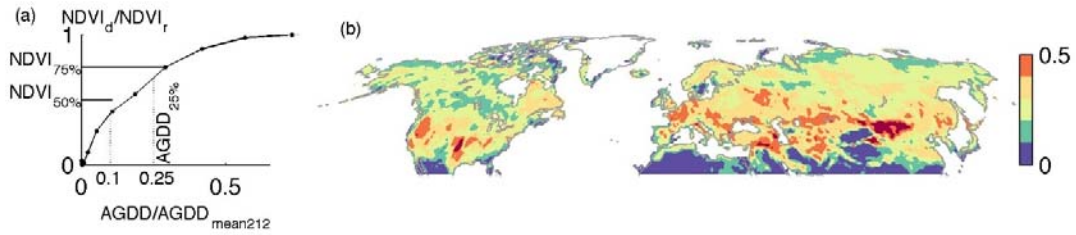

Figure 11. Relationship between AGDDIs and $NDVI_{\%}$. (a) Relationship between AGDD thresholds and NDVI thresholds based on AGDD and NDVI averaged over 1982-2013 at 47.5°N, 93.5°W. AGDD thresholds are calculated by dividing daily AGDD over mean day 212 AGDD ($AGDD_{mean212}$) while NDVI thresholds are based on NDVI departure from annual minimum NDVI ($NDVI-NDVI_{min}$, $NDVI_d$) over annual dynamical range of NDVI ($NDVI_{max}-NDVI_{min}$, $NDVI_r$). (b) Percentage of NDVI change that occurs between $AGDDI_{10\%}$ and $AGDDI_{25\%}$, or ($NDVI(DOY= AGDDI_{10\%})-NDVI(DOY= AGDDI_{25\%})$)/ ($NDVI_{max}-NDVI_{min}$)

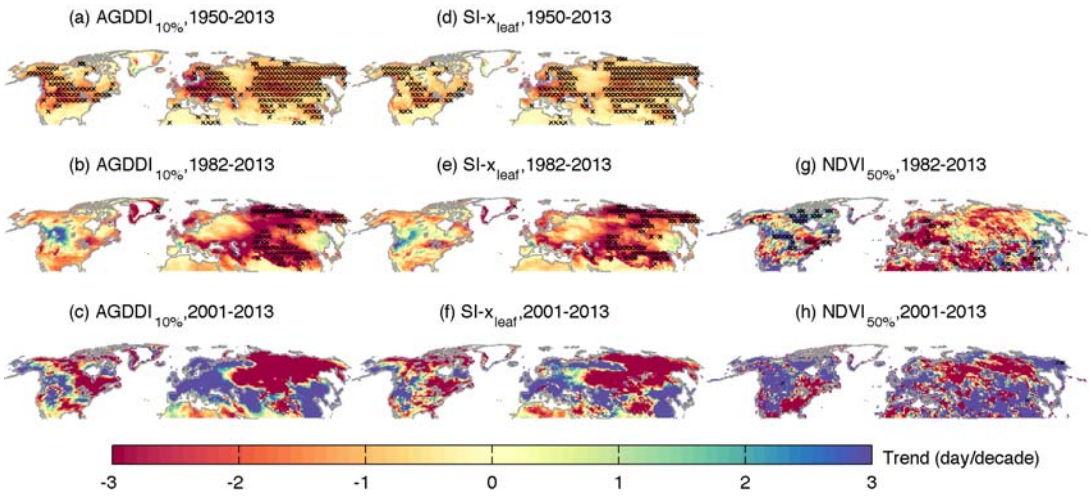

Figure 12. Linear trends of Group I indices over different historical periods. (a)-(c): linear trends of $AGDDI_{10\%}$ over 1950-2013 (a), 1982-2013 (b), and 2001-2013 (c), respectively. (d)-(f): linear trends of $SI\text{-}x_{leaf}$ over 1950-2013 (d), 1982-2013 (e), and 2001-2013 (f). (g)-(h): linear trends of $NDVI_{50\%}$ over 1982-2013 (g) and 2001-2013 (h). Grid points with significant trends after adjusted for false positive are marked with a black "x".

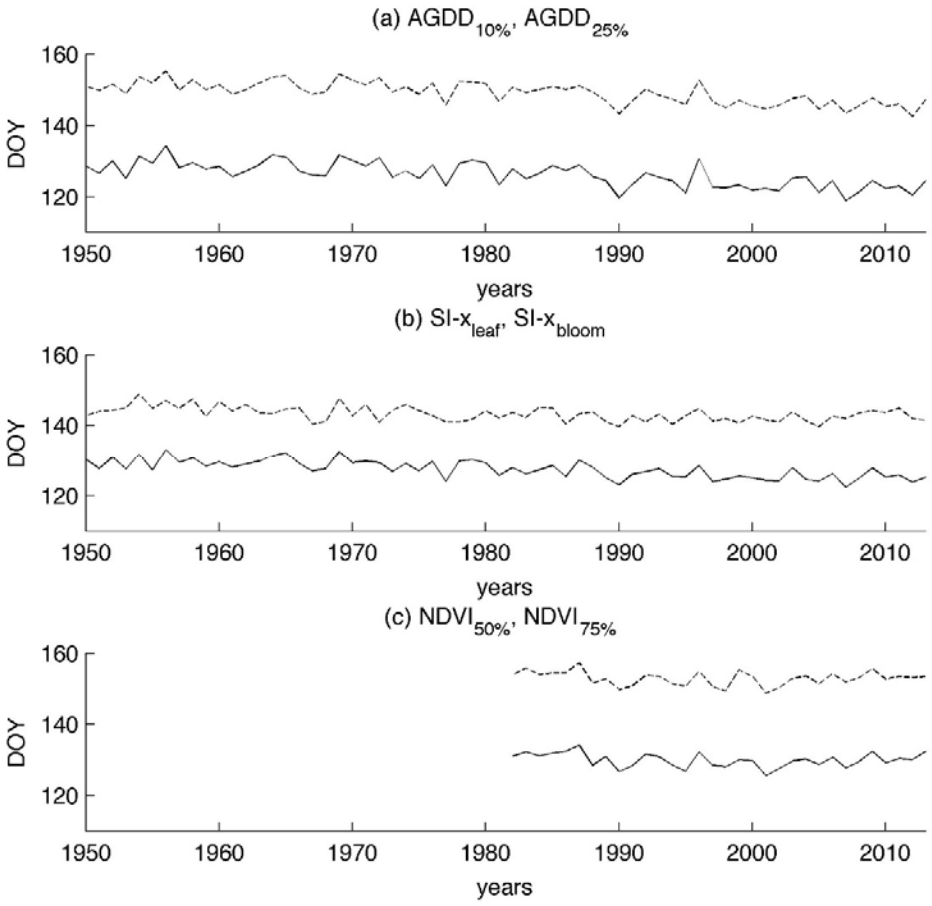

Figure 13. Time series of the mean DOYs of the three set of indices across mid-to-high latitude regions in the Northern Hemisphere. DOYs are calculated by averaging annual DOYs with area-weighting for north of 40°N. (a) mean DOY of $AGDDI_{10\%}$ (solid line) and $AGDDI_{25\%}$ (dashed line) averaged over north of 40°N. (b) mean DOY of $SI\text{-}x_{leaf}$ (solid line) and $SI\text{-}x_{bloom}$ (dashed line) averaged over north of 40°N. (c) mean DOY of $NDVI_{50\%}$ (solid line) and $NDVI_{75\%}$ (dashed line) averaged over north of 40°N.

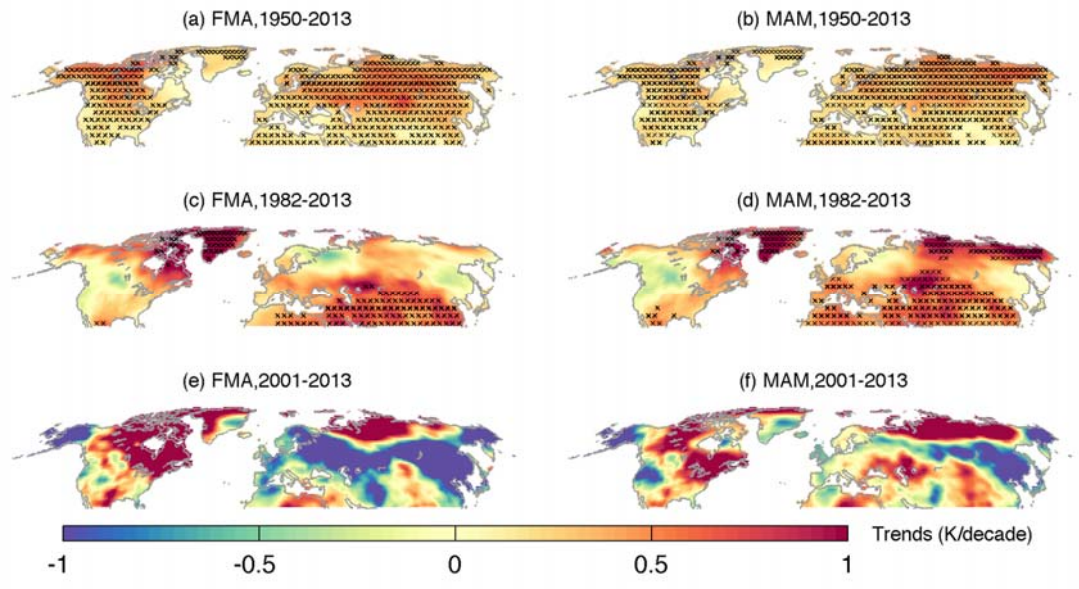

Figure 14. Linear trends of mean spring season temperature over different historical periods. Temperature are averaged over February, March, April (FMA) and March, April, May (MAM), separately. Grid points with significant trends after adjusted for false positive are marked with a black "x".

CHAPTER 2

INDICATORS OF LAND SURFACE PHENOLOGY FROM REMOTE SENSING AND THE COMMUNITY LAND MODEL

Abstract

Large scale changes in the state of the land surface affect the circulation of the atmosphere and the structure and function of ecosystems alike. As global temperatures increase and regional climates change, the timing of key plant phenological events are likely to shift as well. Anticipating those changes requires the use of both observations of large-scale interannual phenological variability, as well as global climate model simulations with realistic land surface phenology routines. Here we evaluate a new suite of phenometrics designed to facilitate an "apples to apples" comparison between remote sensing products and climate model output. Specifically, we derive day-of-year (DOY) thresholds of leaf area index (LAI) from both remote sensing and output from the land surface component (the Community Land Model, or CLM) of the Community Earth System Model (CESM) forced by observational atmospheric variability during recent years. This systematic approach to comparing phenologically-relevant variables reveals broad consistency between the model and observations in terms of large-scale spatial gradients of LAI amplitudes and mean spring onset dates. However, appreciable differences are present in both LAI seasonal cycle and spring onset timing. For example, the model's seasonal amplitude of LAI and growing season length is much greater than observed, owing in part to the amplitude of the LAI cycle in the

subtropical and boreal regions. Likewise, phenological spring onset in the model occurs much later than observed, especially over evergreen and stress deciduous plant functional types. Further, while the more recent version of CLM (v5.0) exhibits seasonal mean LAI values that are in closer agreement with MODIS than its predecessor (CLM4.5), leaf phenology in CLM5.0 is in worse agreement with satellite data. Accordingly, phenology in CLM4.5 and CLM5.0 is fundamentally different from that seen in MODIS, and therefore any coupling between the land surface and the atmosphere that depends on vegetation state might not be fully captured by the existing generation of models. As a result, any future feedback of carbon, moisture, and energy that affect this coupling would be subject to sources of uncertainty originating in model phenology.

Introduction

Plant phenology—the response of vegetation to the seasonal cycle of climate—affects the coupling strength between the atmosphere and the land surface (e.g. Levis & Bonan, 2004), the structure and function of large-scale ecosystems, and the productivity of agricultural regions. It also impacts large scale bird migrations, insect and pest outburst, and human health.

In mid and high latitude regions, where ecosystems experience a prolonged phase of senescence, phenology plays a critical role in determining productivity and therefore the terrestrial carbon budget (e.g. Morisette et al., 2009; Richardson et al., 2009, 2010). As large-scale phenology is most sensitive to climate variability, future

changes in the climate system can alter ecosystem structure and functions as well as the terrestrial carbon cycle dramatically through changing the phenology. For instance, warmer average global temperatures could favor earlier spring onset and longer growing seasons, and hence a larger terrestrial carbon sink. However, the earlier springs and hotter summers of the future could also impose new stresses, including droughts as well as increases in wildfires and destructive insect outbreaks (Guillevic et al., 2002; Peñuelas & Filella, 2009). Together, these impacts will fundamentally affect the total storage of carbon on land.

Characterizing spring onset across the Northern hemisphere--where the largest annual variations due to the large continental land masses in the mid-latitudes--requires information from remote sensing. Furthermore, land surface phenology exhibits considerable year-to-year variability (Richardson et al., 2013; White et al., 2009), and characterizing those fluctuations accurately across space and through time requires multi-year large-scale observations of the ecosystems. Long-lived, high-resolution, and consistent products like MODIS are therefore essential tools for documenting and describing spring onset variations at large scales during the recent historical period.

In addition to remote sensing, land surface models (LSMs) provide insight into the historical coupled land-atmosphere processes that govern the fluxes of water, carbon, and energy through the climate system. Because plants phenology is highly variable across space and through time (White et al., 2009), simulating spring phenology prognostically and accurately is important for modelling future changes in terrestrial ecosystems, land-atmosphere interactions, and the earth system. However,

not all Global Circulation Models (GCMs) in either Coupled Model Intercomparison Project (CMIP) Phase 5 or CMIP6 include LSMs with prognostic phenology. Accordingly, the skill of LSMs in simulating spring onset is yet to be comprehensively evaluated at the global, or at least hemispheric, scales that will be most critical for determining land-atmosphere climate interactions now and into the future. Although a few recent papers have examined site level and large-scale annual cycles of LAI and NPP and found large disagreements between model simulations and observations (e.g. Richardson et al., 2012; Mahowald et al., 2016; Scholze et al., 2017; Klosterman et al., 2018), these studies have tended to focus on small scales (and hence a restricted number of plant functional types) or monthly averages. Moreover, LSM output from GCMs is typically not archived at sufficiently high temporal resolution to compare *day of year* metrics of spring onset with remote sensing products.

In this study, we develop a suite of indices that can be used to describe LSM phenology in a way that is comparable to land surface phenology in remote sensing. We then compared simulations from CLM with MODIS-derived land surface phenology over the Northern Hemisphere. Essentially, we are interested in developing and applying metrics that will reliably characterize the *day of year* (DOY) when various thresholds of spring green-up are crossed. These metrics should accordingly be easily interpretable and meaningful when computed from remote sensing, LSMs forced with historical observations, and fully coupled GCMs with LSMs responding to, and interacting with, a free running atmosphere. This approach therefore represents a novel framework for evaluating land surface phenology vegetation parameterizations and their response to atmospheric forcing.

Data & methods

Remote Sensing LAI data

The indices of primary interest here are the 25%, 50%, and 75% thresholds of dynamical range of annual LAI (maximum LAI minus minimum LAI of each year) computed from LSM and remote sensing data (Figure 1). Our remote sensing data originates from the MODIS TERRA MOD15A2H.v006 (Myneni et al., 2015) LAI product, which itself is based on NDVI and is published at 500m spatial resolution for each eight day time interval. To compare this data to the output from the two LSMs we use-the Community Land Model version 4.5 and 5 (CLM4.5 and CLM5.0)-we aggregate the raw LAI to the CLM finite-volume grid (which has an approximate 1^{o} x 1^{o} lat/lon spatial resolution) through the following procedure. First, all "good quality" data points (e.g., MODIS QA flag = 0) within a given CLM grid cell are averaged together to produce a 1^{o} by 1^{o} product with eight day temporal resolution. Next, a smoothing spline is fit to each time series of the 1^{o} grid cell average for each year, then used to interpolate the data to daily time steps. While the details of the spline fit is somewhat sensitive to the smoothing parameter, we did not find our results to be particularly sensitive to the parameter choices we have employed here.

Land surface model details

The community land model (CLM) is the land component of the community earth system model (CESM). CLM simulates comprehensive biogeophysical, biogeochemical, and hydrological processes at the land surface, permitting it to represent land-atmosphere fluxes of water, carbon, and energy (Oleson et al., 2013;

Lawrence et al., 2018). It may be run in a "coupled" configuration, in which both the atmospheric component of the CESM framework (the community atmosphere model, CAM) and CLM exchange fluxes. Or the land model can be forced with historical observational data, so that the coupled interactions are suppressed and the model's phenology (among many other processes) is determined by boundary conditions during the instrumental era of interest. Running CLM under this configuration for the historical period therefore requires a combination of gridded instrumental data products and reanalysis output to supply the requisite surface radiation, temperature, wind, humidity, and other fields.

The phenology subroutine in CLM governs carbon and nitrogen fluxes for leaf development and litter fall for natural vegetation. It also influences biogeophysical processes such as photosynthesis and canopy hydrology indirectly through modifying leaf area index (LAI). Currently, the 14 natural plant functional types (PFTs) are divided into three phenology PFTs (Table 1). Distribution and area weight of each phenology PFT are shown in Figure 2. While evergreen phenology PFT has a fixed background litter fall rate and no seasonality specified by the phenology subroutine, deciduous phenology is controlled by different environmental factors (Oleson et al., 2013; Lawrence et al., 2018), that is, onset of seasonal deciduous PFTs are triggered by growing degree day thresholds while stress deciduous PFTs start growing only after growing degree day criteria following a chilling requirement, soil water potential threshold, and precipitation requirements are all met. Onset is set to a fixed 30-day window although stress deciduous PFTs can have multiple growing seasons within one year or a long growing season and no dormancy when conditions are favorable.

Due to the model structure of CLM, all area that is occupied by natural vegetation within one grid cell, regardless of their PFT type or phenology PFT type, have the same atmosphere forcing and feedback to the atmosphere and underlying soil as one column. Figure 3 exhibits the annual cycle of LAI for each PFT at the same grid point (i.e. forced by the same atmosphere and soil conditions). Therefore, CLM LAI represents the average of multiple PFTs that are exposed to the exact same climate, whereas LAI in MODIS is the average over multiple land cover types which may have geographical differences and varying microclimates.

Although interannual variability of the start of spring can be as large as 60 days, the trend of spring onset over the past few decades is relatively small, i.e. several days per decade, therefore, to accurately characterize spring onset in both CLM and MODIS, we need daily LAI values from both. CLM by default only outputs monthly total leaf area index (TLAI) history files, therefore, we rerun CLM4.5 with CRUNCEP (Viovy, 2018; as used in Wang et al., 2014) forcing and CLM5.0 with both CRUNCEP and GSWP3 (Müller Schmied et al., 2016) forcing and output daily TLAI and net primary production (NPP) values both as a grid cell average and for each PFT.

Experimental design

Here we run two versions of CLM (4.5 and 5) with two different historical forcing datasets: CRUNCEP and GSPW3. The details of the individual forcings are described elsewhere (e.g., Viovy, 2018; Wang et al., 2014; Muller Schmied et al., 2016; http://hydro.iis.u-tokyo.ac.jp/GSWP3/exp1.html#boundary-conditions). Briefly,

the CRUNCEP forcing was developed from the University of East Anglia's Climate Research Unit's (CRU) TS3.2 monthly data product to constrain most observational fields through 2009 and NCEP reanalysis to fill in the diurnal and daily variability. After 2009 (when the CRU TS3.2 data set ends), NCEP reanalysis data is used for all fields after being statistically adjusted so that its climatology matches that of CRU TS3.2, thus preventing any serious discontinuities in the CLM forcing. GSPW3 data is dynamically downscaled from the 20th Century Reanalysis (20CR, Compo et al., 2011) and corrected using observations.

Both historical forcing datasets (CRUNCEP and GSPW3) were used as boundary conditions to run CLM4.5 and CLM5.0 over the period from January 1 (day1) of 1970 through December 31 (day365) of 2014 for GSWP3 and of 2016 for CRUNCEP. However, for consistency with previous studies (e.g., Wang et al., 2014), we focus primarily on the CRUNCEP results when examining CLM4.5, and for forward compatibility with recent and planned CLM5.0 experiments (such as in LUMIP), we emphasize the GSWP3 results when discussing CLM5.0. Regardless, our results did not depend strongly on the historical forcing data for the regions and variables of interest here. We discarded the first 33 years for spin-up and used 2003-2014 for comparison due to the overlap between GSWP3 and MODIS.

Daily data from each grid point, PFT, and simulation were archived and used to compute the DOY metrics of interest here (see next section). Although we focus on the timing of LAI changes during spring at relatively coarse spatial resolution (by remote sensing standards), the 1^{o} x 1^{o} grid size is relatively standard for climate model simulations. Nevertheless, the process by which information is aggregated to this scale

from either CLM or MODIS is somewhat different. In the case of MODIS, LAI changes at the individual pixel level are averaged together to produce a single LAI value, whereas in CLM LAI changes from individual PFTs are aggregated. Since both CLM and the atmospheric forcing dataset operate at the same spatial scale, all PFTs within a given grid cell must therefore be forced with the same underlying meteorological data regardless of where those PFTs occur within that cell.

LAI-based indices from CLM and MODIS

We computed threshold-based DOY indices for each year of MODIS data from 2003 to 2017 and for CLM4.5 and CLM5.0 from 2000 to 2016 (CRUNCEP)/2014 (GSWP3) based on the annual dynamical range of LAI in each year for each dataset (Figure 1). These indices therefore represent the stage of leaf development or onset of plant growth from an ecosystem perspective. Note that although CLM has a fixed 30-day onset period, because carbon fluxes change with the remaining carbon in the storage pool, rate of LAI changes is still steeper around 50% of its annual dynamical range.

NPP difference and the carbon cycle

We computed annual net primary production difference (estimated using CLM NPP) between CLM simulations and MODIS as CLM NPP produced during difference in their peak growing season (defined by LAI above 75% of annual amplitude) between CLM and MODIS. That is, annual NPP difference is calculated as the mean CLM NPP during peak growing season of each year multiplied by the difference in peak growing season length between CLM and MODIS. These NPP

differences are then averaged across all years to characterize the potential influence of phenology simulations on terrestrial carbon cycle.

Results

Both LAI absolute values and the annual dynamical range has changed dramatically from CLM4.5 to CLM5.0 (Figure 4 and 5). Across CLM simulations, LAI values are too high in evergreen needleleaf forest dominated high latitude regions in spring and early summer months (April, May, and June) compared to MODIS (Figure 2-3). In CLM4.5, mean spring LAI can be as high as $10m^2/m^2$ in Southeast China and Southeast US, and higher than $5m^2/m^2$ across high latitudes regions and in Europe. In CLM5.0, these unrealistic high values have decreased dramatically, but are still higher than MODIS LAI values in the spring (Figure 3).

This geographical pattern of LAI values persists into the annual amplitude and dynamical range of LAI in CLM (Figure 4 and 5). For all CLM experiments, LAI annual range is larger than that in MODIS in most of Canada, Southeast US, most of Europe, South Russia, and East Asia. The magnitude also decreases in CLM5.0, but the spatial pattern is similar to that in CLM4.5 and MODIS (Figure 4). When compared to the annual amplitude in MODIS LAI, CLM4.5 exhibits higher LAI amplitude in polar regions, in the Mediterranean, in Southeast China, and in Southeast US, while the LAI range is lower in CLM4.5 around 60^{o}N. This difference persists in CLM5.0 with an even higher amplitude in the polar regions but a lower or even smaller annual range in Southeast Asia and Southeast US (Figure 5).

Start of spring dates exhibit similar spatial pattern in CLM to that in MODIS

(Figure 6 and 7). Across all dataset, DOY when LAI reaches its 50% annual dynamical range is later at higher latitudes or higher elevations, except for evergreen needleleaf forest and grassland dominated regions in Southwest and Northern North America and the Mediterranean. In MODIS, at the same latitude in the Northern Hemisphere, western coasts of the continents usually experience earlier leaf onset than the eastern coasts, while in CLM, western coasts of the continents are dominated by stress deciduous PFTs and experience later spring onset than in MODIS or the eastern coasts (Figure 6). Overall, the mean DOYs of CLM LAI 50% threshold at mid-to-high latitudes are close to those from MODIS, especially in CLM4.5 (Figure 7). However, large disagreement between CLM and MODIS start of spring dates is present around 60ºN, over the Rocky Mountain regions, in Southeast US, in the Mediterranean, and in Central Asia, where the difference can be larger than 60 days. Notably, locations dominated by evergreen PFTs in CLM tend to show a later spring than in MODIS, while places where stress deciduous occupies a large portion of the vegetation exhibits varying leaf onset behavior when compared to MODIS phenology (Figure 2, 7 and Table 2).

Interannual variability of $LAI_{50\%}$ DOY shows largest agreement between CLM and MODIS in high latitude regions over Eurasia and North America (Figure 8). In CLM4.5, mid-latitude regions in North America and Central Asia also exhibit large and significant correlation with MODIS. In CLM5, although the absolute magnitude of LAI values is closer to that displayed in MODIS, in low- and mid-latitude regions, correlations between $LAI_{50\%}$ DOY from MODIS and CLM are low and not statistically significant, suggesting that interannual variability of the start of spring

may disagree within these two datasets (Figure 8).

To evaluate the potential terrestrial carbon pool or peak growing season length, we also investigated the seasonal window of "peak growth," as indicated by LAI values over 75% of the annual dynamical range (Figure 9-10). Across the Northern Hemisphere, peak growing season length decreases northward, but ecosystems with a more temperature dominant phenology, i.e. seasonal deciduous plant functional types, exhibit shorter peak growing season length than evergreen PFTs or PFTs dominated by both temperature and soil moisture at similar latitudes (Figure 9). In general, CLM has a longer peak growing season than MODIS, especially in mid-to-high latitude regions where stress deciduous phenology dominates, that is, over the great plains in North America, in the Mediterranean, in South Russia, and over the Tibetan Plateau. Notably, although evergreen needleleaf forest north of 60^{o}N experience earlier start of spring in CLM than in MODIS (Figure 9), their peak growing season length is close to or only a little longer in CLM than that in MODIS, suggesting the seasonal cycle might have shifted between the two datasets (Figure 10).

We also calculated the productivity difference in CLM simulations that is due to the longer growing season to estimate the impact of CLM phenology routine on terrestrial carbon cycle (Figure 11 and 14). Over the Northern Hemisphere, NPP is most overestimated in CLM at high-latitude regions, in Midwest regions in the US, in Northern Europe, and in East Asia. Compared to CLM4.5, CLM5.0 improves the overestimation of NPP over mid-latitude regions in East Asia, Europe, and the US, but simulates larger annual NPP in high-latitude regions. This pattern remains when

switching to GSWP3 forcing from CRUNCEP, with small NPP increase in Northern Canada and Alaska (Figure 11). Because total productivity is lower at higher latitudes, the fraction of NPP difference over total CLM NPP is high across the Northern Hemisphere, except for a few evergreen forest and grassland dominated locations (Figure 14).

Discussion

Here we presented a suite of indicators that characterize phenology and seasonal cycle in leaf area index from a land surface phenology perspective. Our results reveal fundamental differences between plant phenology in the community land model and satellite remote sensing from MODIS. Earlier studies have documented a difference in LAI in CLM as compared with remote sensing (e.g. Lawrence et al., 2011; Lawrence et al., submitted). Here we found that this disagreement between CLM and MODIS is strongest in evergreen forest and grassland dominant boreal and temperate phenology types (Figure 2, 5, 10). Although the differences in annual mean LAI range aren't as large in evergreen-dominant regions (Figure 2A and 5), they are still present and mostly negative (Figure 5 and 10).

A variety of reasons may be causing these differences. One possible trigger is a mismatch between CLM PFTs and MODIS land cover types due to both land cover change and the coarse resolution of an earth system model. Another reason can be the different procedures of how leaf area index is generated from MODIS products and CLM simulations. That is, MODIS LAI is calculated based on reflectance and can

have an unrealistic large annual dynamical range while evergreen phenology in land surface models is usually designed to have a flattened annual cycle (Kim et al., 2015; Lawrence & Chase, 2010). Therefore, differences between CLM and MODIS LAI in evergreen-dominant boreal regions likely stem, at least in part, from observational uncertainties in MODIS, which tends to overestimate the magnitude of the winter dormancy signal due to snow cover as MODIS LAI is based on NDVI (Myneni et al., 2015). Meanwhile, the phenology routines governing evergreen LAI in CLM are flattened as there is no onset and offset trigger and growth can happen all year around (as shown by the evergreen PFTs in Figure 12 and 13). However, despite these two reasons, there are still potential problems in the phenology subroutines in CLM that is causing the differences between land surface phenology observations and the modelled phenology. For instance, temperate and boreal evergreen forests can be over-productive and exhibiting a low intra-annual change of LAI, while grassland at mid-to-low latitude regions experiences multiple growing season within one calendar year (Figure 13).

Despite the disagreement between LAI values and annual ranges, CLM can largely reproduce Northern Hemispheric scale patterns of spring onset in remote sensing at mid-to-high latitudes (Figure 7-8). However, CLM phenology generally happens later than MODIS at mid-to-high latitude regions, especially in high-latitude regions where land cover is dominated by evergreen needleleaf trees and in arid mid-latitude regions (Figure 7). This can be partially due to calibrating deciduous phenology spring onset dates with remote sensing records and the 30-day fixed onset period after that (White et al., 1997; Lawrence et al., 2011) as well as the lack of

seasonality in evergreen phenology routine in CLM. Several studies have examined or aimed at improving CLM phenology for different phenology routines (e.g. Dahlin et al., 2015; Chen et al., 2016), here we found that large difference remains in annual cycle and phenology between CLM LAI and MODIS LAI. Although spring onset timing is later in CLM than in MODIS at high latitudes, interannual variability of LAI thresholds also shows highest correlation in high latitude regions (Figure 8). In addition, compared to CLM4.5, although CLM5.0 has a more realistic representation of LAI values and annual range, CLM5.0 also displays a larger difference in mean DOY of LAI thresholds and weaker correlation when compared against MODIS LAI, possibly due to changes in evergreen phenology in temperate and boreal regions. Therefore, when evaluating LSMs, it is important to evaluate phenology/seasonal cycle as well as absolute values of LAI.

Disagreement in phenology can result in large differences in productivity and carbon cycle estimation. Difference between peak growing season length averages around 50 days each year, resulting in a large difference in terrestrial net primary productivity and carbon cycle (Figure 10, 11, 14). Over the Northern Hemisphere, total difference in NPP due to phenology adds up to 6.69 ± 2.43 Pg (one standard deviation) carbon per year in CLM5.0 and 8.78 ± 4.35 Pg carbon per year in CLM4.5, accounting for more than 10% of total NH NPP estimation (Li et al., 2017). Previous studies also showed that phenological differences in land surface models and observations can result in large disagreement in terrestrial carbon cycle (Kucharik et al., 2006; Chiang and Brown, 2007; Migliavacca et al., 2012; Richardson et al., 2012, 2013). This potential overestimation of productivity also increases the uncertainty for

future climate predictions, as terrestrial carbon sequestration can influence atmosphere CO2 concentration and therefore energy balance and biogeochemical processes. Therefore, it is important to understand the difference between CLM or other LSM phenology and land surface phenology observations.

Conclusion

Spring onset indicators based on LAI thresholds are critical for identifying sources of mismatch/bias in timing that would be otherwise hard to see in seasonal mean values at monthly scales. Our results revealed large differences in start of spring dates between MODIS and CLM as well as between CLM4.5 and CLM5.0. Across the Northern Hemisphere, CLM generally simulates later spring onset timing and longer growing season than presented in MODIS. Although CLM5.0 provides better representation of LAI absolute value and seasonal amplitude than CLM4.5, the start of spring timing shows less agreement between CLM5.0 and MODIS. However, because of the relatively short temporal overlap between the forcing dataset and MODIS, correlations are mostly not statistically significant except for higher latitude regions. These findings suggest that there are fundamental differences in phenology derived from MODIS and CLM, especially for evergreen and grassland plant functional types in the Northern Hemisphere. Therefore, the coupling between the land surface and the atmosphere may not be fully captured by the existing generation of models and any future feedback of carbon, moisture, and energy that affect this coupling would be subject to sources of uncertainty originating in model phenology. As a result, refining

phenology in CLM needs to be a priority so that the model can fully capture variability in terrestrial carbon cycles and changes in land-atmospheric interactions.

REFERENCES

Chen, M., Melaas, E. K., Gray, J. M., Friedl, M. A., & Richardson, A. D. (2016). A new seasonal-deciduous spring phenology submodel in the Community Land Model 4.5: impacts on carbon and water cycling under future climate scenarios. *Global change biology*, *22*(11), 3675-3688.

Chiang, J. M., & Brown, K. J. (2007). Improving the budburst phenology subroutine in the forest carbon model PnET. *ecological modelling*, *205*(3-4), 515-526.

Compo, G. P., Whitaker, J. S., Sardeshmukh, P. D., Matsui, N., Allan, R. J., Yin, X., … Bessemoulin, P. (2011). The twentieth century reanalysis project. *Quarterly Journal of the Royal Meteorological Society*, *137*(654), 1–28.

Dahlin, K. M., Fisher, R. A., & Lawrence, P. J. (2015). Environmental drivers of drought deciduous phenology in the Community Land Model. *Biogeosciences*, *12*(16), 5061–5074.

Guillevic, P., Koster, R. D., Suarez, M. J., Bounoua, L., Collatz, G. J., Los, S. O., & Mahanama, S. P. P. (2002). Influence of the interannual variability of vegetation on the surface energy balance—A global sensitivity study. Journal of Hydrometeorology, 3(6), 617-629.

Kim, Y., Moorcroft, P. R., Aleinov, I., Puma, M. J., & Kiang, N. Y. (2015). Variability of phenology and fluxes of water and carbon with observed and simulated soil moisture in the Ent Terrestrial Biosphere Model (Ent TBM version 1.0.1.0.0). *Geoscientific Model Development*, *8*(12), 3837–3865. https://doi.org/10.5194/gmd-8-3837-2015

Klosterman, S., Hufkens, K., & Richardson, A. D. (2018). Later springs green-up faster: the relation between onset and completion of green-up in deciduous forests of North America. International journal of biometeorology, 62(9), 1645-1655.

Kucharik, C. J., Barford, C. C., El Maayar, M., Wofsy, S. C., Monson, R. K., & Baldocchi, D. D. (2006). A multiyear evaluation of a Dynamic Global Vegetation Model at three AmeriFlux forest sites: Vegetation structure, phenology, soil temperature, and CO2 and H2O vapor exchange. *Ecological Modelling*, *196*(1-2), 1-31.

Lawrence, P. J., & Chase, T. N. (2010). Investigating the climate impacts of global land cover change in the community climate system model. *International Journal of Climatology*, *30*(13), 2066–2087.

Lawrence, D.M. R.A. Fisher, C.D. Koven, K.W. Oleson, S.C. Swenson, G. Bonan, N. Collier, B. Ghimire, L. van Kampenhout, D. Kennedy, E. Kluzek, P.J. Lawrence, F. Li, H. Li, D. Lombardozzi, W.J. Riley, W.J. Sacks, M. Shi, M. Vertenstein, W.R. Wieder,, C. Xu, A.A. Ali, A.M. Badger, G. Bisht, M.A. Brunke, S.P. Burns,, J. Buzan, M. Clark, A. Craig, K. Dahlin, B. Drewniak, J.B. Fisher, M. Flanner, A.M. Fox, P. Gentine, F.Hoffman, G. Keppel-Aleks, R., Knox, S.

Kumar, J. Lenaerts, L.R. Leung, W.H. Lipscomb, Y. Lu, A., Pandey, J.D. Pelletier, J. Perket,, J.T. Randerson, D.M. Ricciuto, B.M., Sanderson, A. Slater, Z.M. Subin, J. Tang, R.Q. Thomas, M. Val Martin, and X. Zeng, 2018: The Community Land Model version 5: Description of new features, benchmarking, and impact of forcing uncertainty. Submitted to J. Adv. Model. Earth Syst.

Levis, S., & Bonan, G. B. (2004). Simulating springtime temperature patterns in the community atmosphere model coupled to the community land model using prognostic leaf area. Journal of Climate, 17(23), 4531-4540.

Li, P., Peng, C., Wang, M., Li, W., Zhao, P., Wang, K., … Zhu, Q. (2017). Quantification of the response of global terrestrial net primary production to multifactor global change. *Ecological Indicators*, *76*, 245–255.

Mahowald, N., Lo, F., Zheng, Y., Harrison, L., Funk, C., Lombardozzi, D., & Goodale, C. (2016). Projections of leaf area index in earth system models. *Earth System Dynamics*, *7*(1), 211–229.

Migliavacca, M., Sonnentag, O., Keenan, T. F., Cescatti, A., O'keefe, J., & Richardson, A. D. (2012). On the uncertainty of phenological responses to climate change, and implications for a terrestrial biosphere model. *Biogeosciences*, *9*(6), 2063-2083.

Morisette, J. T., Richardson, A. D., Knapp, A. K., Fisher, J. I., Graham, E. A., Abatzoglou, J., … Liang, L. (2009). Tracking the rhythm of the seasons in the face of global change: phenological research in the 21st century. *Frontiers in Ecology and the Environment*, *7*(5), 253–260. https://doi.org/10.1890/070217

Müller Schmied, H., Adam, L., Eisner, S., Fink, G., Flörke, M., Kim, H., … Riedel, C. (2016). Impact of climate forcing uncertainty and human water use on global and continental water balance components. *Proceedings of the International Association of Hydrological Sciences*, *374*, 53–62.

Myneni, R., Knyazikhin, Y., & Park, T. (2015). MOD15A2H MODIS/terra leaf area index/FPAR 8-day L4 global 500 m SIN grid V006. *NASA EOSDIS Land Processes DAAC*.

Oleson, K. W., Lawrence, D. M., Bonan, G. B., Drewniak, B., Huang, M., Charles, D., … Sacks, W. (2013). CLM 4.5 NCAR Technical Note, (July). https://doi.org/10.1007/s11538-011-9690-0

Peñuelas, J., & Filella, I. (2009). Phenology feedbacks on climate change. Science, 324(5929), 887-888.

Richardson, A. D., Anderson, R. S., Arain, M. A., Barr, A. G., Bohrer, G., Chen, G., … Xue, Y. (2012). Terrestrial biosphere models need better representation of vegetation phenology: Results from the North American Carbon Program Site Synthesis. *Global Change Biology*, *18*(2), 566–584. https://doi.org/10.1111/j.1365-2486.2011.02562.x

Richardson, A. D., Andy Black, T., Ciais, P., Delbart, N., Friedl, M. A., Gobron, N., … Luyssaert, S. (2010). Influence of spring and autumn phenological transitions

on forest ecosystem productivity. *Philosophical Transactions of the Royal Society B: Biological Sciences*, *365*(1555), 3227–3246.

Richardson, A. D., Hollinger, D. Y., Dail, D. B., Lee, J. T., Munger, J. W., & O'keefe, J. (2009). Influence of spring phenology on seasonal and annual carbon balance in two contrasting New England forests. *Tree Physiology*, *29*(3), 321–331. https://doi.org/10.1093/treephys/tpn040

Richardson, A. D., Keenan, T. F., Migliavacca, M., Ryu, Y., Sonnentag, O., & Toomey, M. (2013). Climate change, phenology, and phenological control of vegetation feedbacks to the climate system. *Agricultural and Forest Meteorology*, *169*, 156–173. https://doi.org/10.1016/j.agrformet.2012.09.012

Scholze, M., Buchwitz, M., Dorigo, W., Guanter, L., & Quegan, S. (2017). Reviews and syntheses: Systematic Earth observations for use in terrestrial carbon cycle data assimilation systems. *Biogeosciences*, *14*(14), 3401–3429. https://doi.org/10.5194/bg-14-3401-2017

Viovy, N. (2018). CRUNCEP Version 7–Atmospheric Forcing Data for the Community Land Model. *Research Data Archive at the National Center for Atmospheric Research, Computational and Information Systems Laboratory, Boulder CO, USA*.

Wang, X., Piao, S., Ciais, P., Friedlingstein, P., Myneni, R. B., Cox, P., … Wang, T. (2014). A two-fold increase of carbon cycle sensitivity to tropical temperature variations. *Nature*, *506*(7487), 212.

White, M. A., Thornton, P. E., & Running, S. W. (1997). A continental phenology model for monitoring vegetation responses to interannual climatic variability. *Global biogeochemical cycles*, *11*(2), 217-234.

White, M. A., De Beurs, K. M., Didan, K., Inouye, D. W., Richardson, A. D., Jensen, O. P., … Lauenroth, W. K. (2009). Intercomparison, interpretation, and assessment of spring phenology in North America estimated from remote sensing for 1982–2006. *Global Change Biology*, *15*(10), 2335–2359. https://doi.org/10.1111/j.1365-2486.2009.01910.x

TABLES

Table 1. Summary information for the three different phenology routines used in CLM (left column) and the PFTs that invoke them (right).

Pheno PFT	PFT
evergreen	needleleaf evergreen temperate tree, needleleaf evergreen boreal tree, broadleaf evergreen tropical tree, broadleaf evergreen temperate tree, broadleaf evergreen shrub,
stress deciduous	broadleaf deciduous tropical tree, broadleaf deciduous temperate shrub, c3 non-arctic grass, c4 grass, c3 crop/crop1, c3 irrigated/crop2,
seasonal deciduous	needleleaf deciduous boreal tree, broadleaf deciduous temperate tree, broadleaf deciduous boreal tree, broadleaf deciduous boreal shrub, c3 arctic grass,

Table 2. Summary of differences in land cover type, LAI value, and LAI seasonality between varying geographical locations

	Evergreen needleleaf forest across 60°N	Mediterranean	Central Asia (near Kazakhstan)	Southeast China	Southeast US
Dominant phenology PFT type	Evergreen	Stress deciduous	Stress deciduous	Stress deciduous	Stress deciduous, seasonal deciduous, evergreen
Mean annual LAI range	High	High	Low	High	High
Difference in annual LAI range between MODIS and CLM	Lower in CLM	Higher in CLM	Near 0	Higher in CLM4.5 but lower in CLM5	Higher in CLM4.5 but lower in CLM5
Difference in mean $LAI_{25\%}$ DOY between MODIS and CLM	Later in CLM	Earlier in CLM	Later in CLM	Earlier in CLM4.5 but close in CLM5	Mostly earlier in CLM
Correlation of $LAI_{25\%}$ DOYs	Relatively high in CLM4.5 but low or no correlation in CLM5	Low	Low	Low	Low

FIGURES

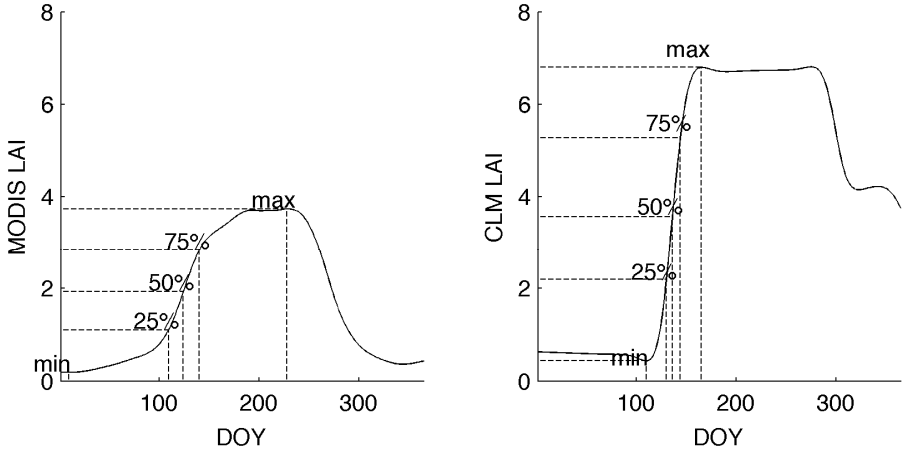

Figure 1. Schematic diagram of how our DOY threshold-based indices are computed from remote sensing (left) and CLM output (right).

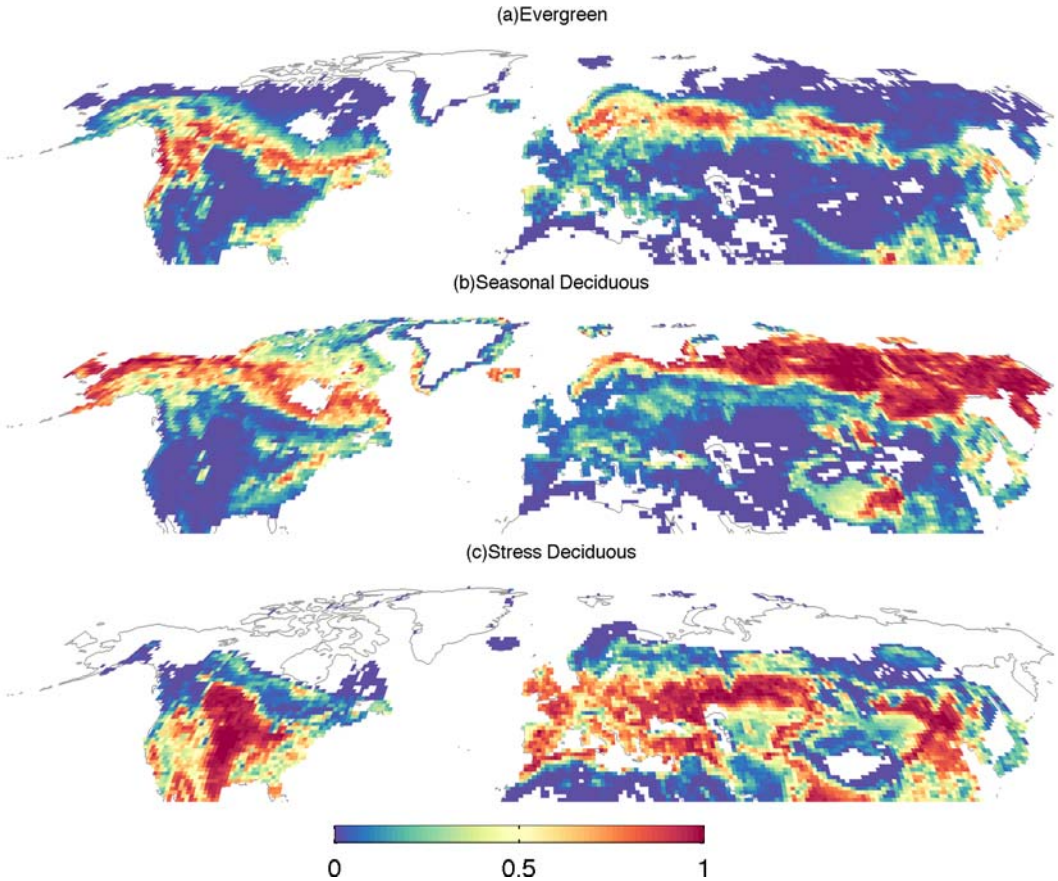

Figure 2. Maps showing the area weight of different phenology plant functional type in CLM5.0 Year 2000 initial condition land surface input dataset

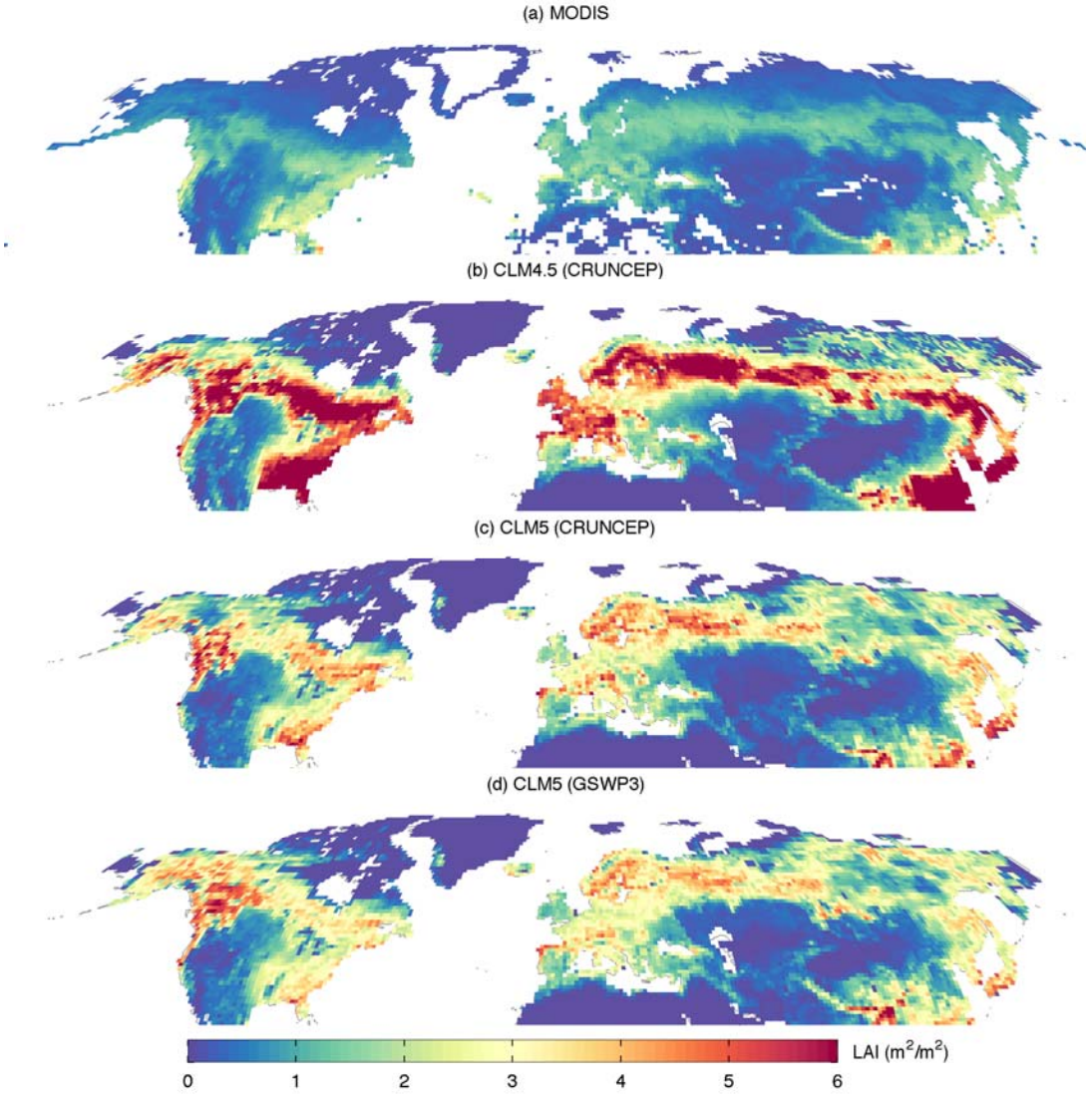

Figure 3. Mean spring (April, May, and June) LAI values from (A) MODIS, (B) CLM4.5 with CRUNCEP, (C) CLM5.0 with CRUNCEP, and (D) CLM5.0 with GSWP3 averaged between 2003-2014

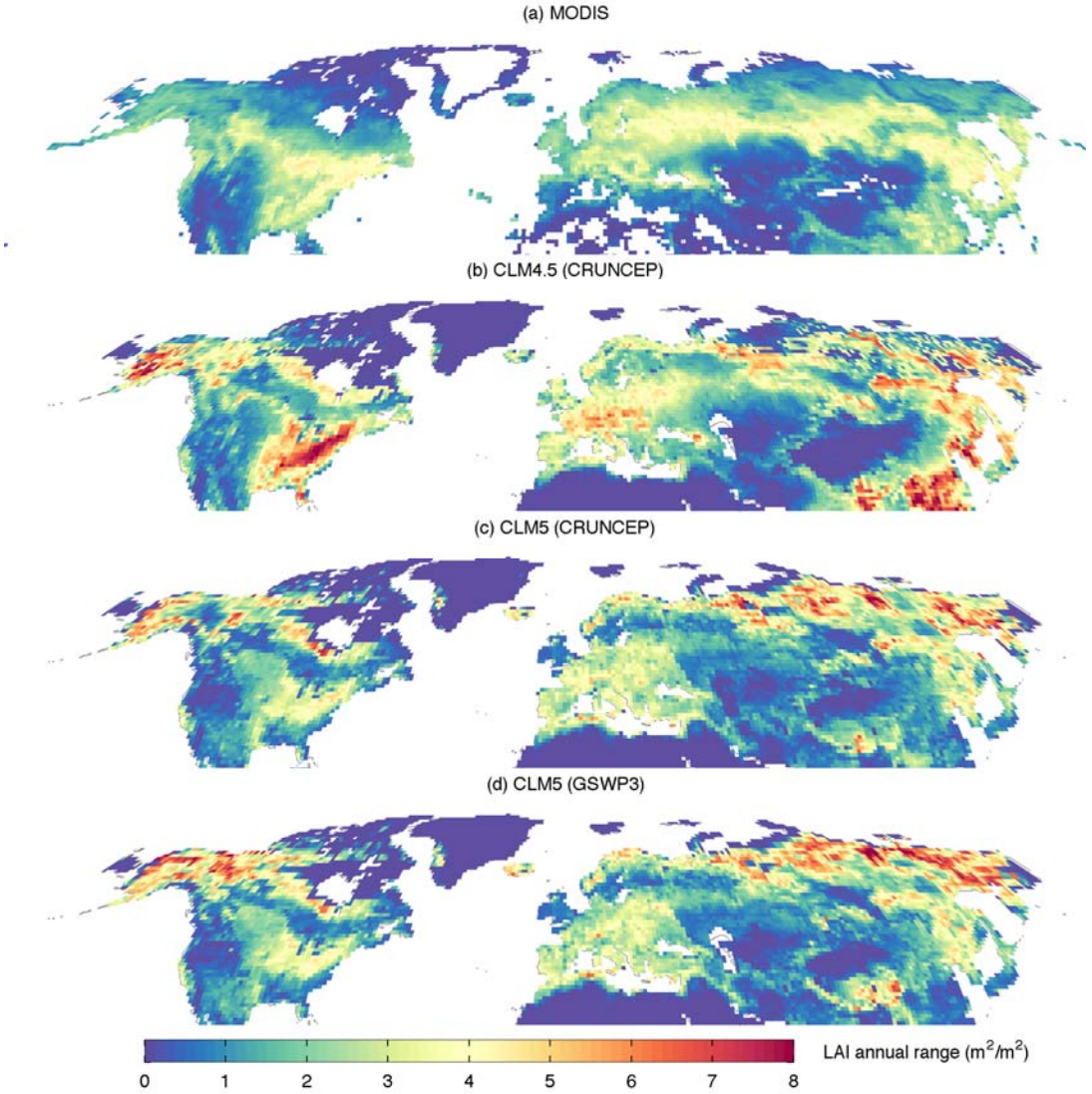

Figure 4. Mean annual range of LAI (annual maximum minus annual minimum) from (A) MODIS, (B) CLM4.5 with CRUNCEP, (C) CLM5.0 with CRUNCEP, and (D) CLM5.0 with GSWP3 averaged between 2003-2014

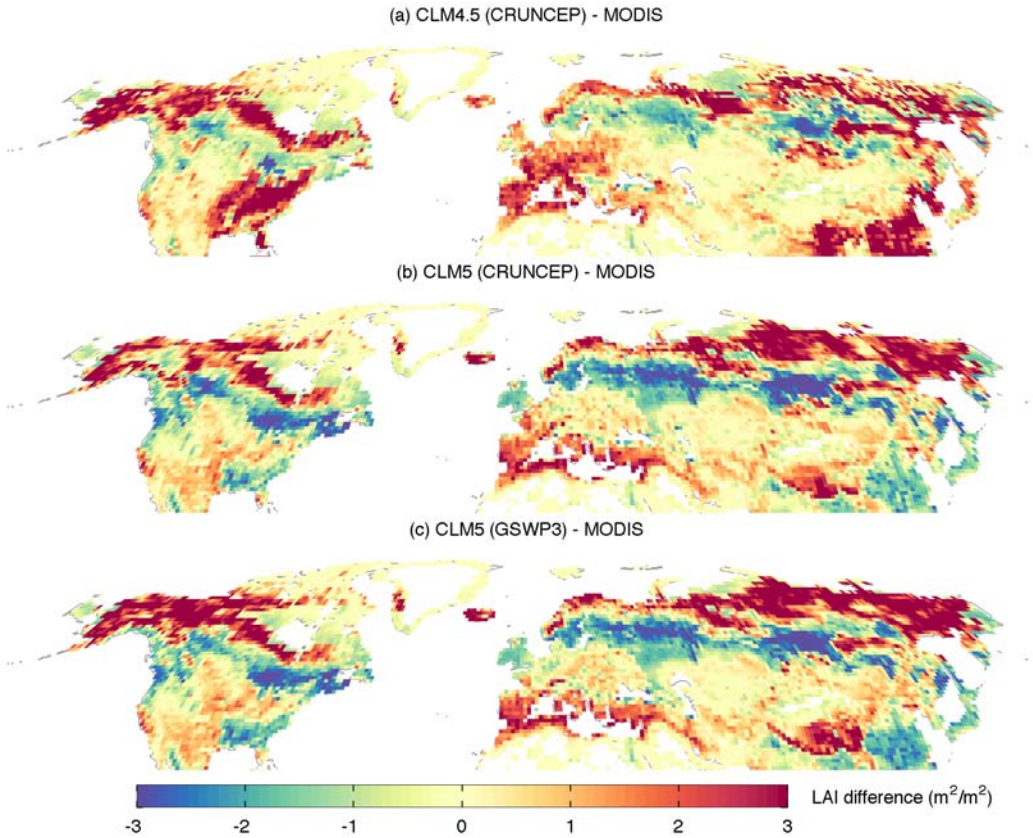

Figure 5. Difference in mean annual range of LAI (annual maximum minus annual minimum) between (A) CLM4.5 with CRUNCEP, (B) CLM5.0 with CRUNCEP, and (C) CLM5.0 with GSWP3 and MODIS, averaged between 2003-2014

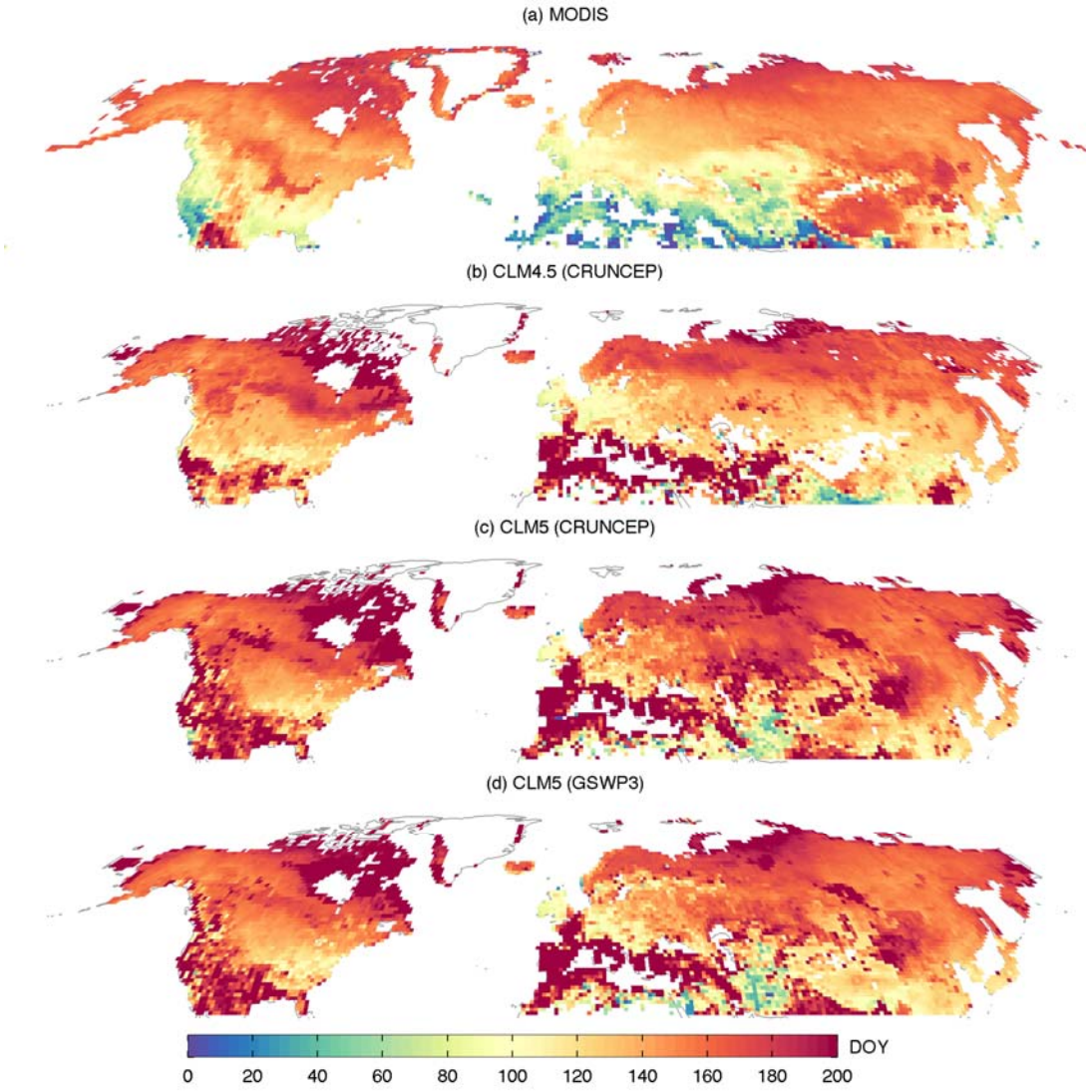

Figure 6. Mean DOY when LAI crosses 50% threshold of annual dynamical range from (A) MODIS, (B) CLM4.5 with CRUNCEP, (C) CLM5.0 with CRUNCEP, and (D) CLM5.0 with GSWP3, averaged between 2003-2014

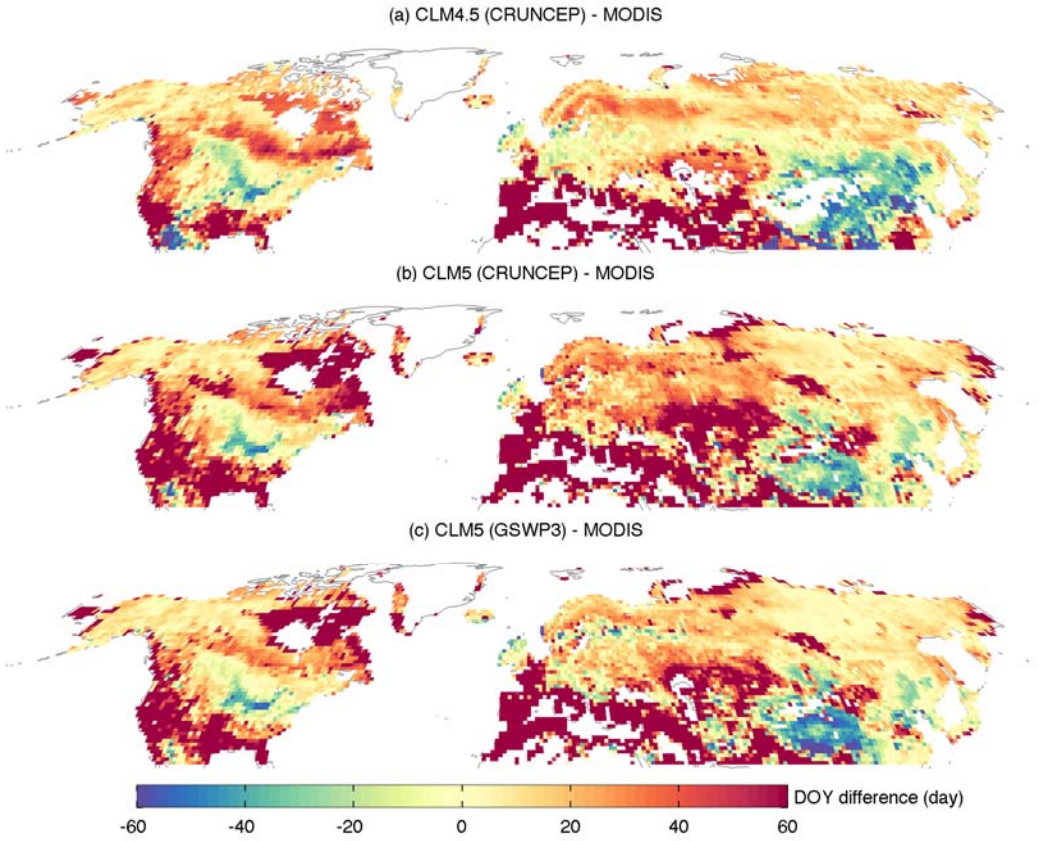

Figure 7. Difference between mean DOY when LAI reaches 50% threshold in (A) CLM4.5 with CRUNCEP, (B) CLM5.0 with CRUNCEP, and (C) CLM5.0 with GSWP3 and in MODIS, averaged between 2003-2014.

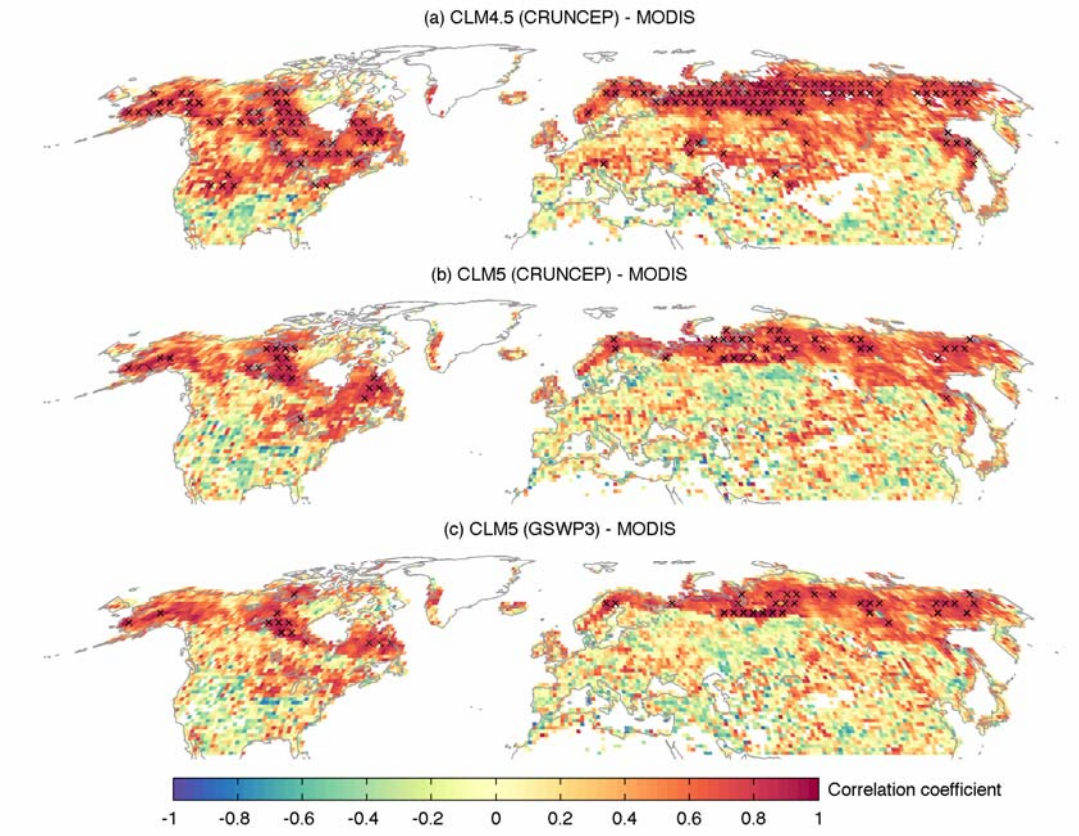

Figure 8. Correlations between (A) CLM4.5 with CRUNCEP, (B) CLM5.0 with CRUNCEP, and (C) CLM5.0 with GSWP3 with MODIS LAI-based DOYs at 50% threshold of annual dynamical range during 2003-2016.

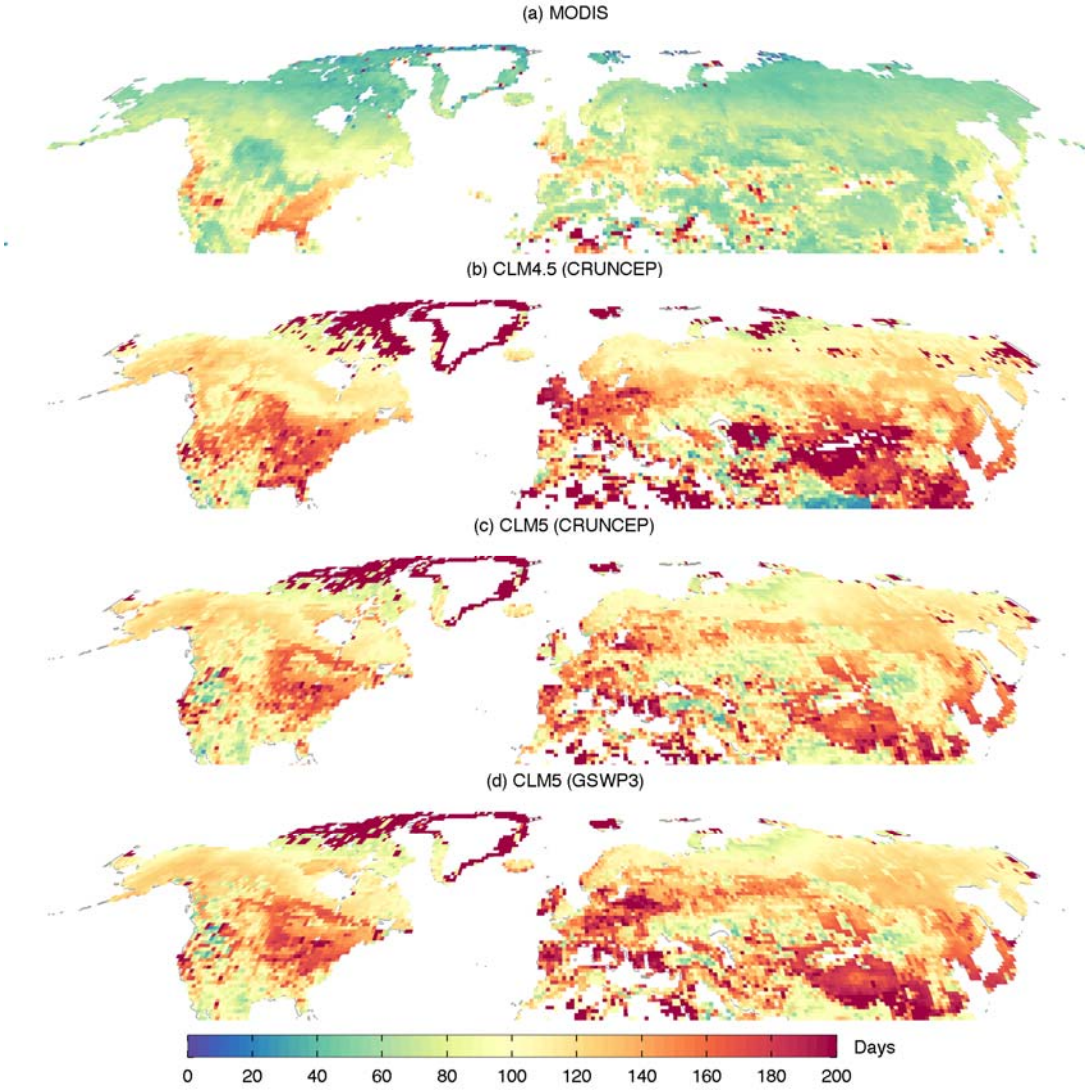

Figure 9. Peak growing season length as indicated by LAI 75% threshold from (A) MODIS, (B) CLM4.5 with CRUNCEP, (C) CLM5.0 with CRUNCEP, and (D) CLM5.0 with GSWP3, averaged between 2003-2014

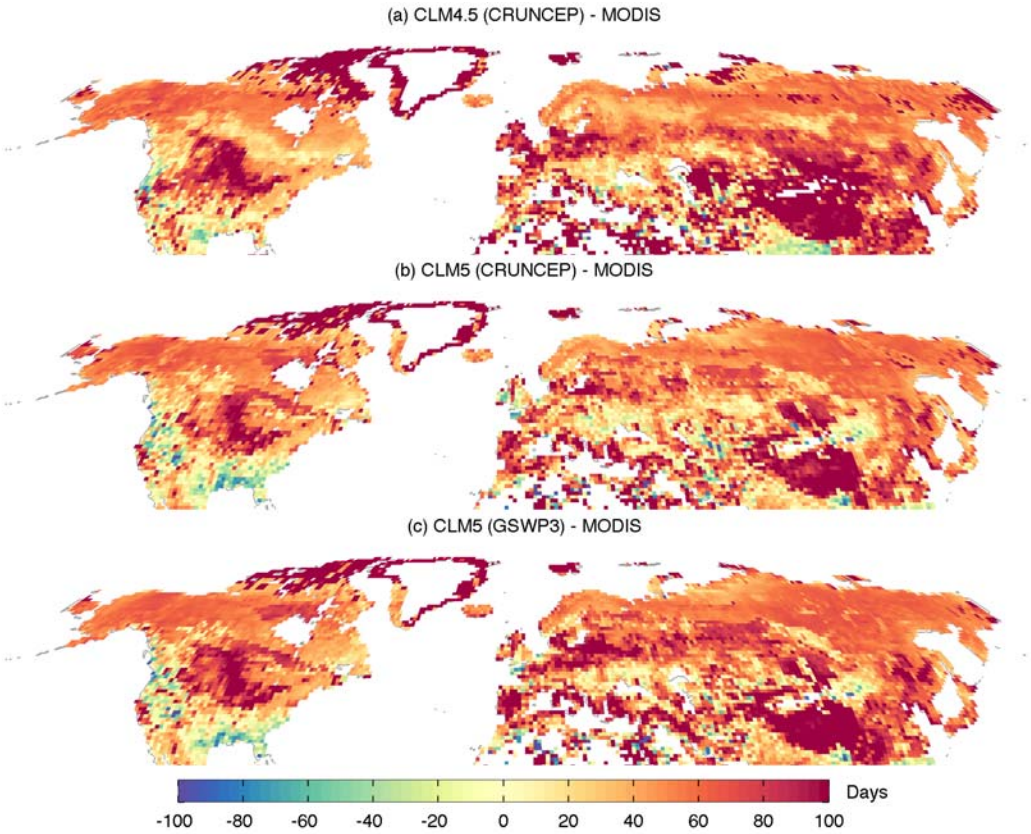

Figure 10. Difference in peak growing season length as indicated by LAI 75% threshold between (A) CLM4.5 with CRUNCEP, (B) CLM5.0 with CRUNCEP, and (C) CLM5.0 with GSWP3 and MODIS, averaged between 2003-2014

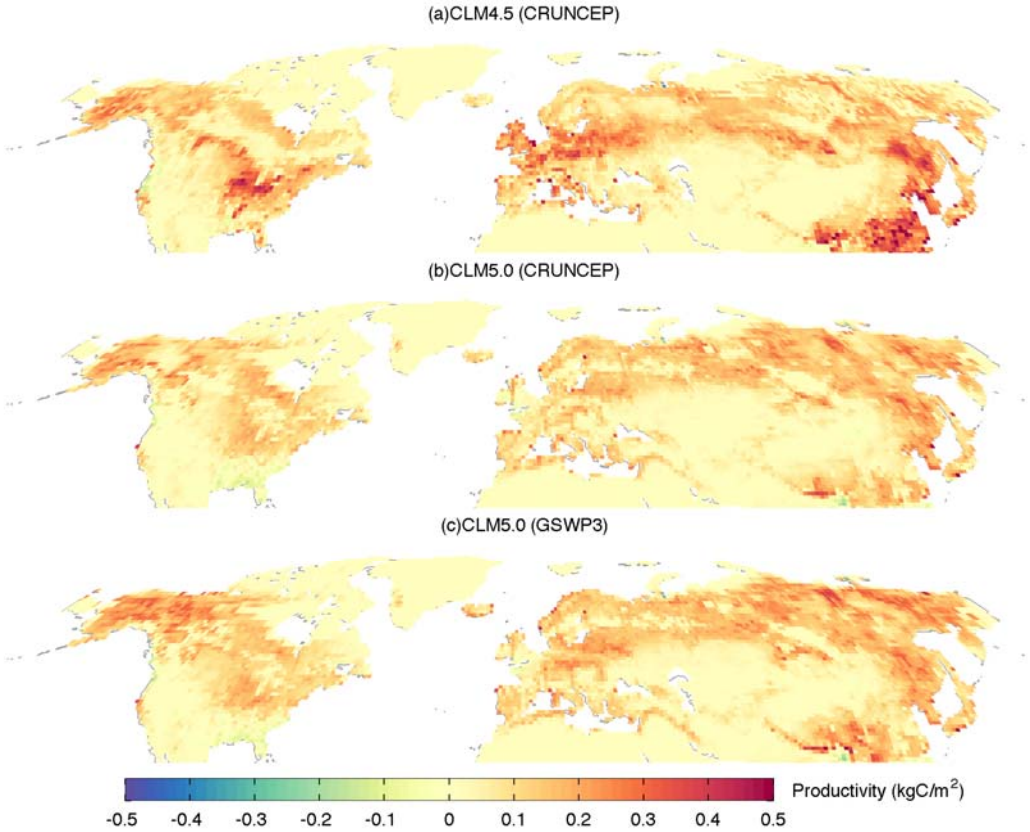

Figure 11. Annual net primary production (NPP) produced during the difference between MODIS peak growing season as indicated by LAI 75% threshold and that of (A) CLM4.5 with CRUNCEP, (B) CLM5.0 with CRUNCEP, and (C) CLM5.0 with GSWP3 and MODIS, averaged between 2003-2014

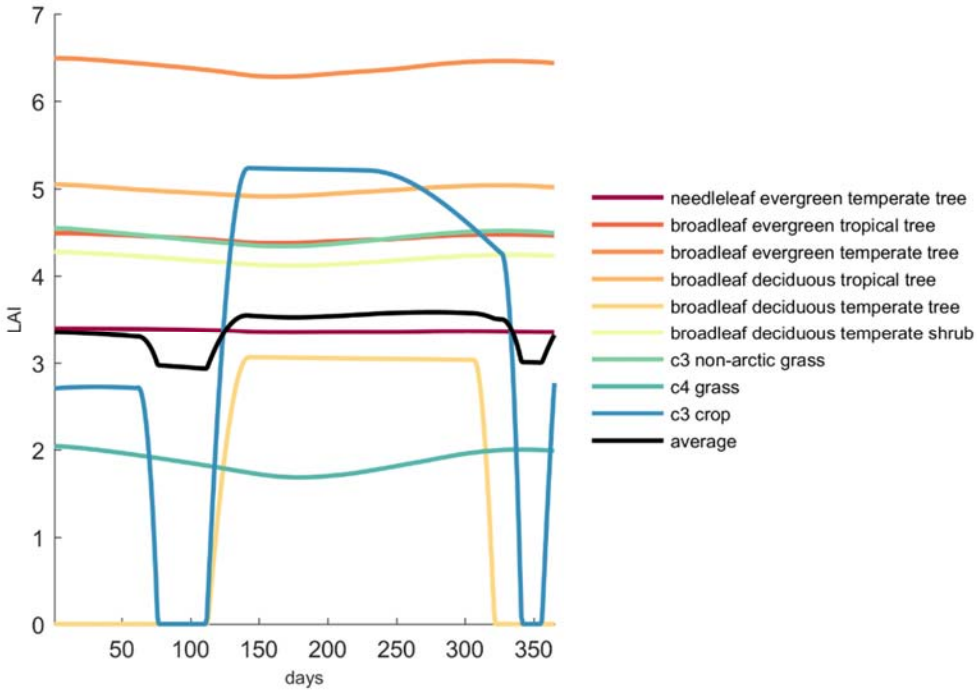

Figure 12. Annual cycle of LAI of different PFTs from CLM5.0 (GSWP3) simulation at one grid point (28.74°N, 81.25°W) in 2009. The PFTs that coexist in this grid cell are needleleaf evergreen temperate tree (phenology routine: evergreen); broadleaf evergreen tropical tree (evergreen); broadleaf evergreen temperate tree (evergreen); broadleaf deciduous tropical tree (stress deciduous); broadleaf deciduous temperate tree (seasonal deciduous); broadleaf deciduous temperate shrub (stress deciduous); c3 non-arctic grass (stress deciduous); c4 grass (stress deciduous); C3 crop: generic crop that is treated as C3 grass (stress deciduous).

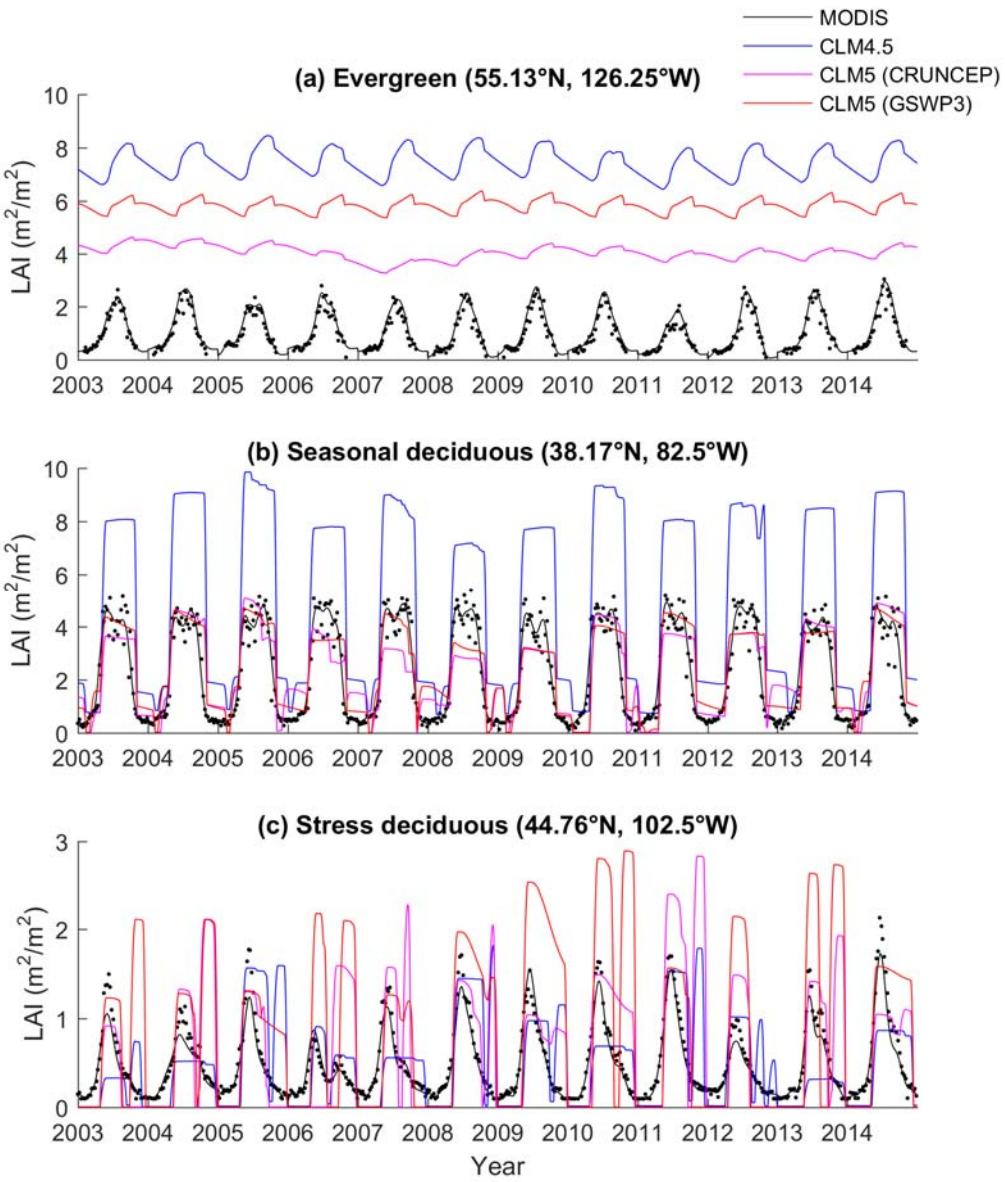

Figure 13. LAI time series at three illustrative grid points. (a) LAI seasonal cycles at a needleleaf evergreen boreal tree dominated grid cell (CLM phenology: evergreen). (b) LAI seasonal cycles at a broadleaf deciduous temperate tree dominated grid cell (CLM phenology: seasonal deciduous). (c) LAI seasonal cycles at a grassland dominated grid cell (CLM phenology: stress deciduous). Original 8-day composite of MODIS LAI is represented with black dots and the fitted smoothing spline is plotted using black lines. LAIs from CLM5.0 with GSWP3 forcing is colored red while CLM5.0 with CRUNCEP forcing is in magenta. LAIs from CLM4.5 with CRUNCEP forcing is colored blue.

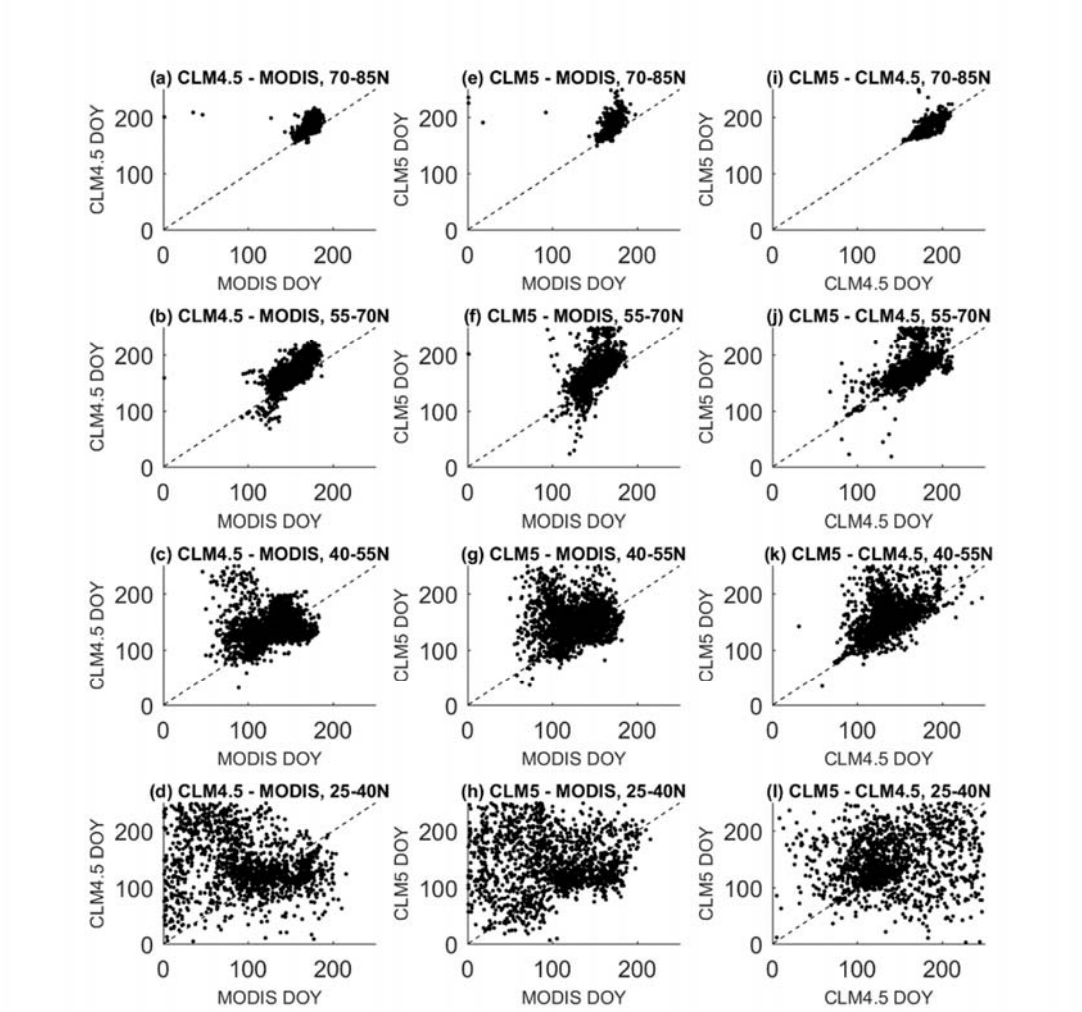

Figure 14. Comparison of LAI 50% threshold DOYs derived from different dataset at different latitudes. (a)-(h): LAI 50% threshold DOYs derived from CLM4.5 with CRUNCEP forcing and MODIS, averaged between 2003-2014, for each latitudinal band. (e)-(h): LAI 50% threshold DOYs derived from CLM5.0 with GSWP3 forcing and MODIS, averaged between 2003-2014, for each latitudinal band. (i)-(l): LAI 50% threshold DOYs derived from CLM4.5 with CRUNCEP forcing and CLM5.0 with CRUNCEP forcing, averaged between 2003-2014, for each latitudinal band.

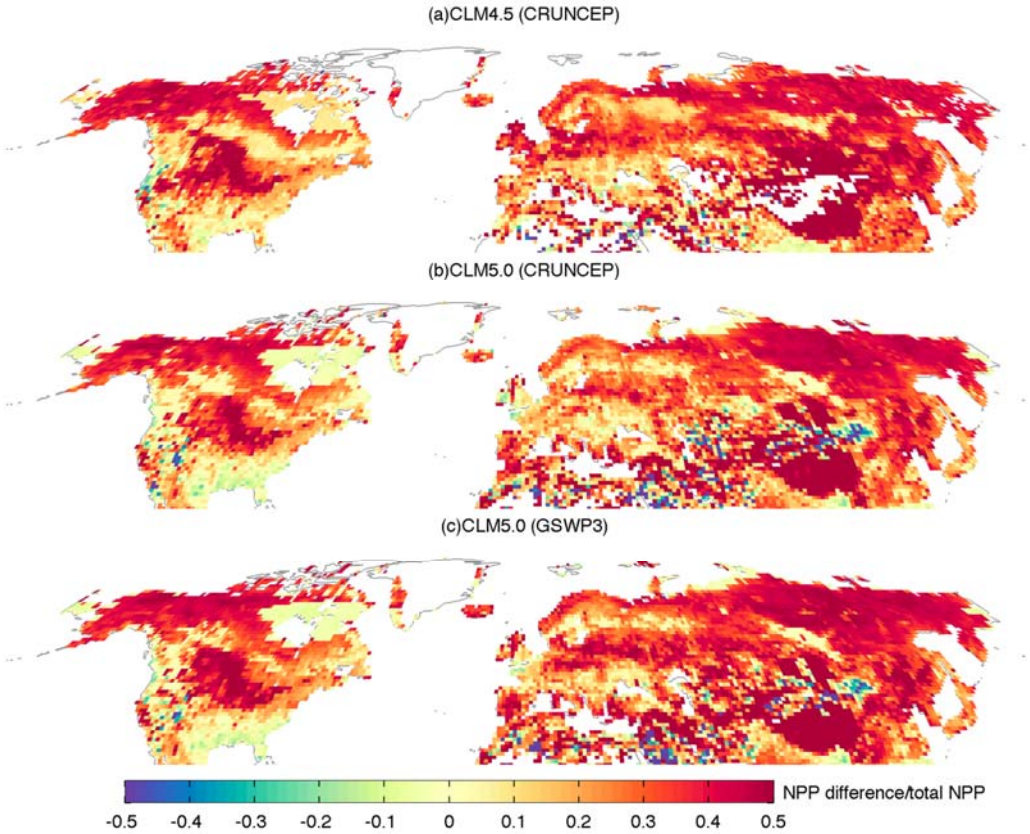

Figure 15. Fraction of total annual net primary production (NPP) that is produced during the difference between MODIS peak growing season as indicated by LAI 75% threshold and that of (A) CLM4.5 with CRUNCEP, (B) CLM5.0 with CRUNCEP, and (C) CLM5.0 with GSWP3 and MODIS, averaged between 2003-2014

CHAPTER 3

UNDERSTANDING LEAF PHENOLOGY OF DIFFERENT VEGETATION TYPES FROM LOCAL TO HEMISPHERIC SCALE: COMPARISONS OF LEAF AREA INDEX AND SEASONALITY OF VARYING CLM PLANT FUNCTIONAL TYPES AND CORRESPONDING MODIS LAND COVER TYPES

Abstract

Leaf phenology is important in both living ecosystems and land surface models as it modifies ecosystem structure and functions, land-atmosphere coupling, and the terrestrial carbon cycle. Therefore, simulating seasonal variations of leaf area index accurately for different plant functional types is crucial for future land use and climate projections. To understand grid-level differences between CLM and MODIS LAI values, seasonal amplitude, and seasonal variation and to ensure that the model produces realistic LAI values for the right reason, we compared LAI seasonal cycles in CLM and MODIS at plant functional type/land cover type level at various spatial scales. We found that, although CLM5 has better representation of MODIS LAI values and seasonal amplitude over most natural PFTs, larger disagreement is present between CLM5 and MODIS LAI seasonal cycles. We also discovered that some PFTs may display zero LAI but grid-cell averages will not reflect this phenomenon, resulting in a "right" overall LAI for the wrong reason. Overall, seasonal deciduous PFTs exhibit good agreement with MODIS in LAI seasonal variations while evergreen and stress deciduous PFTs have more room for improvement. Despite larger

differences in their LAI values, high-latitude regions show more consistent spring onset timing across different PFTs.

Introduction

Phenology is important in both real-life ecosystems and land surface models as it influences land-atmosphere coupling, structure and functions of ecosystems, and the global carbon cycle (e.g. Fitzjarrald et al., 2001; Lawrence & Chase, 2010; Richardson et al., 2013). In the community land model (CLM), coupling between vegetated land surface and its atmosphere happens at the plant functional type level, although both underlying soil layers and the atmosphere above receive output from the land surface as aggregated over all PFTs within the soil column (see methods section). In the model, start of growth for deciduous vegetation types is triggered by a subroutine that determines leaf phenophase (Oleson et al., 2013; Lawrence et al., submitted). Therefore, to understand land-atmosphere interactions and the carbon cycle in CLM, as well as other similar modeling frameworks, it is critical to examine LAI seasonal cycles at the PFT level.

The majority of previous studies evaluating phenology in CLM and other land surface models have focused on comparisons at small spatial scales to either fit parameters or characterize fundamental ecological processes. These studies have used either in-situ measurements or remote sensing at specific sites or for specific PFTs. For instance, Scholze et al. (2017) used data assimilation approaches at the site level and tuned parameterizations in land surface models to reproduce observed seasonal

cycles. Dahlin et al. (2015, 2017) examined stress deciduous phenology in CLM in tropical drylands and found that a precipitation criterion is necessary to prevent rapid onset of growing seasons due to soil moisture fluctuations. Chen et al. (2016) implemented different spring onset triggers for seasonal deciduous trees in CLM and improved the model's simulation of productivity. While these studies are crucial for developing model parameters and evaluating ecological processes, accurately simulating the land surface is a critical component for future climate projections at the global scale. It is therefore important to evaluate the skill of CLM to simulate key aspects of spring "green up" across different climate zones and over varying vegetation types at the hemispheric and continental scales that will be most important for future climate feedbacks and carbon sinks or sources.

Large-scale comparisons between CLM and observed LAI seasonal cycles can be misleading due to the large uncertainties that are present in ground observations, satellite remote sensing records, and CLM simulations. These uncertainties emerge from different sources including definitions of spring onset, deriving procedure of simulated and observed variables, as well as biases in observations and in land surface models. Satellite-derived LAI values, for instance, are based on reflectance and therefore subject to influences of snow cover and atmospheric conditions like cloud cover and diffusion (Myneni, Knyazikhin, & Park, 2015). Reducing these biases and characterizing distinct sources of uncertainty requires comparisons at the vegetation type level.

As illustrated in Chapter 2, large disagreements between both CLM and MODIS--and even different versions of CLM---are present in land surface phenology.

For example, CLM5 exhibits better representation of LAI values and seasonal amplitude but fails to represent LAI annual cycle and interannual variability accurately. However, the sources of these disagreement remains unknown. Therefore, in this chapter, we compare leaf phenology at the plant functional type (CLM) - land cover type (MODIS) level at both grid cell level and hemispheric scale and seek to answer:

1. Across PFTs, how well can CLM simulate LAI variability in MODIS, what are the PFTs that have most room for improvement?
2. What are the primary sources of uncertainties in defining PFT-specific LAIs from remote sensing and CLM output?
3. What causes the difference between CLM and MODIS LAI? Why is there an improvement in CLM LAI values and amplitude in CLM5 but not in LAI seasonal cycles? And why is the interannual correlation of the day of year (DOY) indices worse between MODIS and CLM5 than with CLM4.5?

Data and method

CLM land surface data structure and plant functional types

To represent spatial heterogeneity in the land surface, CLM adopts a "nested subgrid hierarchy" (Lawrence et al., submitted). Under this scheme, grid cells are divided into multiple land units and if a grid cell has vegetated land surface in it, then one of its land units is a vegetated land unit. This land unit consists of one single soil

column and the soil column are then divided into different plant functional types. Currently when crop model is disabled in CLM, each grid cell can have a maximum of 14 natural plant functional types (PFTs), two generic crop PFTs, and bare ground. The area weight of different PFTs in CLM5 for a case run with a standard "year 2000" land surface configuration (e.g., land use/land cover as well as atmospheric boundary conditions are taken to be representative of the early 2000s) is shown in Figure 1. Both fluxes and vegetation state variables (e.g. leaf area index and vegetation temperature) are defined at the PFT level. However, coupling between CLM and the atmosphere component, either data atmosphere or dynamical atmosphere model, happens at grid cell level, and within CLM, interactions between land surface and below ground soil layers takes place at the "column" level. Therefore, although different PFTs can have different biogeophysical and biogeochemical processes, when communicating to the atmosphere or the soil layers, they receive the same input data and output variables are averaged across PFTs based normally on their area weight.

MODIS land cover types and LAI for different land cover types

As in Chapter 2, our remote sensing LAI originates from the MODIS TERRA MOD15A2H.v006 (Myneni et al., 2015) product. In order to compare against different PFTs in CLM, we now separate MODIS LAI into different land cover types. The land cover type is based on the MODIS Terra land cover type data product (MCD12Q1, Friedl et al., 2010). Like in Chapter 2, within each CLM finite-volume grid cell, raw LAIs with a "good quality" flag (i.e., MODIS QA flag = 0) from each land cover type

are averaged together to produce a 1° by 1° product with eight-day temporal resolution. A cubic spline is then fit to each time series of the 1° grid cell average for each year and used to interpolate the data to daily time steps. We matched CLM PFTs to MODIS land cover type based on the dominant plant functional type and location. Figure 2 shows the spatial distribution and area weight of each MODIS land cover type. and Table 1 reports the match between CLM PFTs and MODIS land cover types.

Grid-level comparison of LAI seasonal cycle

MODIS and CLM do not characterize all land cover types in exactly the same way throughout all CLM grid cells. To control for these possible differences introduced by mixed MODIS land cover types, or mismatches between MODIS land cover type and CLM PFT, we selected grid points where MODIS land cover type is more consistent within the grid cell. That is, we ranked area weights for each MODIS land cover type across the Northern Hemisphere and compared LAIs of the most dominant land cover type(s) with those of corresponding PFTs in CLM. We also sampled grid points across North America to examine the reason for the shift of correlation strength. Note that, although we chose year 2012 for all analysis, the shape of LAI seasonal cycles is similar across simulated years from the same CLM experiment or MODIS observations (grassland may have larger variations from one year to the next). We also plotted LAI from the "satellite phenology" (SP) mode in CLM, which by default has the same annual cycle throughout all model years.

LAI ratios

At grid points where both CLM PFT and corresponding MODIS land cover (Table 1) are present, we defined the LAI ratio as annual summation of LAI values in CLM divided by summation of both CLM LAI and MODIS LAI (Equation 1).

$$LAI\ ratio = \frac{\sum_{n=1}^{365}(CLM\ LAI)}{\sum_{n=1}^{365}(CLM\ LAI) + \sum_{n=1}^{365}(MODIS\ LAI)} \quad \text{(Equation 1)}$$

$LAI_{CLM\text{-}MODIS}$ ratio ranges from 0 to 1. A LAI ratio of 0 means CLM simulates zero LAI across the year: i.e. the PFT is "dead" in CLM. When LAI ratio equals or is close to 0.5, CLM LAI values is close to MODIS LAI from an annual average perspective, although no information is provided on how well their seasonal cycles agree. If LAI ratio is close to one, then MODIS LAI is very small compared to CLM LAI, meaning CLM may have overestimated LAI at those locations.

Root mean square error of normalized annual LAIs

We also calculated the root mean square error (RMSE) between normalized CLM LAIs and MODIS LAIs. For each year between 2003 and 2014, we first normalized daily LAIs from MODIS and CLM, respectively, to remove the impact of differences in mean LAI values and LAI seasonal amplitude. Then we calculated the RMSE using the normalized LAIs to determine how well the seasonal cycle of LAI agree between CLM and MODIS (Equation 2).

$$RMSE_{normLAI} = \sqrt{\frac{\sum_{DOY=1}^{365} \left(\frac{CLM\ LAI - CLM\ LAI\ annual\ mean)}{CLM\ LAI\ annual\ standard\ deviation} - \frac{MODIS\ LAI - MODIS\ LAI\ annual\ mean)}{MODIS\ LAI\ annual\ standard\ deviation}\right)^2}{365}}^2$$

(Equation 2)

If the RMSE is large, then normalized CLM LAIs differ from normalized MODIS LAIs constantly over the year, suggesting CLM seasonal cycle differs from that in MODIS. When the RMSE is close to 0, CLM and MODIS LAI have good agreement on their seasonal variation.

To combine these two indices, we also calculated a match ratio (Equation 3) that reflects both LAI values and seasonal variation.

$$Match\ ratio = \sqrt{RMSE_{normLAI}^2 + (LAI\ ratio - 0.5)^2} \quad \text{(Equation 3)}$$

A large negative number means MODIS LAIs are larger than CLM LAIs and their seasonal cycles match poorly while a large positive number indicates that CLM LAIs are larger and their seasonal variations still differ. When the match ratio is close to zero, LAI estimations from CLM and MODIS are close and/or seasonal cycle of LAI from the two datasets match well with each other. We also calculated NH averages of the three ratios over each CLM PFT.

LAI threshold-based spring onset timing

Using the approaches documented in Chapter 1 and 2, we calculated spring onset timing based on day of the year when LAI reaches different threshold of its

annual dynamical ranges. We compared the difference in start of spring dates using standard deviations and difference in mean DOYs.

Results

Grid-level analysis for different MODIS land cover types

We first analyzed LAI seasonal cycles of different CLM PFT-MODIS land cover combinations to characterize the potential sources and importance of uncertainties in LAI estimates. For grid cells dominated by evergreen needleleaf forest in MODIS, there are good agreements between the MODIS land cover type and CLM PFT type (needleleaf evergreen temperate tree and needleleaf evergreen boreal tree, or NETt and NETb), although some grid points are classified as temperate PFTs in CLM5 and as boreal PFTs in CLM4.5. However, large differences are present between simulated LAIs and observed satellite LAIs. CLM5 generally displays lower and more realistic LAI values than CLM4.5, but the seasonal amplitudes are also lower and peak growing season is delayed into late summer or autumn (Figure 3 and 4). Compared to MODIS LAI and MODIS-based satellite phenology, CLM simulates larger LAI values and lower LAI seasonal amplitudes. MODIS LAI also displays steeper onset periods and earlier peak growing season (Figure 3 and 4).

Grid cells dominated by evergreen broadleaf forest in MODIS exhibit large LAI variation throughout the year, possibly due to large uncertainties triggered by cloud cover and other atmosphere influences in the tropics (Figure 5). Over these grid cells, MODIS land cover and CLM PFT still agrees well. Although CLM4.5 still

simulates higher LAI values, CLM5 LAI simulations are close to, or sometimes lower than, the annual mean MODIS LAI over this land cover type.

Although deciduous needleleaf forest only covers at most 50% area of the grid cells in the MODIS classification scheme, coverage of needleleaf deciduous boreal tree in corresponding CLM5 grid cell can be close to 100% (Figure 6). The area weights in CLM4.5 are much lower, and most grid cells simulate zero LAIs, which means the PFT dies under the corresponding forcing after a few years, though the PFT classification remains unchanged. CLM5 LAIs at these grid points are also generally lower than MODIS LAIs, but the growing season is both delayed and prolonged. Some of these grid cells are mainly characterized as needleleaf evergreen boreal tree in CLM4.5 and therefore follow the evergreen phenology (Figure 7). Compared to CLM4.5, the improvement in PFT classification results in a more realistic LAI simulations over these regions (Figure 6 and 7).

Both area weight and LAI seasonal cycle agree well between CLM and MODIS for deciduous broadleaf forest dominated grid cells, especially in CLM5 (Figure 8 and 9). Although CLM4.5 shows generally good agreement of leaf phenology with MODIS, LAI values and seasonal amplitude are too high in CLM4.5 in temperate regions as well as some boreal locations (Figure 8 and 9). Compared to CLM4.5, CLM5 has lower and more realistic LAI values and annual amplitude for temperate trees, but LAI can be too low for boreal ones (Figure 9). Overall, both leaf phenology and growing season length show good agreement among CLM4.5, CLM5, and MODIS.

Large variation and disagreement across datasets and temporal scales are present over grasslands (Figure 10 and 11). Agreement between area weight of MODIS grassland and corresponding CLM PFTs is still high, but the stress deciduous phenology routine in CLM can hardly capture variation of grassland LAI in MODIS. In 2012, CLM4.5 exhibits multiple growing seasons at most of the grassland dominated grid points. While this problem is partially solved in CLM5.0 and only one growing season is retained at most of the grid cells, growth generally starts later in CLM5.0 than in MODIS and the growing season length disagrees at most of the locations as well.

Broadleaf deciduous boreal shrub in CLM generally display similar onset timing and seasonal cycle to that of open shrublands in MODIS (Figure 12). However, CLM5 peak LAI can be two times higher than MODIS LAI at most locations and growing seasons in CLM5 also last much longer. CLM4.5 simulates zero LAI at about half of the locations, while both LAI value and growing season length are much larger than MODIS ones at the other grid cells. Overall, agreement on PFT area weight, onset timing, and seasonal cycle between CLM and MODIS is high, especially in CLM5, but LAI values and growing season length are generally too high in CLM.

Closed shrublands in MODIS are mostly mixed with grasslands and the agreement depends on whether the CLM grid cell is more tuned to temperature or soil moisture as the primary growth limiting factor (Figure 13-17). For shrub PFTs in CLM (Figure 13 and 14), CLM5 exhibits simulates both LAI values and seasonality over boreal shrubs, while CLM4.5 simulates zero LAIs at some grid points (Figure 13). However, although CLM5 PFTs match with MODIS closed shrublands over

temperate regions, CLM5 exhibits either zero LAI or a prolonged growing season and cannot simulate the multiple growing seasons displayed in MODIS (Figure 14). For grasslands at these locations, CLM4.5 is able to simulate multiple growing seasons in the low-latitude regions and the single summer growing season at high latitudes, but LAI values are generally higher than those in MODIS (Figure 15 and 16). CLM5 also simulates reasonable seasonal cycles and higher LAI values at high latitudes (Figure 15), but still shows a flattened seasonal cycle in low-latitude regions (Figure 16). In CLM4.5, a large proportion of the low-latitude grid points are classified as deciduous broadleaf tropical trees and display zero LAI, but these areas have been classified into shrubs in CLM5 (Figure 17).

Croplands display multiple growing seasons in CLM but show less inter-seasonal variation in MODIS (Figure 18). When biogeochemical cycles are enabled but the crop model is disabled in CLM, croplands are mostly treated as C3 generic grasses and follow the stress deciduous phenology subroutine. Accordingly, croplands in CLM can have multiple growing seasons. In MODIS, locations in mid-to-high latitude regions generally only have one growing season in the summer. At low-latitude locations where MODIS LAI display multiple growing seasons due to planting, CLM simulates even more growing cycles within the year or zero LAIs (Figure 18).

Across different PFTs in the Northern Hemisphere, there is generally a good agreement between CLM PFT and MODIS land cover types, especially in CLM5. However, the skill of CLM in simulating LAI annual amplitude and seasonal cycles varies across PFTs and locations. Therefore, in the next section, we extend this

comparison between CLM and MODIS to a hemispheric scale and characterized how LAI values and seasonal cycle differ between CLM and MODIS LAI.

Hemispheric scale comparison of LAI values and seasonal variation

Both LAI values and seasonal variation of LAI over evergreen needleleaf tree PFTs in CLM5 is different from that in MODIS in boreal regions, but LAI values match well with MODIS evergreen needleleaf forest in temperate regions (Figure 19 and 20). Across evergreen forests along 60^0N, LAI ratio is greater than 0.8, except in South Siberia, and RMSE of normalized LAIs is close to 2. These results indicate that CLM LAIs are consistently much higher than MODIS LAIs and seasonal variations of LAI differ between the two products (Figure 19). For temperate evergreen needleleaf trees, although RMSE is still high in South Canada and central Europe, LAI ratio drops to around 0.7, suggesting the mean and seasonal amplitude of LAI matches better between CLM and MODIS in temperate regions although the seasonal cycles still disagree. At locations where evergreen needleleaf forest is present in the Mediterranean, LAI ratio decreases to 0 or near 0, indicating that the PFT dies in this region in CLM5 (Figure 20).

For evergreen broadleaf forests, CLM5 LAI estimates are close to those in MODIS, especially for tropical trees (Figure 21 and 22). CLM5 overestimates LAIs for evergreen broadleaf temperate trees in subtropical regions in East and Southeast Asia, Southeast US, and Mexico (Figure 21), while CLM LAIs are close to, or a little lower than, MODIS values for evergreen broadleaf tropical trees in Southeast Asia,

Central America, and Sahel (Figure 22). RMSE between normalized CLM and MODIS LAI is generally greater than 1 across these regions, indicating that LAI seasonal cycle in CLM differs from the spline-fitted seasonal variations in MODIS LAI.

Both LAI seasonal amplitude and variation agree between CLM5 and MODIS deciduous needleleaf forest at locations where deciduous needleleaf trees survive in CLM5 (Figure 23). CLM LAIs decrease to zero before the analyzing period in some regions in South, East, and West Siberia and North Canada. At places where deciduous needleleaf trees survive in CLM5, i.e. along 55^0N in East Asia and West and Central Siberia, both LAI ratio and the RMSE decreases from North to South, suggesting that both LAI values and seasonal cycles are more similar between CLM and MODIS at lower latitudes for deciduous needleleaf PFT.

CLM5 and MODIS also display similar LAI seasonal amplitude and variation at deciduous broadleaf dominated boreal and temperate regions (Figure 24 and 25). LAI ratio is close to or lower than 0.5 and RMSE is around 0.5 in Eastern US, Europe, East Asia, and along 55^0N in Central Asia, suggesting that CLM LAIs are close to or lower than MODIS LAIs in these regions, but the seasonal cycles are similar. RMSE also decreases when moving to lower latitudes in these regions (Figure 24 and 25). However, at locations occupied by tropical deciduous broadleaf trees in Southeast Asia, India, and Mexico, LAI ratio is either zero or higher than 0.6 and the RMSEs are generally above 1, indicating that CLM LAIs are either zero or higher than MODIS LAIs and exhibit different seasonal cycles (Figure 26).

CLM5 estimates much larger LAIs than MODIS does in high-latitude regions across the Northern Hemisphere, but LAI seasonal cycles still match (Figure 27). Based on their area weight, Savannas at high latitudes in MODIS are classified as C3 arctic grass in CLM5 (Figure 1 and 2). Across high-latitude regions (around 60^0N) in North America and Eurasia, LAI ratio is 0.7 or higher while RMSE is 1 or lower, suggesting that CLM LAIs are much larger than MODIS values, although they display similar seasonal cycles. Both LAI ratio and RMSE decreases when moving to lower latitudes, indicating that LAI seasonal amplitude and variation of these two communities are more similar at lower latitudes (Figure 27).

Agreement between grassland LAI in CLM5 and MODIS varies dramatically across space and PFT (Figure 28 and 29). For the C3 non-arctic grass PFT in CLM5 (Figure 28), CLM exhibits larger LAIs with the LAI ratio higher than 0.6 in Eastern US, South Canada, Central America, the majority of Europe, as well as Central and Eastern Asia. LAI ratio is lower than 0.5 (but still non-zero) at a few locations in the Western US, Northern UK, Eastern Europe, and Central Asia, and decreases to zero in the surrounding regions. RMSE of normalized LAIs are largest and larger than 1.5 in the Southeast US and Western Europe and decreases from low to high latitude. Overall, aggregating both LAI amplitude and seasonal variation, CLM LAIs are most similar to MODIS grassland LAIs at locations around 50^0N in Eastern Europe, Central Asia, and part of North America (Figure 28d). The C4 grass PFT in CLM5 exhibits a better agreement on LAI values and seasonal cycles than C3 non-arctic grass (Figure 29). CLM LAI values of C4 grass are close to or lower than MODIS ones in the Eastern US and Sahel, while higher in Rocky Mountain regions in the US, Central

America, Eastern Europe, India, and Southeast, East, and Central Asia. LAI annual cycle in CLM agrees with that in MODIS in Southern US, Mexico, Sahel, and North India. Overall, C4 grass exhibits better agreement between CLM and MODIS than C3 grass (Figure 29d).

Like other high-latitude PFTs, CLM overestimates LAI values of broadleaf deciduous shrub (Figure 30 and 31). Across high-latitude regions in North America and Eurasia, CLM5 exhibits a LAI ratio either close to one or zero, suggesting that CLM5 boreal shrubland LAI is either too high or zero in these regions (Figure 30). RMSE of normalized LAI is around 1 and lower at lower latitudes, indicating that lower latitudes display better agreement between CLM and MODIS LAI seasonality over boreal shrublands (Figure 30). LAI ratio of temperate shrub is slightly lower than that of boreal shrub but is still over 0.8 when it is not zero (Figure 31). This suggests that if temperate shrub survives in CLM5, the LAI values are much higher than MODIS ones. The RMSE of temperate shrubs is also higher than that of boreal ones. RMSE of normalized LAIs are around 1.5 in the Rocky Mountain regions in the US, the Mediterranean, and Central Asia.

CLM5 simulates higher LAI values and varying seasonal cycles over living croplands (Figure 32). Because crop model is disabled in CLM for these experiments, C3 crop PFT is generic C3 crop that has stress deciduous phenology and largely follows grassland behavior. Compared to C3 grass, crop LAI ratio is lower and yet still above 0.5, indicating higher LAI values in CLM than MODIS croplands. Despite disagreement in LAI values, RMSE of normalized LAI is lower than 1 in Northern US, South Canada, Mexico, and Sahel, suggesting that seasonal cycle of LAI agrees in

these regions.

Agreement between MODIS and CLM LAI values and seasonal cycles depend largely on the plant functional type in CLM. In general, CLM LAIs are higher than corresponding MODIS land cover types for needleleaf evergreen trees, shrubs, and grass PFTs (Figure 33). CLM5 also has a higher survival rate (i.e. LAI is not consistently zero at every time step) of needleleaf deciduous trees, broadleaf evergreen trees, and C3 grass. From CLM4.5 to CLM5, LAI estimation of broadleaf deciduous trees decreases to lower than MODIS LAI while increases to higher MODIS LAI for broadleaf evergreen temperate trees (Figure 33egh). However, CLM5 LAI seasonal cycles generally have poorer agreement with corresponding MODIS land cover types over all PFTs (Figure 34). This is also shown when comparing across PFTs. Compared to CLM4.5, CLM5 LAI simulations are closer to MODIS LAIs but exhibit larger disagreement with MODIS in their seasonal variations (Figure 35). Considering both LAI values and seasonal variation, overall, CLM shows most agreement with MODIS LAI in broadleaf deciduous temperate tree PFT and least agreement in shrub PFTs (Table 2 and 3).

Although these ratios can help characterize the seasonal amplitude and variation of the two types of LAI estimations, they cannot provide information of phenology or consistency of seasonal variation across different PFTs. Therefore, in the next section, we examined how spring onset timing and phenology vary across CLM PFTs and differ between CLM and MODIS.

Threshold-based spring onset timing and phenology

Spring onset timing varies substantially across space and among different PFTs over the Northern Hemisphere. Within each PFT in CLM5, day of the year when LAI reaches each threshold generally decreases southward, except for grass and C3 crop in Southeast US, Western Europe, and East China where spring onset occurs after day 200 (Figure 36). When multiple PFTs coexist at the same location, spring onset usually appears later in evergreen PFTs than deciduous ones. Across the Northern Hemisphere, start of spring dates are more consistent among different PFTs at higher latitudes and for earlier thresholds (Figure 37). For instance, difference between LAI 50% threshold dates of different PFTs at the same grid cell is around 35 days north of 50^0N and yet can be as high as 100 days in subtropical regions in the west coast of the US and Europe (Figure 37b). When examining peak LAI timing, the difference now exceeds 100 days in high-latitude regions as well (Figure 37d). This pattern remains similar in CLM4.5. Because evergreen spring onset is not as late in CLM4.5 as in CLM5 (Figure 38ab), CLM4.5 exhibit more consistent spring onset timing among different PFTs (Figure 39).

Start of spring also occurs later southward in MODIS, but consistency between different land cover types exhibits a different pattern from that in CLM (Figure 40 and 41). Spring onset timing among different land cover types in MODIS is most consistent in mid-latitude regions, especially for earlier LAI thresholds (Figure 41abc). Large cross land cover difference is present in MODIS start of spring dates at high-latitude regions dominated by shrublands and savannas. This difference decreases over the grassland-dominated regions northward and forest-dominated regions at mid

latitudes. The cross land cover difference increases again in subtropical regions (Figure 41abc). Overall, MODIS displays smaller difference between spring onset timing among different land cover types than that among different CLM PFTs, especially for peak LAI timing.

Across different PFTs in the Northern Hemisphere, CLM5 simulates later spring onset than MODIS does, except for a few grass-dominated mid-latitude locations, but difference between CLM5 and CLM4.5 phenology varies across vegetation types. CLM5 spring onset exhibits largest difference from MODIS start of spring timing in high-latitude regions that are dominated by needleleaf evergreen trees, broadleaf deciduous shrubs, or C3 arctic grasses (Figure 42abkl). This difference remains large in boreal regions in other PFTs, such as broadleaf deciduous trees and C3 non-arctic grass, but decreases in mid-latitude regions across the Northern Hemisphere (Figure 42ghmn). It then increases again over grassland in subtropical regions (Figure 42mno). Difference between CLM4.5 and CLm5 spring onset timing depends largely on the vegetation type (Figure 43). Across the Northern Hemisphere, CLM5 exhibit later spring onset than CLM4.5 over needleleaf evergreen trees (Figure 43ab), but earlier spring onset over the deciduous PFTs at mid-to-high latitudes (Figure 43ghklm). CLM5 also simulateds later spring onset over temperate vegetation types in subtropical regions (Figure 43jmno).

Discussion

Agreement between CLM and MODIS LAI varies across space and vegetation

types. Over the Northern Hemisphere, greater agreement between CLM and MODIS LAI values and seasonal amplitude is present at lower latitudes and over temperate and tropical PFTs, while better alignment of CLM and MODIS LAI seasonal variation exhibits in mid-latitude regions and over deciduous trees. The influence of latitude on the agreement between CLM and MODIS on LAI values and seasonal cycles also changes across different plant functional types. In general, LAI values match better between CLM5 and MODIS at lower latitudes for deciduous and evergreen trees, but grass and crop display a more varying pattern where largest disagreement is present in mid-latitude regions. Therefore, although site-level analysis and comparison can provide critical information in model development and validation (Dahlin et al., 2015; Kim et al., 2015; Stöckli et al., 2008), because vegetation within the same PFT in CLM shares the same set of parameters, it is important to examine PFT-level consistency across large spatial scales or at the hemispheric level to evaluate model performance or improvement. In addition, LAI over some PFTs may keep decreasing and results in zero values over the period of interest, however, as long as other PFTs within the same grid cell remain alive, total LAI aggregated over the grid cell may not reflect the dead vegetation type and only display signals from the surviving PFTs, resulting in a potential underestimation of both LAI and productivity in CLM. Therefore, to fully understand vegetation responses and feedback as well as characterizing changes in the terrestrial carbon cycle in climate models, it is important to evaluate model simulations against observations at both large spatial scales and plant functional type level.

Large uncertainty can emerge from the procedure of producing MODIS LAI

from satellite reflectance measurements and CLM phenology. Because MODIS LAI is produced using normalized difference vegetation index (NDVI) based on reflectance measurements (Myneni et al., 2015), uncertainties in MODIS NDVI persist into the LAI estimations. That is, in high-latitude regions, snow presence and melting may cause unrealistic low LAI values and false LAI growing signal in winter and spring seasons (White et al., 2009). In the tropics, cloud cover and cloud disturbances can also cause missing records and large uncertainty in LAI predictions. In addition, while reflectance and NDVI exhibit changes in both leaf density and leaf color, CLM LAI only reflects leaf development and changes in leaf carbon pool, resulting in a potential bias in using satellite-derived LAI values to evaluate CLM LAI predictions. For instance, MODIS displays an annual amplitude of more than $2 m^2/m^2$ over needleleaf evergreen forests in boreal regions (Figure 3 and 4), covering nearly 100% of the peak LAIs in those regions, and yet seasonal variations in leaf area are small over evergreen vegetation types by definition. Therefore, although comparison against satellite remote sensing records are crucial due to their large spatial coverage and long temporal coverage, ground observations from flux tower sites (Baldocchi et al., 2001), PhenoCams (Richardson et al., 2018), and phenological observations are also important for evaluating CLM leaf phenology and seasonal variations, especially in boreal and tropical regions where large uncertainty is present in remote sensing measurements.

Despite uncertainties in both satellite observations and CLM simulations, grid cell and Northern Hemispheric scale PFT-level comparison between CLM and MODIS LAI annual cycles and between different versions of CLM reveals

fundamental differences in leaf development process in these two state-of-the-art large-scale products. Although mismatch between CLM PFT and MODIS land cover type area weight can cause misrepresentation of MODIS LAI in CLM, especially at locations where temperate and boreal PFTs of the same vegetation type coexist (Figure 3, 4, 6, and 7), the main reason why CLM and MODIS LAIs disagree lies in difference between the seasonal cycle of LAI in CLM and MODIS. While leaf phenology in seasonal deciduous PFTs largely agrees between CLM and MODIS, LAI of evergreen PFTs in boreal and temperate regions peaks too late and changes too small within each year. Stress deciduous PFTs in moisture limited temperate and tropical regions can have several growing seasons within one year while usually only one or two growing period are displayed in MODIS LAI. Agreement with MODIS also changes from CLM4.5 to CLM5. Over most PFTs, CLM5 improves simulations of LAI values, but alignment of LAI seasonal cycle between MODIS and CLM decreases from CLM4.5 to CLM5. We note, however, the survival rate of different PFTs also changes from CLM4.5 to CLM5, so it is possible that the increasing disagreement results from the PFTs that have zero LAI in CLM4.5 but is alive in CLM5. Because these PFTs are often faced with climate conditions that are less suitable for growth and tend to have unrealistic seasonal cycles, if they are dead in CLM4.5 but alive in CLM5, then including them in the grid cell aggregation may result in less agreement between CLM and MODIS although it is still an improvement of CLM because their phenology is now represented in the model. Furthermore, as fluxes are calculated at PFT level in CLM, changes in PFT survival rate may also influence surface energy balance, exchange of gases between the land and the

atmosphere, and the global carbon cycle. Therefore, it is important to examine PFT level variables to understand changes in model performance. An alternative is to use a dynamical vegetation model instead of the big-leaf fixed-PFT CLM, however, global dynamical vegetation experiments are computationally expensive and may not be able to explain why the difference between simulated and observed land cover emerges.

Although large difference is present in LAI seasonal amplitude and seasonal cycle in high-latitude regions, interseasonal and interannual variability of spring onset is most consistent across PFTs and datasets at high latitudes (Figure 19-32, 37, and 39). Spring onset timing shows largest agreement across vegetation types at high-latitude regions in CLM4.5, CLM5, and peak LAI timing in MODIS. This is also present in phenological changes in observational data products (see Chapter 1). Because temperature dominates growth in high-latitude regions, interseasonal and interannual variations of leaf phenology is more tuned to temperature variability and therefore are more consistent across PFTs or among different datasets. Moving to lower latitude and more arid regions, as grassland and crop occupy more area and moisture has larger influence on plant growth, consistency of spring onset timing or agreement of LAI seasonal cycle across PFTs also decreases. This is also true when examining later thresholds into the growing season. Both CLM4.5 and CLM5 show larger cross-PFT difference in later LAI thresholds, suggesting that changes in leaf phenology are more consistent across PFTs earlier in the growing season. That is, each spring, as the temperature warms up and soil moisture becomes more limited for plant growth, phenological changes among different vegetation types differ and show less consistency (e.g., as illustrated schematically in Figure 44). As shown in Chapter 1,

thermal-based indices are good indicators of spring onset timing at locations where temperature dominates growth, therefore, we can also use thermal-based indices to characterize and compare spring onset timing between different data products.

Future work is still needed to explain why certain PFTs cannot survive and why LAI seasonal cycle displays larger disagreement with MODIS although LAI values have been improved. In addition, as LAI seasonal variations also influence land-atmosphere coupling and terrestrial carbon cycle, it is important to characterize impacts of the different LAI seasonal cycles on land-atmospheric interactions. Further research could also fix certain PFTs to the annual cycle while allowing others to respond prognostically to climate forcings. Such experiments would shed new light into the role of land-surface/atmosphere coupling as a function of individual PFTs, or cohorts of PFTs, throughout the start of spring.

These findings should help guide future modeling studies, observational campaigns, and even ecological theory to help explain phenological sensitivity to both climate forcing and interannual variability. Furthermore, in a changing climate, the temperature-dominated response of many PFTs is likely to change. Diagnosing the ecological dynamics of those changes in sensitivity will require researchers to archive a larger number of required LAI and land surface variables to compute the indices used here, which we argue are critical for identifying sources of model bias that are not typically seen using other standard diagnostic metrics.

Conclusion

CLM displays large cross-PFT variation in LAI values, seasonal amplitude, and seasonal cycle, and they are influenced by both coexisting PFTs within the grid cell and the location. This information may be lost when aggregated to grid cell level averages, resulting in good LAI and productivity simulations for the wrong reason. Therefore, it is important to examine LAI variability and related fluxes at PFT-level over large spatial scales.

Despite large uncertainties in both MODIS and CLM LAIs, there are fundamental differences between leaf phenology in different versions of CLM and MODIS. While LAI seasonal cycles agree well over seasonal deciduous PFTs, evergreen and stress deciduous PFTs exhibit large differences between CLM and MODIS LAI values and seasonal variation, especially over boreal and temperate regions. Compared to CLM4.5, CLM5 improves over LAI values but has less agreement with LAI seasonal cycles in MODIS. Therefore, it is critical to evaluate seasonal variations when examining model performance.

Spring onset timing and LAI seasonal cycle are more consistent across vegetation types at higher latitudes and earlier in the growing season, indicating that there may be a temperature dominated signal in spring phenological changes in both CLM and observations. Therefore, thermal-based indices and LAI threshold-based indices can be helpful in characterizing spring onset variability in these data products.

REFERENCE

Baldocchi, D., Falge, E., Gu, L., Olson, R., Hollinger, D., Running, S., … Evans, R. (2001). FLUXNET: A new tool to study the temporal and spatial variability of ecosystem-scale carbon dioxide, water vapor, and energy flux densities. *Bulletin of the American Meteorological Society*, *82*(11), 2415–2434.

Chen, M., Melaas, E. K., Gray, J. M., Friedl, M. A., & Richardson, A. D. (2016). A new seasonal-deciduous spring phenology submodel in the Community Land Model 4.5: impacts on carbon and water cycling under future climate scenarios. *Global Change Biology*, *22*(11), 3675–3688.

Dahlin, K. M., Fisher, R. A., & Lawrence, P. J. (2015). Environmental drivers of drought deciduous phenology in the Community Land Model. *Biogeosciences*, *12*(16), 5061–5074.

Dahlin, K. M., Ponte, D. Del, Setlock, E., & Nagelkirk, R. (2017). Global patterns of drought deciduous phenology in semi-arid and savanna-type ecosystems. *Ecography*, *40*(2), 314–323. https://doi.org/10.1111/ecog.02443

Fitzjarrald, D. R., Acevedo, O. C., & Moore, K. E. (2001). Climatic consequences of leaf presence in the eastern United States. *Journal of Climate*, *14*(4), 598–614.

Friedl, M. A., Sulla-Menashe, D., Tan, B., Schneider, A., Ramankutty, N., Sibley, A., & Huang, X. (2010). MODIS Collection 5 global land cover: Algorithm refinements and characterization of new datasets. *Remote Sensing of Environment*, *114*(1), 168–182.

Kim, Y., Moorcroft, P. R., Aleinov, I., Puma, M. J., & Kiang, N. Y. (2015). Variability of phenology and fluxes of water and carbon with observed and simulated soil moisture in the Ent Terrestrial Biosphere Model (Ent TBM version 1.0.1.0.0). *Geoscientific Model Development*, *8*(12), 3837–3865. https://doi.org/10.5194/gmd-8-3837-2015

Lawrence, P. J., & Chase, T. N. (2010). Investigating the climate impacts of global land cover change in the community climate system model. *International Journal of Climatology*, *30*(13), 2066–2087.

Lawrence, D.M. R.A. Fisher, C.D. Koven, K.W. Oleson, S.C. Swenson, G. Bonan, N. Collier, B. Ghimire, L. van Kampenhout, D. Kennedy, E. Kluzek, P.J. Lawrence, F. Li, H. Li, D. Lombardozzi, W.J. Riley, W.J. Sacks, M. Shi, M. Vertenstein, W.R. Wieder,, C. Xu, A.A. Ali, A.M. Badger, G. Bisht, M.A. Brunke, S.P. Burns,, J. Buzan, M. Clark, A. Craig, K. Dahlin, B. Drewniak, J.B. Fisher, M.

Flanner, A.M. Fox, P. Gentine, F.Hoffman, G. Keppel-Aleks, R., Knox, S. Kumar, J. Lenaerts, L.R. Leung, W.H. Lipscomb, Y. Lu, A., Pandey, J.D. Pelletier, J. Perket,, J.T. Randerson, D.M. Ricciuto, B.M., Sanderson, A. Slater, Z.M. Subin, J. Tang, R.Q. Thomas, M. Val Martin, and X. Zeng, 2018: The Community Land Model version 5: Description of new features, benchmarking, and impact of forcing uncertainty. Submitted to J. Adv. Model. Earth Syst.

Myneni, R., Knyazikhin, Y., & Park, T. (2015). MOD15A2H MODIS/terra leaf area index/FPAR 8-day L4 global 500 m SIN grid V006. *NASA EOSDIS Land Processes DAAC*.

Oleson, K. W., Lawrence, D. M., Bonan, G. B., Drewniak, B., Huang, M., Charles, D., … Sacks, W. (2013). CLM 4.5 NCAR Technical Note, (July). https://doi.org/10.1007/s11538-011-9690-0

Richardson, A. D., Hufkens, K., Milliman, T., Aubrecht, D. M., Chen, M., Gray, J. M., … Kosmala, M. (2018). Tracking vegetation phenology across diverse North American biomes using PhenoCam imagery. *Scientific Data*, *5*, 180028.

Richardson, A. D., Keenan, T. F., Migliavacca, M., Ryu, Y., Sonnentag, O., & Toomey, M. (2013). Climate change, phenology, and phenological control of vegetation feedbacks to the climate system. *Agricultural and Forest Meteorology*, *169*, 156–173. https://doi.org/10.1016/j.agrformet.2012.09.012

Scholze, M., Buchwitz, M., Dorigo, W., Guanter, L., & Quegan, S. (2017). Reviews and syntheses: Systematic Earth observations for use in terrestrial carbon cycle data assimilation systems. *Biogeosciences*, *14*(14), 3401–3429. https://doi.org/10.5194/bg-14-3401-2017

Stöckli, R., Lawrence, D. M., Niu, G., Oleson, K. W., Thornton, P. E., Yang, Z., … Running, S. W. (2008). Use of FLUXNET in the Community Land Model development. *Journal of Geophysical Research: Biogeosciences*, *113*(G1).

White, M. A., De Beurs, K. M., Didan, K., Inouye, D. W., Richardson, A. D., Jensen, O. P., … Lauenroth, W. K. (2009). Intercomparison, interpretation, and assessment of spring phenology in North America estimated from remote sensing for 1982–2006. *Global Change Biology*, *15*(10), 2335–2359. https://doi.org/10.1111/j.1365-2486.2009.01910.x

TABLES

Table 1. lookup table between MODIS land cover types and CLM plant functional types

MODIS land cover	**CLM PFT**
evergreen needleleaf forest	needleleaf evergreen temperate tree
evergreen needleleaf forest	needleleaf evergreen boreal tree
deciduous needleleaf forest	needleleaf deciduous boreal tree
evergreen broadleaf forest	broadleaf evergreen tropical tree
evergreen broadleaf forest	broadleaf evergreen temperate tree
deciduous broadleaf forest	broadleaf deciduous tropical tree
deciduous broadleaf forest	broadleaf deciduous temperate tree
deciduous broadleaf forest	broadleaf deciduous boreal tree
closed shrublands	broadleaf evergreen shrub
open shrublands	broadleaf deciduous temperate shrub
open shrublands	broadleaf deciduous boreal shrub
savannas	c3 arctic grass
grasslands	c3 non-arctic grass
grasslands	c4 grass
croplands	c3 crop
croplands	c3 irrigated

Table 2. Mean LAIs and ratios for each CLM PFT-MODIS land cover type combination in CLM4.5 with CRUNCEP forcing, averaged between 2003-2014

CLM PFT	MODIS land cover	CLM mean LAI	CLM mean alive LAI	MODIS mean LAI	total area weight	LAI ratio	RMSE of normalized LAI	match
needleleaf evergreen temperate tree	Evergreen Needleleaf forest	4.70	5.28	1.68	0.06	0.65	1.14	0.27
needleleaf evergreen boreal tree	Evergreen Needleleaf forest	4.07	4.86	1.68	0.13	0.66	1.27	0.44
needleleaf deciduous boreal tree	Deciduous Needleleaf forest	0.19	0.94	0.57	0.02	0.09	0.75	0.09
broadleaf evergreen tropical tree	Evergreen Broadleaf forest	2.92	3.78	3.88	0.08	0.38	1.35	0.16
broadleaf evergreen temperate tree	Evergreen Broadleaf forest	2.97	3.66	3.88	0.01	0.42	1.31	0.16
broadleaf deciduous tropical tree	Deciduous Broadleaf forest	3.08	5.98	1.80	0.07	0.20	1.04	0.23
broadleaf deciduous temperate tree	Deciduous Broadleaf forest	2.16	2.46	1.80	0.05	0.55	0.57	0.05
broadleaf deciduous boreal tree	Deciduous Broadleaf forest	1.44	1.92	1.80	0.02	0.61	0.66	0.16

broadleaf evergreen shrub	Closed shrublands	3.58	4.51	0.32	0.00	0.73	1.26	0.34
broadleaf deciduous temperate shrub	Open shrublands	2.49	3.69	0.19	0.02	0.39	1.12	0.38
broadleaf deciduous boreal shrub	Open shrublands	1.68	2.97	0.19	0.11	1.28	0.93	1.85
c3 arctic grass	Savannas	2.59	3.85	1.21	0.06	0.70	0.80	0.35
c3 non-arctic grass	Grasslands	2.91	4.13	0.68	0.11	0.48	1.12	0.32
c4 grass	Grasslands	5.78	6.02	0.68	0.08	0.74	1.19	0.38
Crop1	Croplands	4.38	4.81	0.92	0.17	0.66	1.14	0.32

Table 3. Mean LAIs and ratios for each CLM PFT-MODIS land cover type combination in CLM5 with GSWP3 forcing, averaged between 2003-2014

CLM PFT	MODIS land cover	CLM mean LAI	CLM mean alive LAI	MODIS mean LAI	total area weight	LAI ratio	RMSE of normalized LAI	match
needleleaf evergreen temperate tree	Evergreen Needleleaf forest	3.31	3.67	1.68	0.07	0.54	1.56	0.34
needleleaf evergreen boreal tree	Evergreen Needleleaf forest	2.71	3.24	1.68	0.08	0.68	1.67	0.52
needleleaf deciduous boreal tree	Deciduous Needleleaf forest	0.37	1.19	0.57	0.03	0.28	0.79	0.41
broadleaf evergreen tropical tree	Evergreen Broadleaf forest	3.10	3.96	3.88	0.09	0.48	1.41	0.07
broadleaf evergreen temperate tree	Evergreen Broadleaf forest	5.71	6.05	3.88	0.01	0.63	1.48	0.26
broadleaf deciduous tropical tree	Deciduous Broadleaf forest	2.34	5.48	1.80	0.01	0.32	1.34	0.25
broadleaf deciduous temperate tree	Deciduous Broadleaf forest	0.65	1.52	1.80	0.04	0.31	0.57	0.04
broadleaf deciduous boreal tree	Deciduous Broadleaf forest	0.41	0.87	1.80	0.01	0.44	0.64	0.24

broadleaf evergreen shrub	Closed shrublands	2.45	3.05	0.32	0.00	0.43	1.54	0.51
broadleaf deciduous temperate shrub	Open shrublands	1.90	2.86	0.19	0.02	0.30	1.21	0.38
broadleaf deciduous boreal shrub	Open shrublands	2.21	2.48	0.19	0.06	1.41	0.88	1.29
c3 arctic grass	Savannas	2.00	2.35	1.21	0.12	0.85	0.69	0.38
c3 non-arctic grass	Grasslands	2.03	2.70	0.68	0.17	0.53	1.17	0.31
c4 grass	Grasslands	1.33	1.56	0.68	0.14	0.46	1.17	0.30
C3 Crop	Croplands	1.07	1.68	0.92	0.13	0.35	1.08	0.22
C3 Crop Irrigated	Croplands	0.00	NaN	0.92	0.03	0.00	NaN	NaN

FIGURES

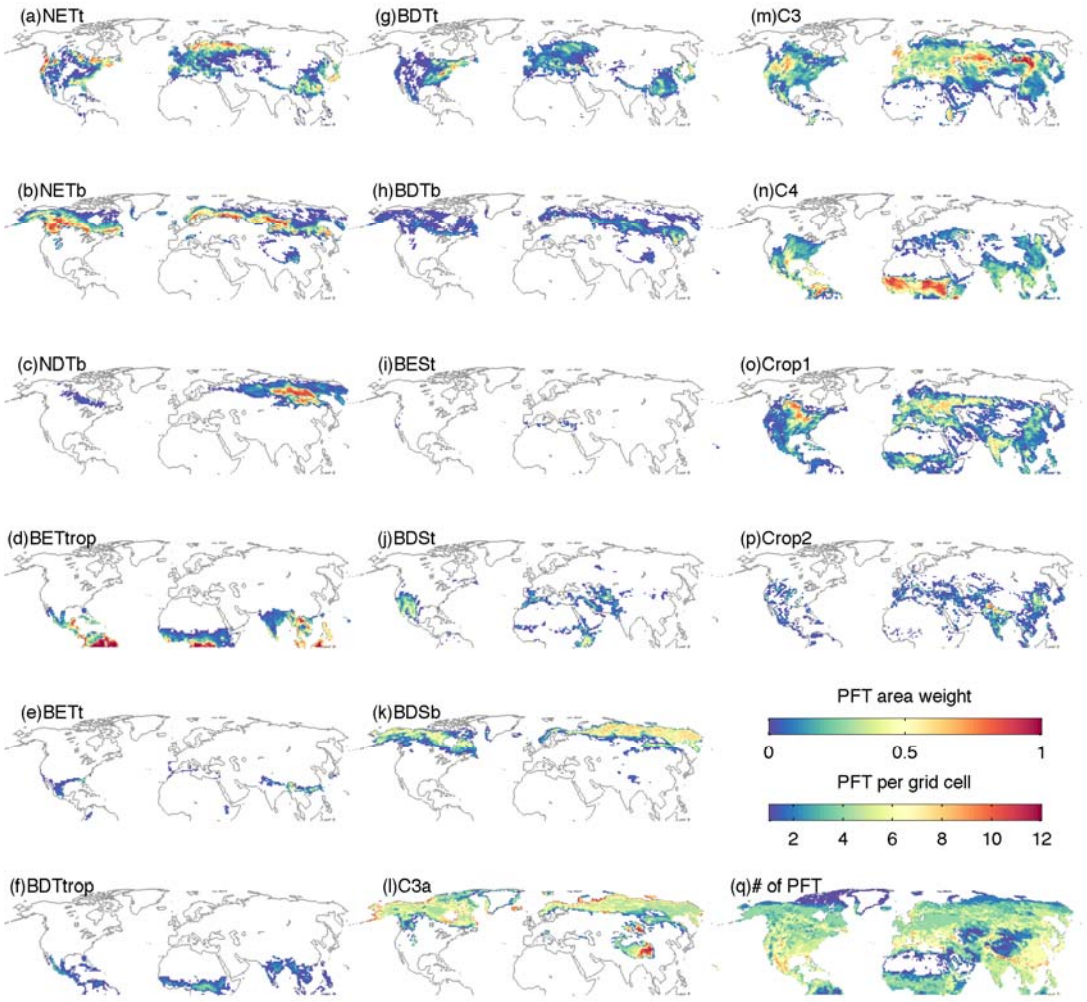

Figure 1. PFT area weight within each grid cell for all 14 natural PFTs and two crop PFTs in CLM5.0 "2000 initial conditions (panels a-i), and number of PFTs in vegetated land unit within each grid cell (panel q). The fourteen natural PFTs include: NETt: needleleaf evergreen temperate tree; NETb: needleleaf evergreen boreal tree; NDTb: needleleaf deciduous boreal tree; BETtrop: broadleaf evergreen tropical tree; BETt: broadleaf evergreen temperate tree; BDTtrop: broadleaf deciduous tropical tree; BDTt: broadleaf deciduous temperate tree; BDTb: broadleaf deciduous boreal tree; BES: broadleaf evergreen temperate shrub; BDSt: broadleaf deciduous temperate shrub; BDSb: broadleaf deciduous boreal shrub; C3a: C3 arctic grass; C3: C3 non-arctic grass; C4: C4 grass. Two crop PFTs are: C3Crop: C3 generic crops; C3CropIr: C3 irrigated crops.

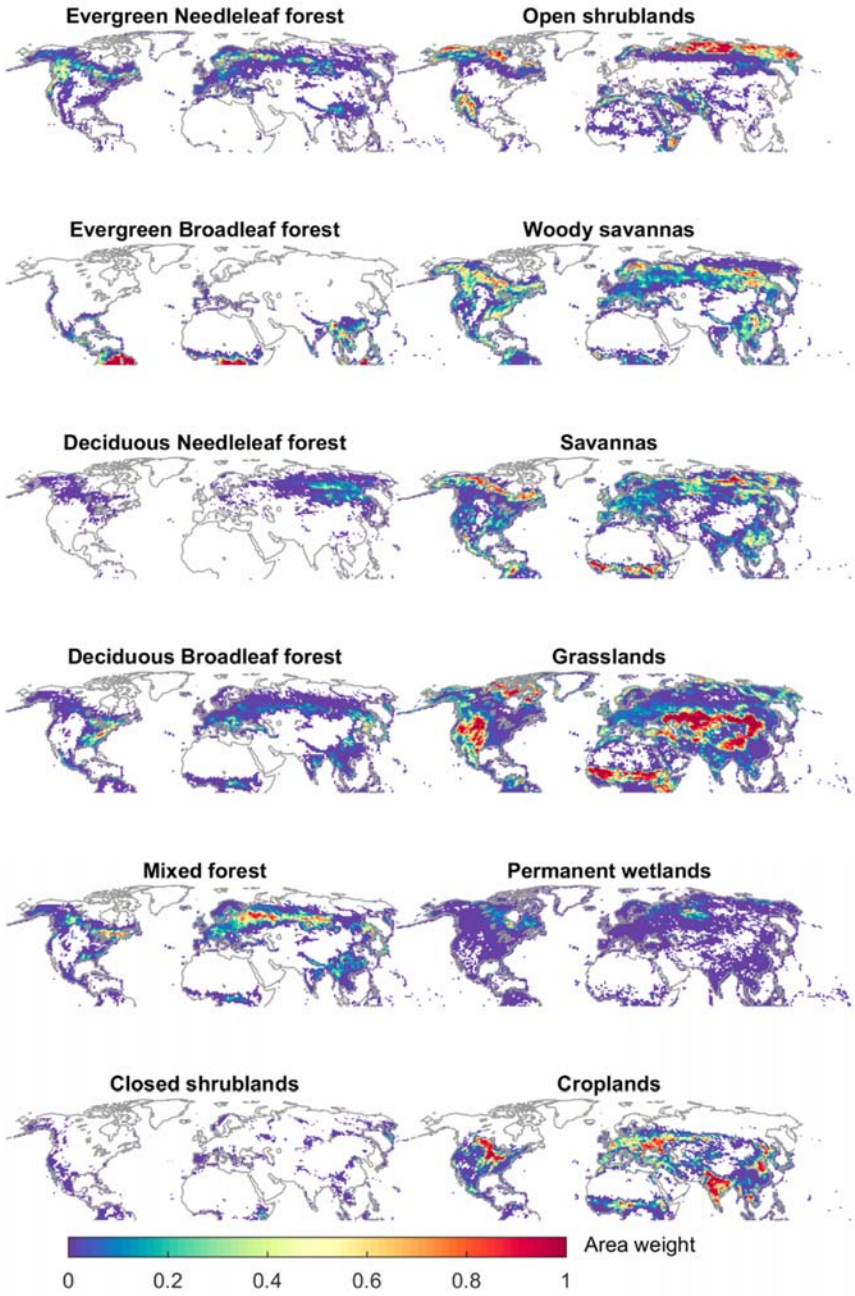

Figure 2. Mean area weight within the grid cell for different MODIS land cover types averaged between 2003-2014. MODIS land cover type and area weight are based on MOD12Q1 product (Friedl et al., 2002).

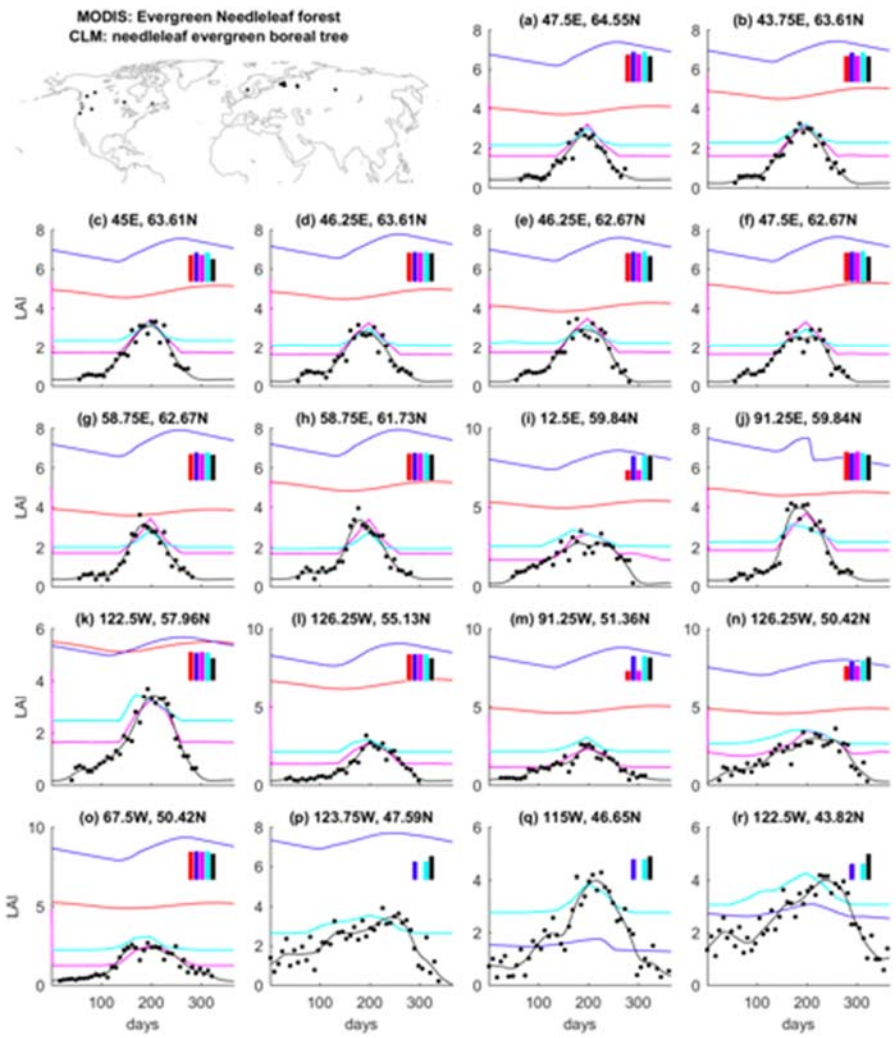

Figure 3. LAI seasonal cycles at evergreen locations dominated by needleleaf forests for the year 2012. Grid points were selected based on area weight rank of evergreen needleleaf forests over the Northern Hemisphere in MODIS in the year of 2012. Corresponding CLM plant functional type plotted in this figure is needleleaf evergreen boreal tree (NETb). LAIs from CLM5 with GSWP3 forcing in 2012 is colored red while CLM4.5 with CRUNCEP forcing in 2012 is in blue. LAI from CLM5 satellite phenology mode is colored magenta and CLM4.5 SP is in cyan. Original 8-day composite of MODIS LAI in 2012 is represented with black dots and the fitted smoothing spline is plotted using black lines. Upper left panel shows the locations of all the grid cells. Panel (a)-(r) show the 2012 annual cycle of LAIs from different datasets at each grid cell with grid cell coordinates indicated in the panel title. The boxes in the upper right corner of each panel show the area weight of the land cover type or plant functional type within the grid cell in each dataset.

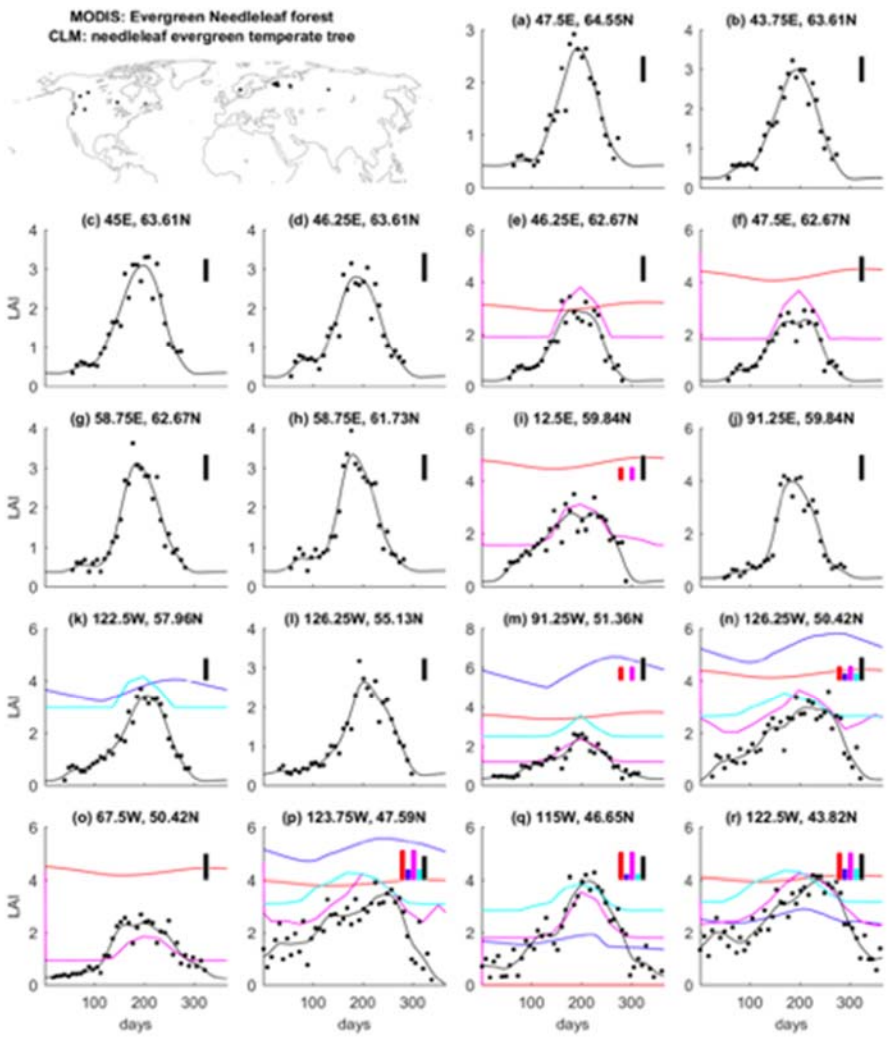

Figure 4. LAI seasonal cycles at evergreen needleleaf forest dominated locations in 2012. Grid points were selected based on area weight rank of evergreen needleleaf forests over the Northern Hemisphere in MODIS in the year of 2012. Corresponding CLM plant functional type plotted in this figure is needleleaf evergreen temperate tree (NETt). LAIs from CLM5 with GSWP3 forcing in 2012 is colored red while CLM4.5 with CRUNCEP forcing in 2012 is in blue. LAI from CLM5 satellite phenology mode is colored magenta and CLM4.5 SP is in cyan. Original 8-day composite of MODIS LAI in 2012 is represented with black dots and the fitted smoothing spline is plotted using black lines. Upper left panel shows the locations of all the grid cells. Panel (a)-(r) show the 2012 annual cycle of LAIs from different datasets at each grid cell with grid cell coordinates indicated in the panel title. The boxes in the upper right corner of each panel show the area weight of the land cover type or plant functional type within the grid cell in each dataset.

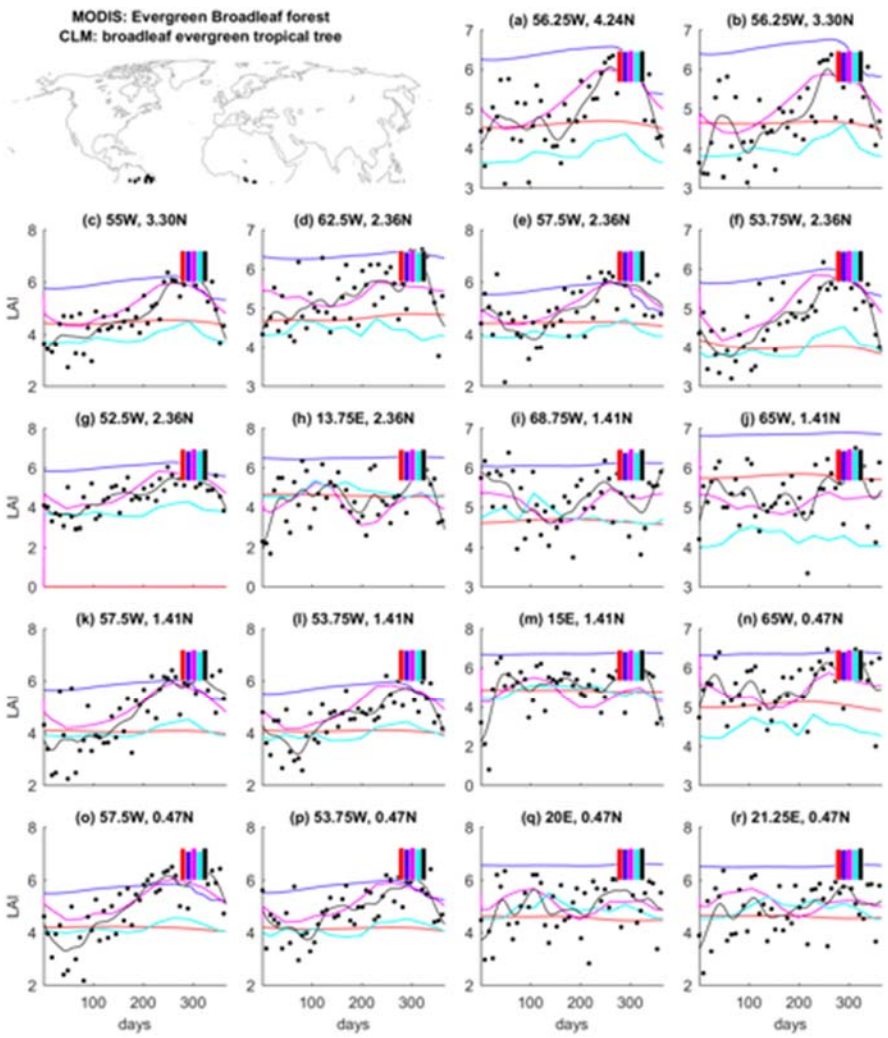

Figure 5. LAI seasonal cycles at evergreen broadleaf forest dominated locations in 2012. Grid points were selected based on area weight rank of evergreen broadleaf forests over the Northern Hemisphere in MODIS in the year of 2012. Corresponding CLM plant functional type plotted in this figure is broadleaf evergreen tropical tree (BETtrop). LAIs from CLM5 with GSWP3 forcing in 2012 is colored red while CLM4.5 with CRUNCEP forcing in 2012 is in blue. LAI from CLM5 satellite phenology mode is colored magenta and CLM4.5 SP is in cyan. Original 8-day composite of MODIS LAI in 2012 is represented with black dots and the fitted smoothing spline is plotted using black lines. Upper left panel shows the locations of all the grid cells. Panel (a)-(r) show the 2012 annual cycle of LAIs from different datasets at each grid cell with grid cell coordinates indicated in the panel title. The boxes in the upper right corner of each panel show the area weight of the land cover type or plant functional type within the grid cell in each dataset.

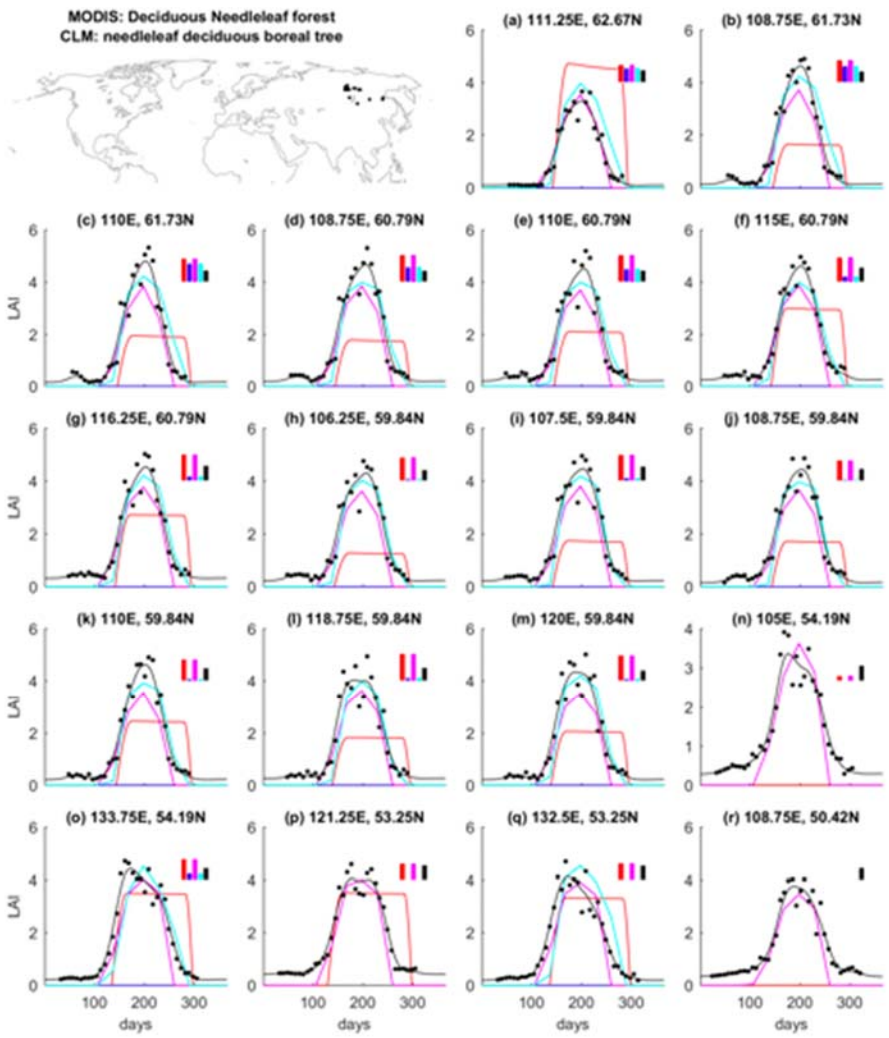

Figure 6. LAI seasonal cycles at deciduous needleleaf forest dominated locations in 2012. Grid points were selected based on area weight rank of deciduous needleleaf forests over the Northern Hemisphere in MODIS in the year of 2012. Corresponding CLM plant functional type plotted in this figure is needleleaf deciduous boreal tree (NDTb). LAIs from CLM5 with GSWP3 forcing in 2012 is colored red while CLM4.5 with CRUNCEP forcing in 2012 is in blue. LAI from CLM5 satellite phenology mode is colored magenta and CLM4.5 SP is in cyan. Original 8-day composite of MODIS LAI in 2012 is represented with black dots and the fitted smoothing spline is plotted using black lines. Upper left panel shows the locations of all the grid cells. Panel (a)-(r) show the 2012 annual cycle of LAIs from different datasets at each grid cell with grid cell coordinates indicated in the panel title. The boxes in the upper right corner of each panel show the area weight of the land cover type or plant functional type within the grid cell in each dataset.

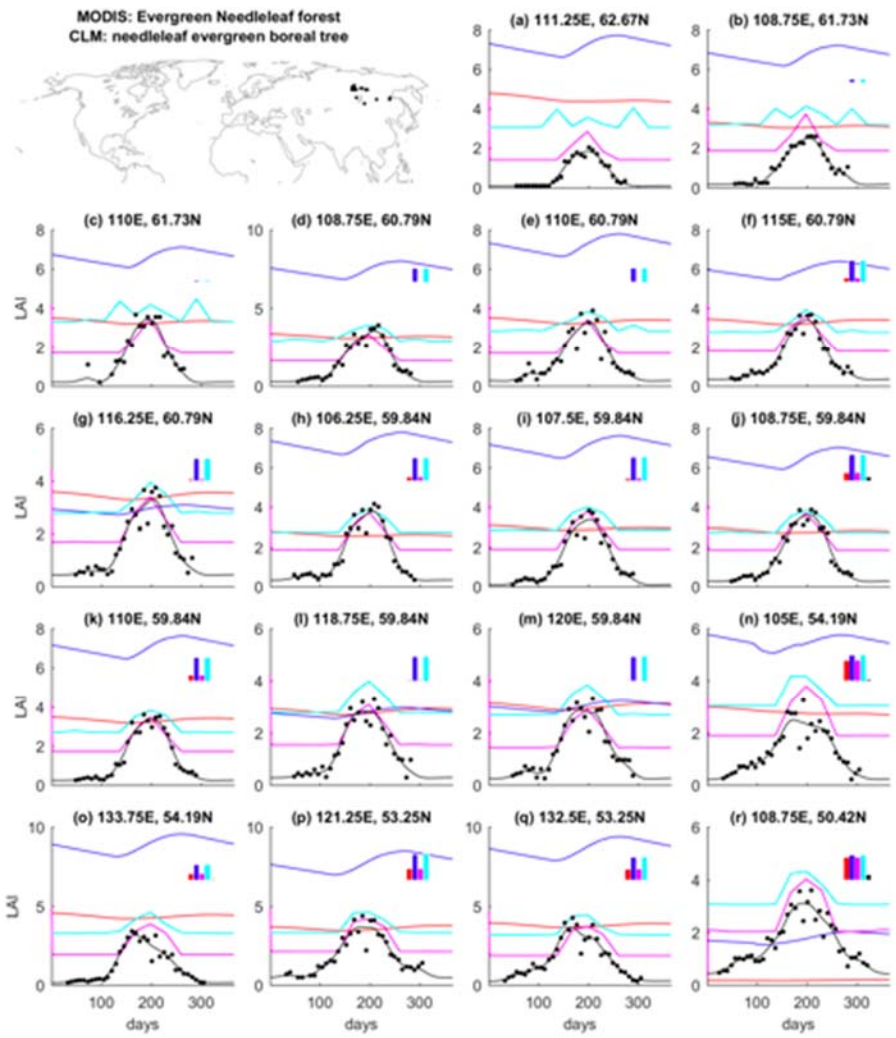

Figure 7. LAI seasonal cycles of evergreen needleleaf forests at deciduous needleleaf forest dominated locations in 2012. Grid points were selected based on area weight rank of deciduous needleleaf forests over the Northern Hemisphere in MODIS in the year of 2012. LAI seasonal cycles of evergreen needle forests are displayed in this figure. Corresponding CLM plant functional type is needleleaf evergreen boreal tree (NETb). LAIs from CLM5 with GSWP3 forcing in 2012 is colored red while CLM4.5 with CRUNCEP forcing in 2012 is in blue. LAI from CLM5 satellite phenology mode is colored magenta and CLM4.5 SP is in cyan. Original 8-day composite of MODIS LAI in 2012 is represented with black dots and the fitted smoothing spline is plotted using black lines. Upper left panel shows the locations of all the grid cells. Panel (a)-(r) show the 2012 annual cycle of LAIs from different datasets at each grid cell with grid cell coordinates indicated in the panel title. The boxes in the upper right corner of each panel show the area weight of the land cover type or plant functional type within the grid cell in each dataset.

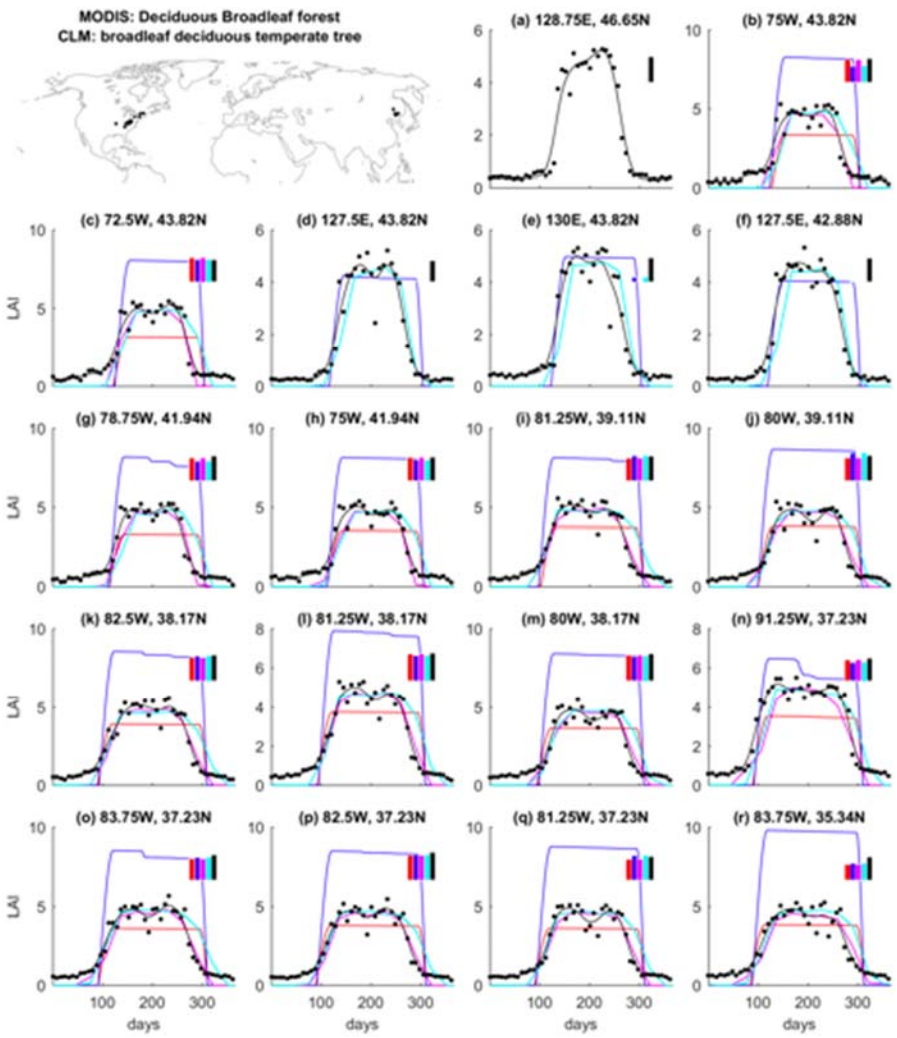

Figure 8. LAI seasonal cycles at deciduous broadleaf forest dominated locations in 2012. Grid points were selected based on area weight rank of deciduous broadleaf forests over the Northern Hemisphere in MODIS in the year of 2012. Corresponding CLM plant functional type plotted in this figure is broadleaf deciduous temperate tree (NDTt). LAIs from CLM5 with GSWP3 forcing in 2012 is colored red while CLM4.5 with CRUNCEP forcing in 2012 is in blue. LAI from CLM5 satellite phenology mode is colored magenta and CLM4.5 SP is in cyan. Original 8-day composite of MODIS LAI in 2012 is represented with black dots and the fitted smoothing spline is plotted using black lines. Upper left panel shows the locations of all the grid cells. Panel (a)-(r) show the 2012 annual cycle of LAIs from different datasets at each grid cell with grid cell coordinates indicated in the panel title. The boxes in the upper right corner of each panel show the area weight of the land cover type or plant functional type within the grid cell in each dataset.

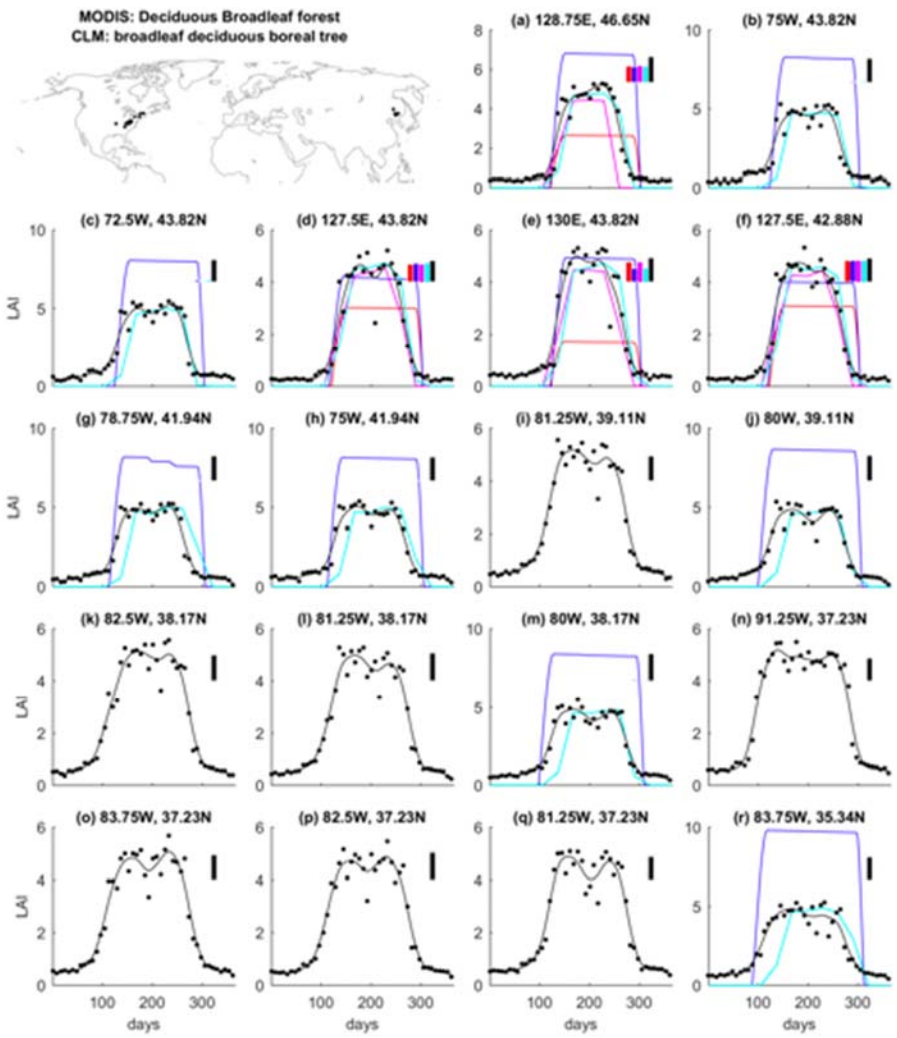

Figure 9. LAI seasonal cycles at deciduous broadleaf forest dominated locations in 2012. Grid points were selected based on area weight rank of deciduous broadleaf forests over the Northern Hemisphere in MODIS in the year of 2012. Corresponding CLM plant functional type plotted in this figure is broadleaf deciduous boreal tree (NDTb). LAIs from CLM5 with GSWP3 forcing in 2012 is colored red while CLM4.5 with CRUNCEP forcing in 2012 is in blue. LAI from CLM5 satellite phenology mode is colored magenta and CLM4.5 SP is in cyan. Original 8-day composite of MODIS LAI in 2012 is represented with black dots and the fitted smoothing spline is plotted using black lines. Upper left panel shows the locations of all the grid cells. Panel (a)-(r) show the 2012 annual cycle of LAIs from different datasets at each grid cell with grid cell coordinates indicated in the panel title. The boxes in the upper right corner of each panel show the area weight of the land cover type or plant functional type within the grid cell in each dataset.

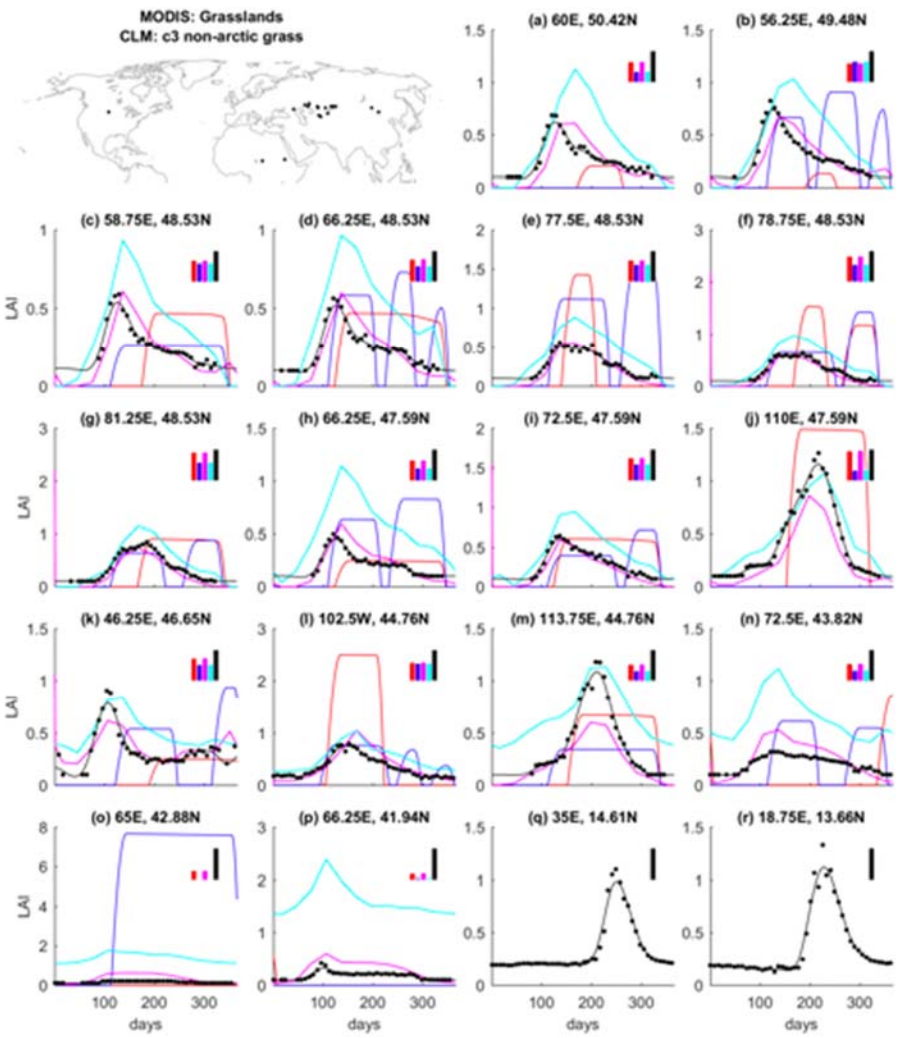

Figure 10. LAI seasonal cycles at grassland dominated locations in 2012. Grid points were selected based on area weight rank of grasslands over the Northern Hemisphere in MODIS in the year of 2012. Corresponding CLM plant functional type plotted in this figure is C3 non-arctic grass (C3). LAIs from CLM5 with GSWP3 forcing in 2012 is colored red while CLM4.5 with CRUNCEP forcing in 2012 is in blue. LAI from CLM5 satellite phenology mode is colored magenta and CLM4.5 SP is in cyan. Original 8-day composite of MODIS LAI in 2012 is represented with black dots and the fitted smoothing spline is plotted using black lines. Upper left panel shows the locations of all the grid cells. Panel (a)-(r) show the 2012 annual cycle of LAIs from different datasets at each grid cell with grid cell coordinates indicated in the panel title. The boxes in the upper right corner of each panel show the area weight of the land cover type or plant functional type within the grid cell in each dataset.

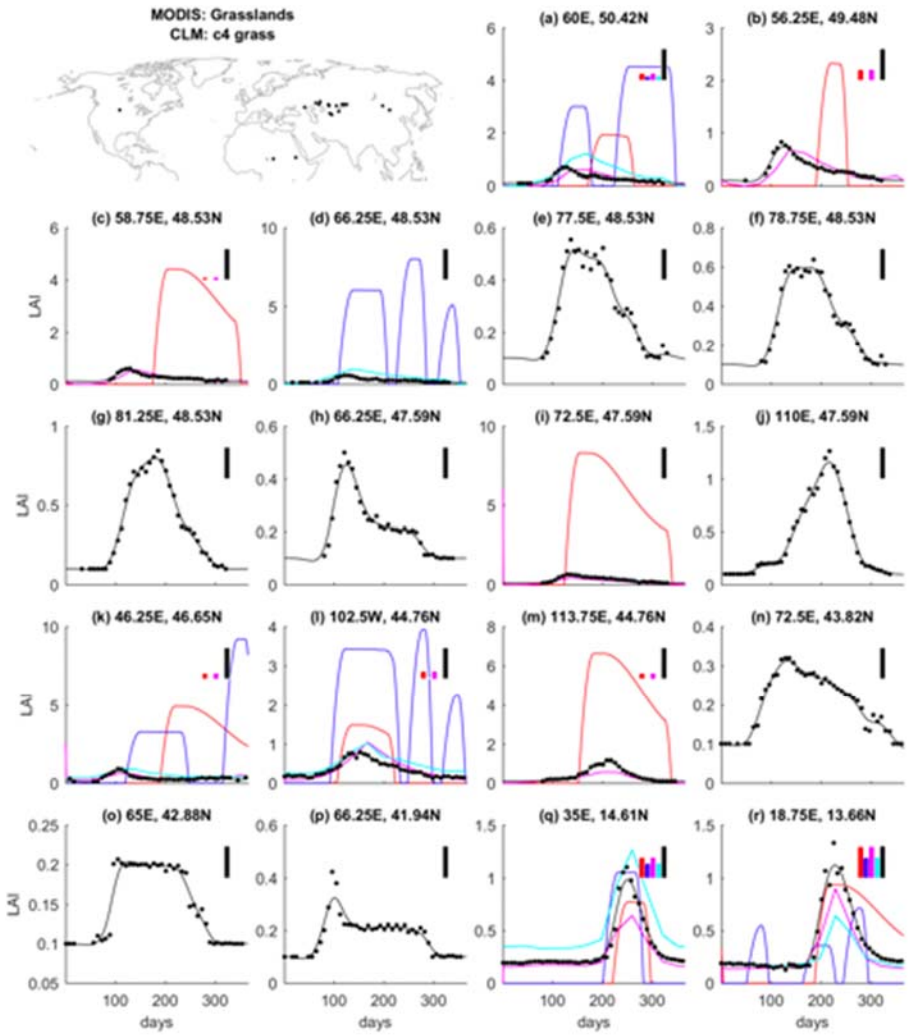

Figure 11. LAI seasonal cycles at grassland dominated locations in 2012. Grid points were selected based on area weight rank of grasslands over the Northern Hemisphere in MODIS in the year of 2012. Corresponding CLM plant functional type plotted in this figure is C4 grass (C4). LAIs from CLM5 with GSWP3 forcing in 2012 is colored red while CLM4.5 with CRUNCEP forcing in 2012 is in blue. LAI from CLM5 satellite phenology mode is colored magenta and CLM4.5 SP is in cyan. Original 8-day composite of MODIS LAI in 2012 is represented with black dots and the fitted smoothing spline is plotted using black lines. Upper left panel shows the locations of all the grid cells. Panel (a)-(r) show the 2012 annual cycle of LAIs from different datasets at each grid cell with grid cell coordinates indicated in the panel title. The boxes in the upper right corner of each panel show the area weight of the land cover type or plant functional type within the grid cell in each dataset.

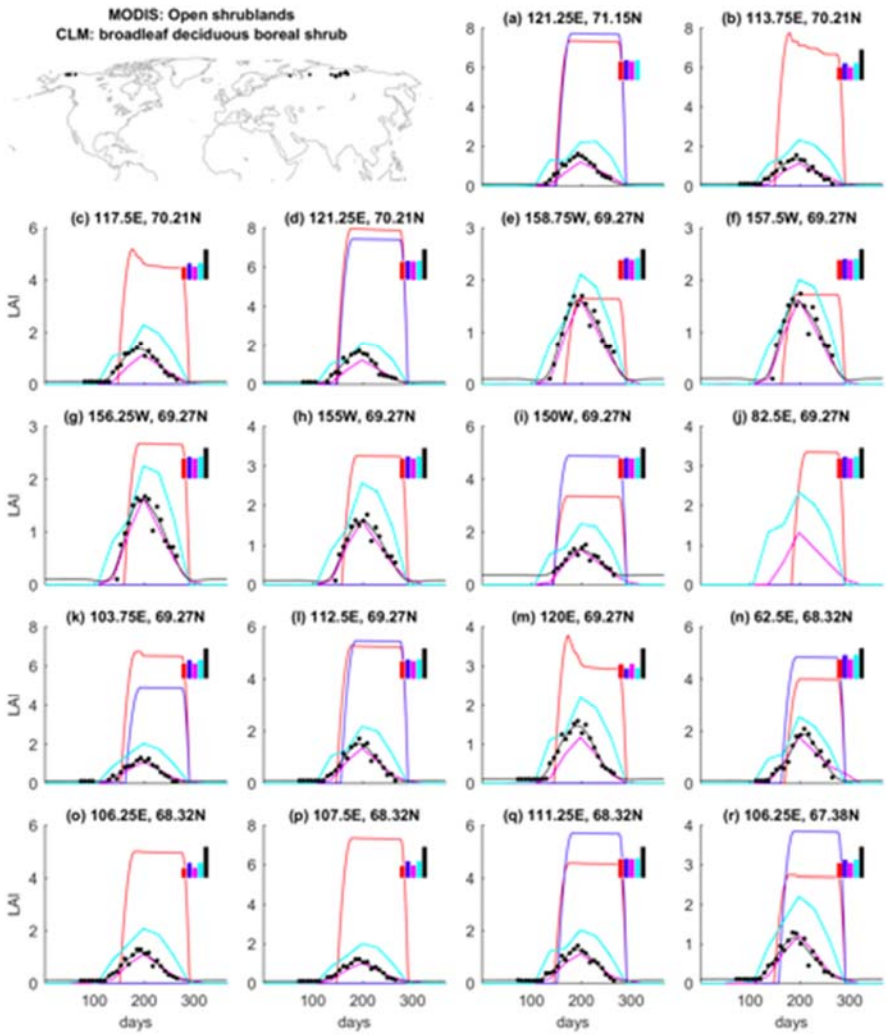

Figure 12. LAI seasonal cycles at open shrubland dominated locations in 2012. Grid points were selected based on area weight rank of open shrublands over the Northern Hemisphere in MODIS in the year of 2012. Corresponding CLM plant functional type plotted in this figure is broadleaf deciduous boreal shrub (BDSb). LAIs from CLM5 with GSWP3 forcing in 2012 is colored red while CLM4.5 with CRUNCEP forcing in 2012 is in blue. LAI from CLM5 satellite phenology mode is colored magenta and CLM4.5 SP is in cyan. Original 8-day composite of MODIS LAI in 2012 is represented with black dots and the fitted smoothing spline is plotted using black lines. Upper left panel shows the locations of all the grid cells. Panel (a)-(r) show the 2012 annual cycle of LAIs from different datasets at each grid cell with grid cell coordinates indicated in the panel title. The boxes in the upper right corner of each panel show the area weight of the land cover type or plant functional type within the grid cell in each dataset.

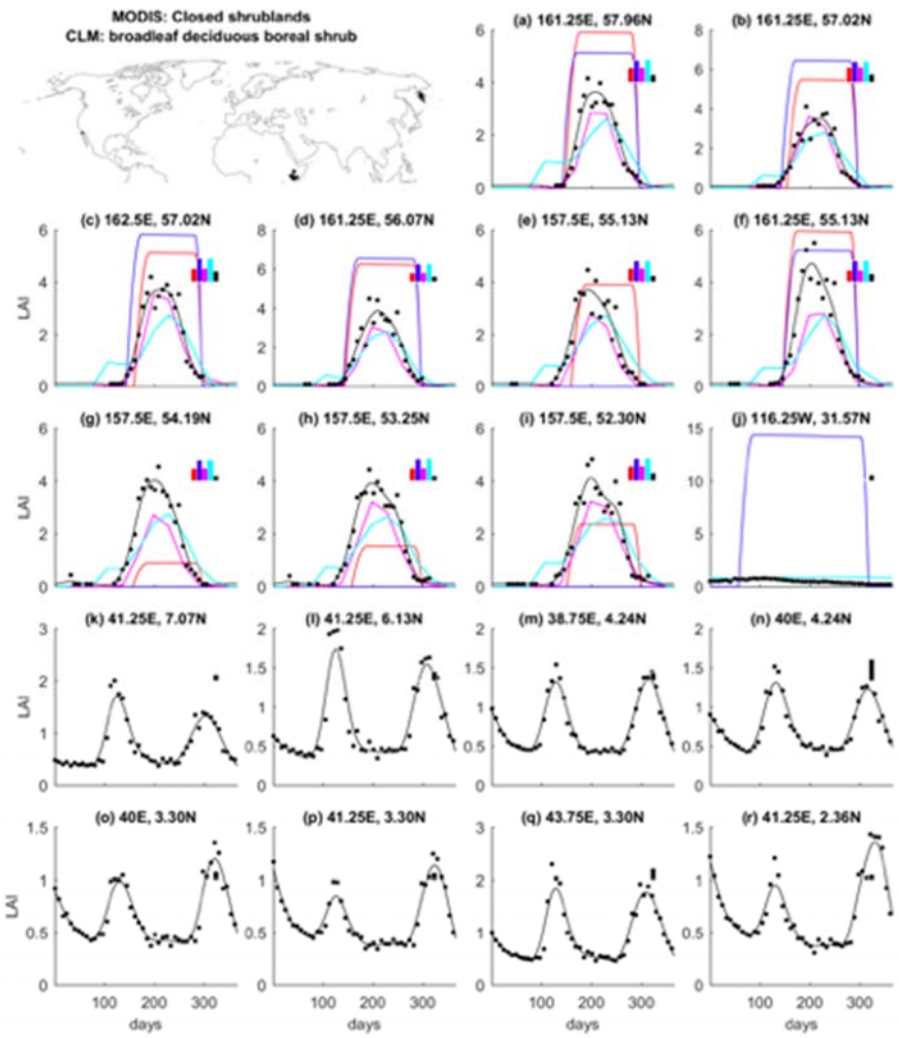

Figure 13. LAI seasonal cycles at closed shrubland dominated locations in 2012. Grid points were selected based on area weight rank of closed shrublands over the Northern Hemisphere in MODIS in the year of 2012. Corresponding CLM plant functional type plotted in this figure is broadleaf deciduous boreal shrub (BDSb). LAIs from CLM5 with GSWP3 forcing in 2012 is colored red while CLM4.5 with CRUNCEP forcing in 2012 is in blue. LAI from CLM5 satellite phenology mode is colored magenta and CLM4.5 SP is in cyan. Original 8-day composite of MODIS LAI in 2012 is represented with black dots and the fitted smoothing spline is plotted using black lines. Upper left panel shows the locations of all the grid cells. Panel (a)-(r) show the 2012 annual cycle of LAIs from different datasets at each grid cell with grid cell coordinates indicated in the panel title. The boxes in the upper right corner of each panel show the area weight of the land cover type or plant functional type within the grid cell in each dataset.

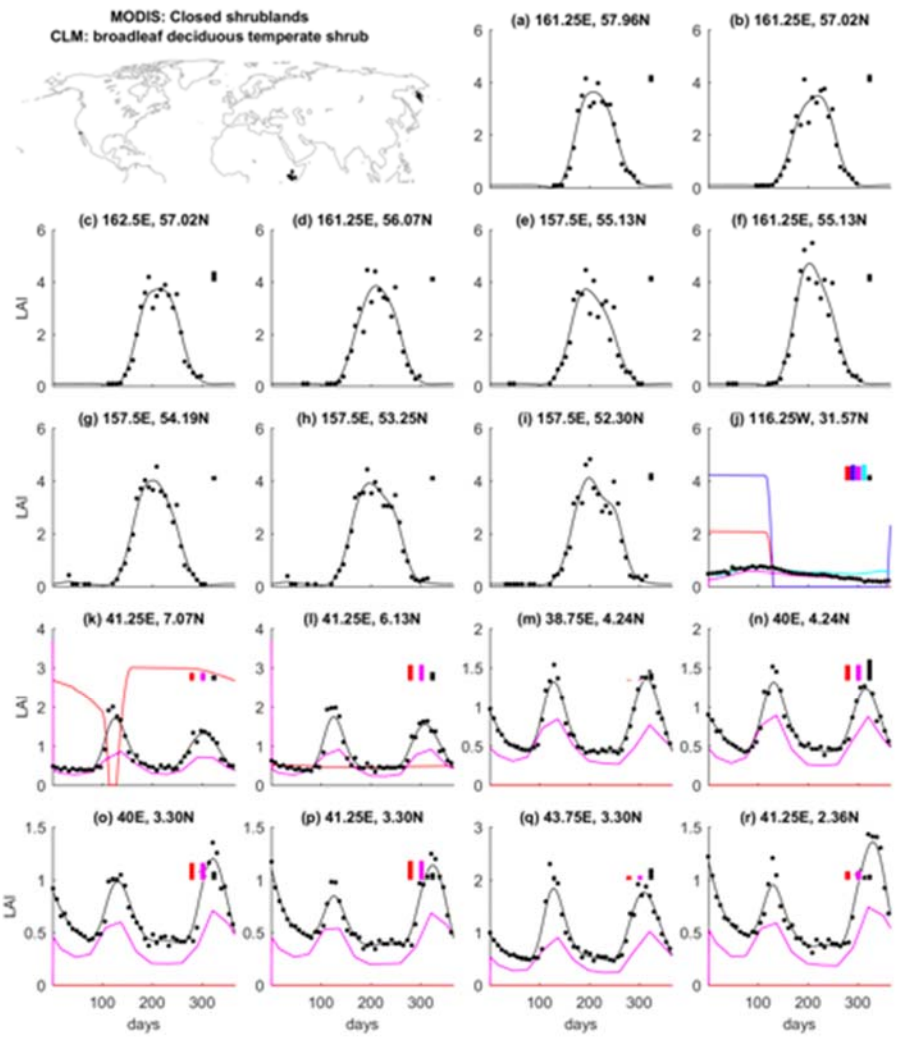

Figure 14. LAI seasonal cycles at closed shrubland dominated locations in 2012. Grid points were selected based on area weight rank of closed shrublands over the Northern Hemisphere in MODIS in the year of 2012. Corresponding CLM plant functional type plotted in this figure is broadleaf deciduous temperate shrub (BDSt). LAIs from CLM5 with GSWP3 forcing in 2012 is colored red while CLM4.5 with CRUNCEP forcing in 2012 is in blue. LAI from CLM5 satellite phenology mode is colored magenta and CLM4.5 SP is in cyan. Original 8-day composite of MODIS LAI in 2012 is represented with black dots and the fitted smoothing spline is plotted using black lines. Upper left panel shows the locations of all the grid cells. Panel (a)-(r) show the 2012 annual cycle of LAIs from different datasets at each grid cell with grid cell coordinates indicated in the panel title. The boxes in the upper right corner of each panel show the area weight of the land cover type or plant functional type within the grid cell in each dataset.

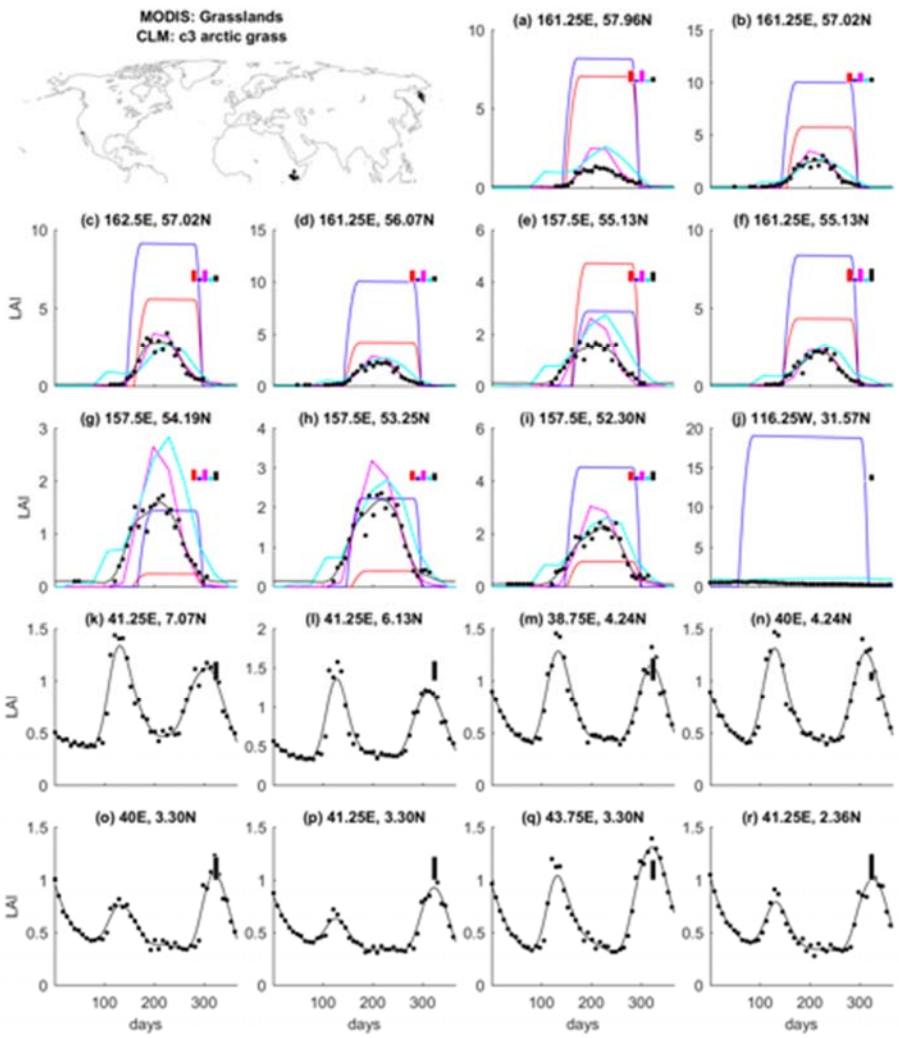

Figure 15. LAI seasonal cycles at closed shrubland dominated locations in 2012. Grid points were selected based on area weight rank of closed shrublands over the Northern Hemisphere in MODIS in the year of 2012. LAI seasonal cycles of grasslands are shown in this figure. Corresponding CLM plant functional type is C3 arctic grass (C3a). LAIs from CLM5 with GSWP3 forcing in 2012 is colored red while CLM4.5 with CRUNCEP forcing in 2012 is in blue. LAI from CLM5 satellite phenology mode is colored magenta and CLM4.5 SP is in cyan. Original 8-day composite of MODIS LAI in 2012 is represented with black dots and the fitted smoothing spline is plotted using black lines. Upper left panel shows the locations of all the grid cells. Panel (a)-(r) show the 2012 annual cycle of LAIs from different datasets at each grid cell with grid cell coordinates indicated in the panel title. The boxes in the upper right corner of each panel show the area weight of the land cover type or plant functional type within the grid cell in each dataset.

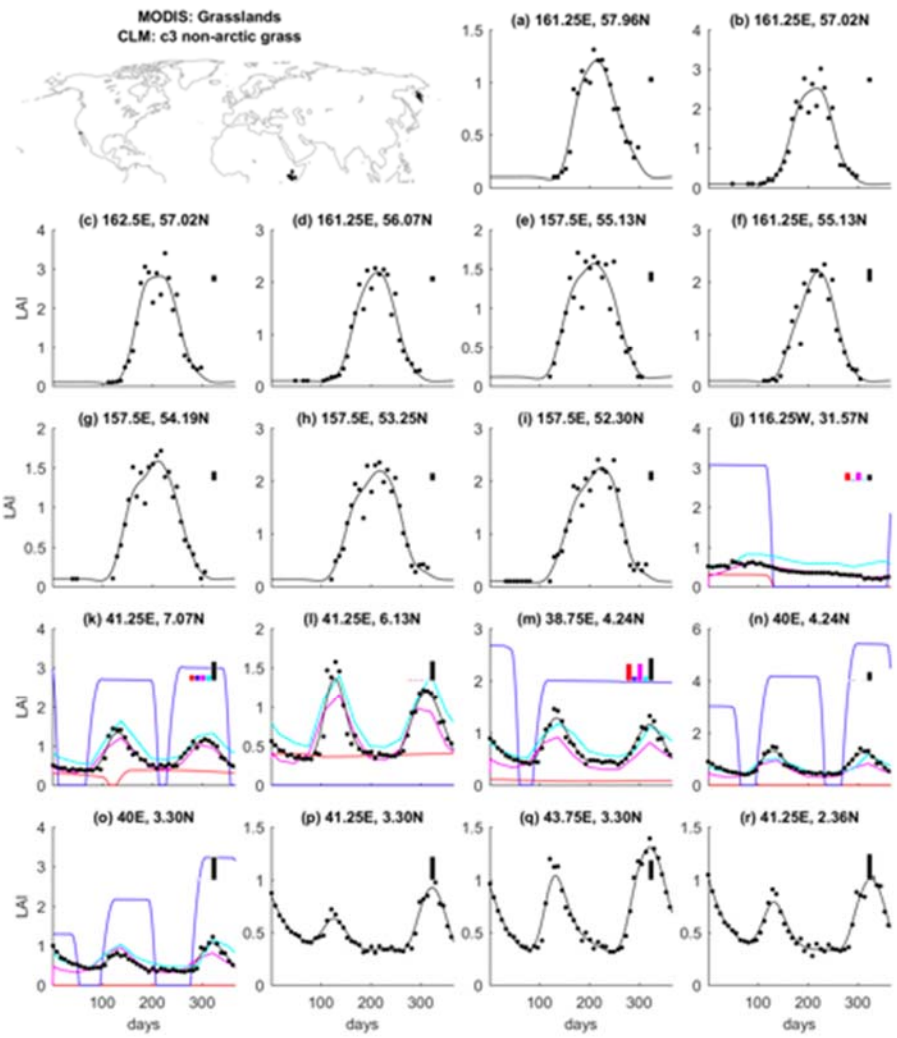

Figure 16. LAI seasonal cycles at closed shrubland dominated locations in 2012. Grid points were selected based on area weight rank of closed shrublands over the Northern Hemisphere in MODIS in the year of 2012. MODIS LAI seasonal cycles of grasslands are shown in this figure. Corresponding CLM plant functional type is C3 non-arctic grass (C3). LAIs from CLM5 with GSWP3 forcing in 2012 is colored red while CLM4.5 with CRUNCEP forcing in 2012 is in blue. LAI from CLM5 satellite phenology mode is colored magenta and CLM4.5 SP is in cyan. Original 8-day composite of MODIS LAI in 2012 is represented with black dots and the fitted smoothing spline is plotted using black lines. Upper left panel shows the locations of all the grid cells. Panel (a)-(r) show the 2012 annual cycle of LAIs from different datasets at each grid cell with grid cell coordinates indicated in the panel title. The boxes in the upper right corner of each panel show the area weight of the land cover type or plant functional type within the grid cell in each dataset.

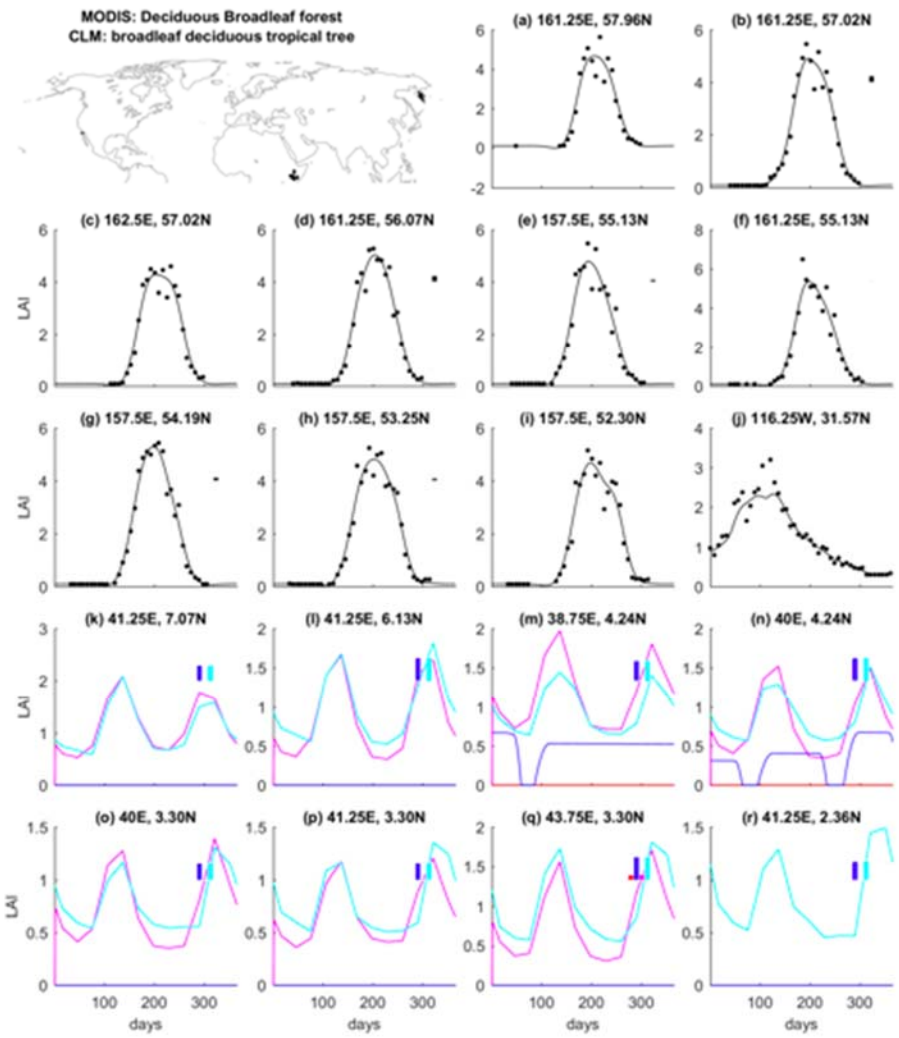

Figure 17. LAI seasonal cycles at closed shrubland dominated locations in 2012. Grid points were selected based on area weight rank of closed shrublands over the Northern Hemisphere in MODIS in the year of 2012. MODIS LAI seasonal cycles of broadleaf deciduous forests are shown in this figure. Corresponding CLM plant functional type is broadleaf deciduous tropical tree (BDTtrop). LAIs from CLM5 with GSWP3 forcing in 2012 is colored red while CLM4.5 with CRUNCEP forcing in 2012 is in blue. LAI from CLM5 satellite phenology mode is colored magenta and CLM4.5 SP is in cyan. Original 8-day composite of MODIS LAI in 2012 is represented with black dots and the fitted smoothing spline is plotted using black lines. Upper left panel shows the locations of all the grid cells. Panel (a)-(r) show the 2012 annual cycle of LAIs from different datasets at each grid cell with grid cell coordinates indicated in the panel title. The boxes in the upper right corner of each panel show the area weight of the land cover type or plant functional type within the grid cell in each dataset.

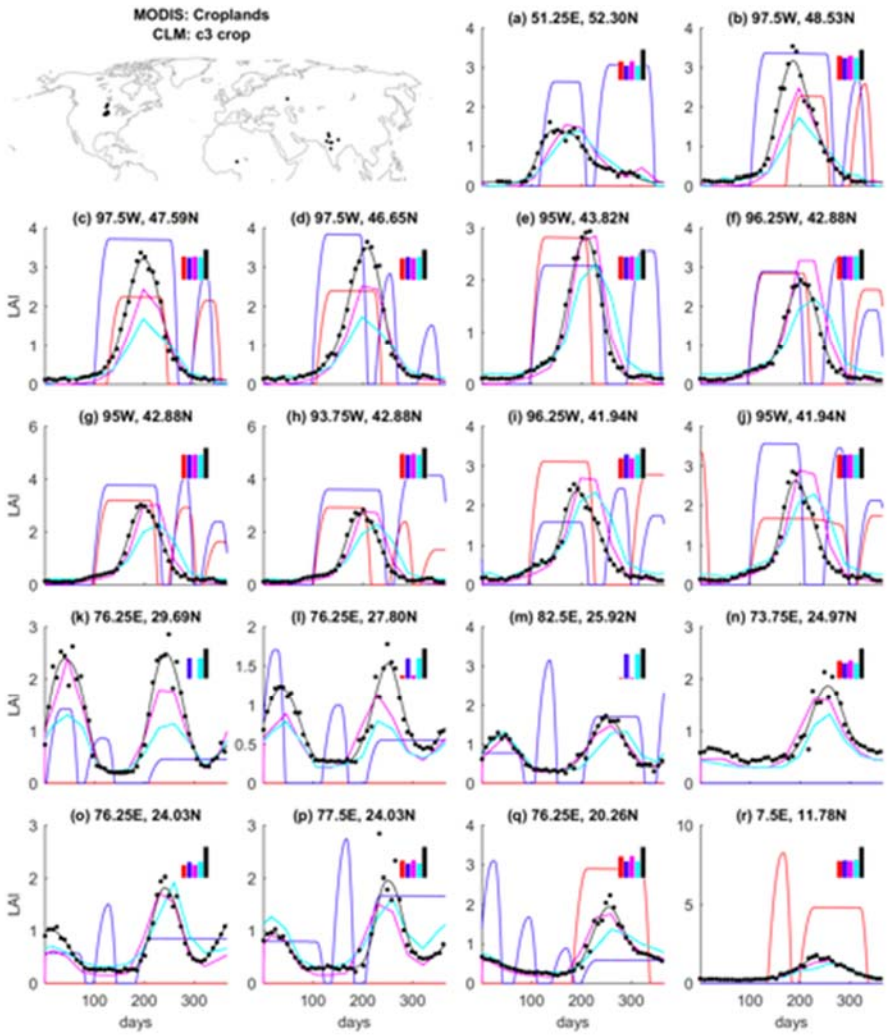

Figure 18. LAI seasonal cycles at cropland dominated locations in 2012. Grid points were selected based on area weight rank of croplands over the Northern Hemisphere in MODIS in the year of 2012. Corresponding CLM plant functional type is Crop1 in CLM4.5 and C3 Crop in CLM5. LAIs from CLM5 with GSWP3 forcing in 2012 is colored red while CLM4.5 with CRUNCEP forcing in 2012 is in blue. LAI from CLM5 satellite phenology mode is colored magenta and CLM4.5 SP is in cyan. Original 8-day composite of MODIS LAI in 2012 is represented with black dots and the fitted smoothing spline is plotted using black lines. Upper left panel shows the locations of all the grid cells. Panel (a)-(r) show the 2012 annual cycle of LAIs from different datasets at each grid cell with grid cell coordinates indicated in the panel title. The boxes in the upper right corner of each panel show the area weight of the land cover type or plant functional type within the grid cell in each dataset.

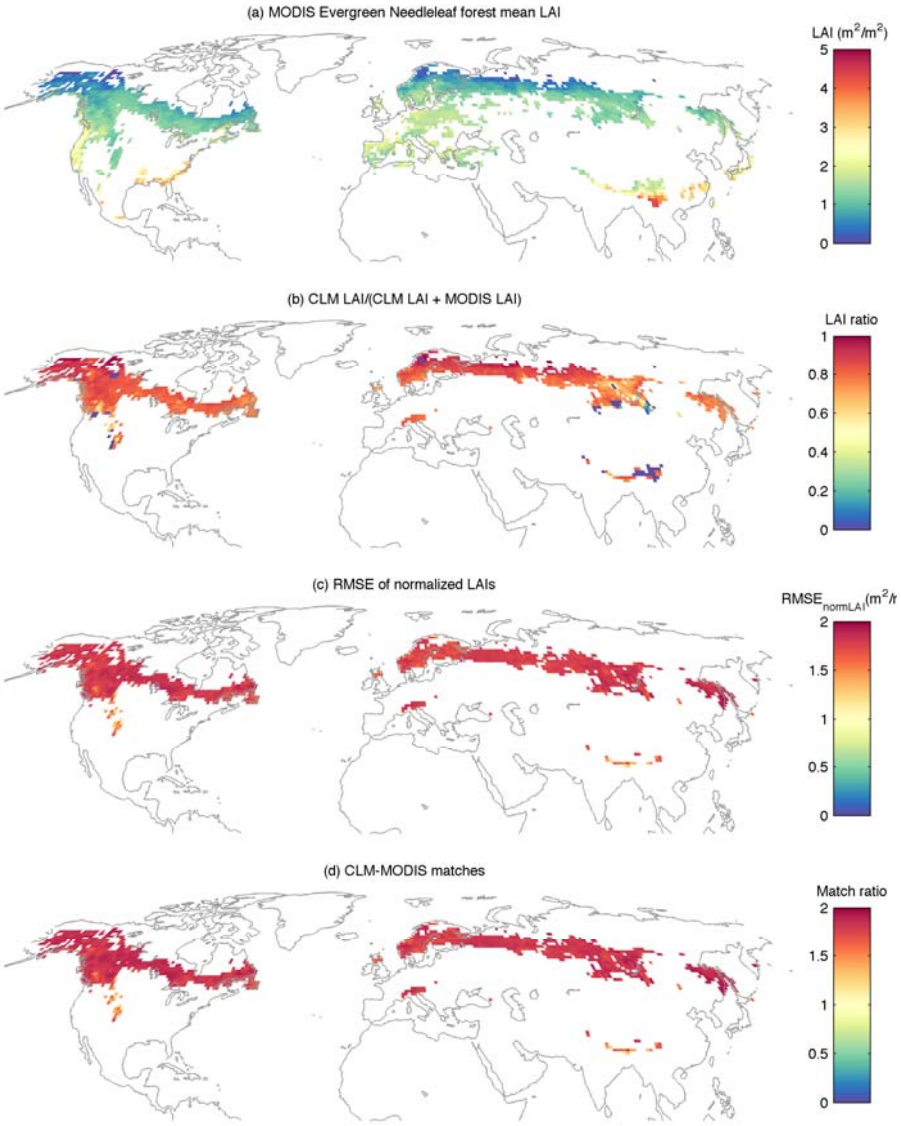

Figure 19. Maps showing agreement of LAI values and seasonal cycle between CLM5 with GSWP3 forcing and MODIS. (a): mean LAI for MODIS evergreen needleleaf forest averaged over 2003-2014. (b): summation of annual CLM evergreen needleleaf boreal tree LAI divided by summation of annual CLM evergreen needleleaf boreal tree LAI and annual MODIS evergreen needleleaf forest LAI, or the LAI ratio, averaged over 2003-2014. This ratio reflects how well CLM LAI values and seasonal amplitude match with MODIS. A LAI ratio close to 0.5 means good match. If LAI ratio is less than 0.5, then MODIS LAI is larger than CLM LAI over the course of a year, and vice versa. (c) RMSE between annually normalized LAIs in CLM and MODIS, averaged over 2003-2014. This ratio indicates agreement of LAI seasonal cycle between CLM and MODIS and smaller RMSE means better agreement. (d) overall match between CLM and MODIS LAI considering both LAI values and seasonal variation. Values closer to zero indicate larger agreement.

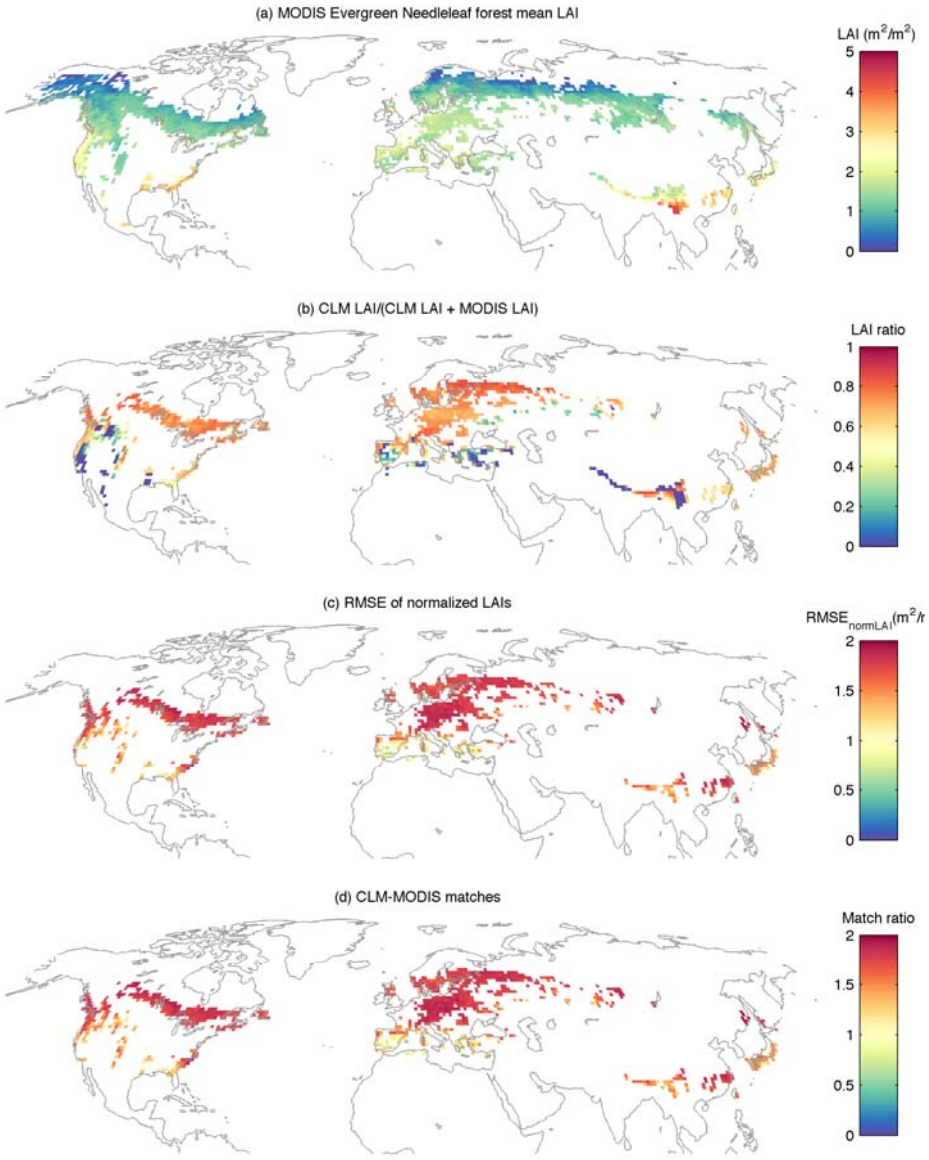

Figure 20. Maps showing agreement of LAI values and seasonal cycle between CLM5 with GSWP3 forcing and MODIS. (a): mean LAI for MODIS evergreen needleleaf forest averaged over 2003-2014. (b): summation of annual CLM evergreen needleleaf temperate tree LAI divided by summation of annual CLM evergreen needleleaf temperate tree LAI and annual MODIS evergreen needleleaf forest LAI, or the LAI ratio, averaged over 2003-2014. This ratio reflects how well CLM LAI values and seasonal amplitude match with MODIS. A LAI ratio close to 0.5 means good match. If LAI ratio is less than 0.5, then MODIS LAI is larger than CLM LAI over the course of a year, and vice versa. (c) RMSE between annually normalized LAIs in CLM and MODIS, averaged over 2003-2014. This ratio indicates agreement of LAI seasonal cycle between CLM and MODIS and smaller RMSE means better agreement. (d) overall match between CLM and MODIS LAI considering both LAI values and seasonal variation. Values closer to zero indicate larger agreement.

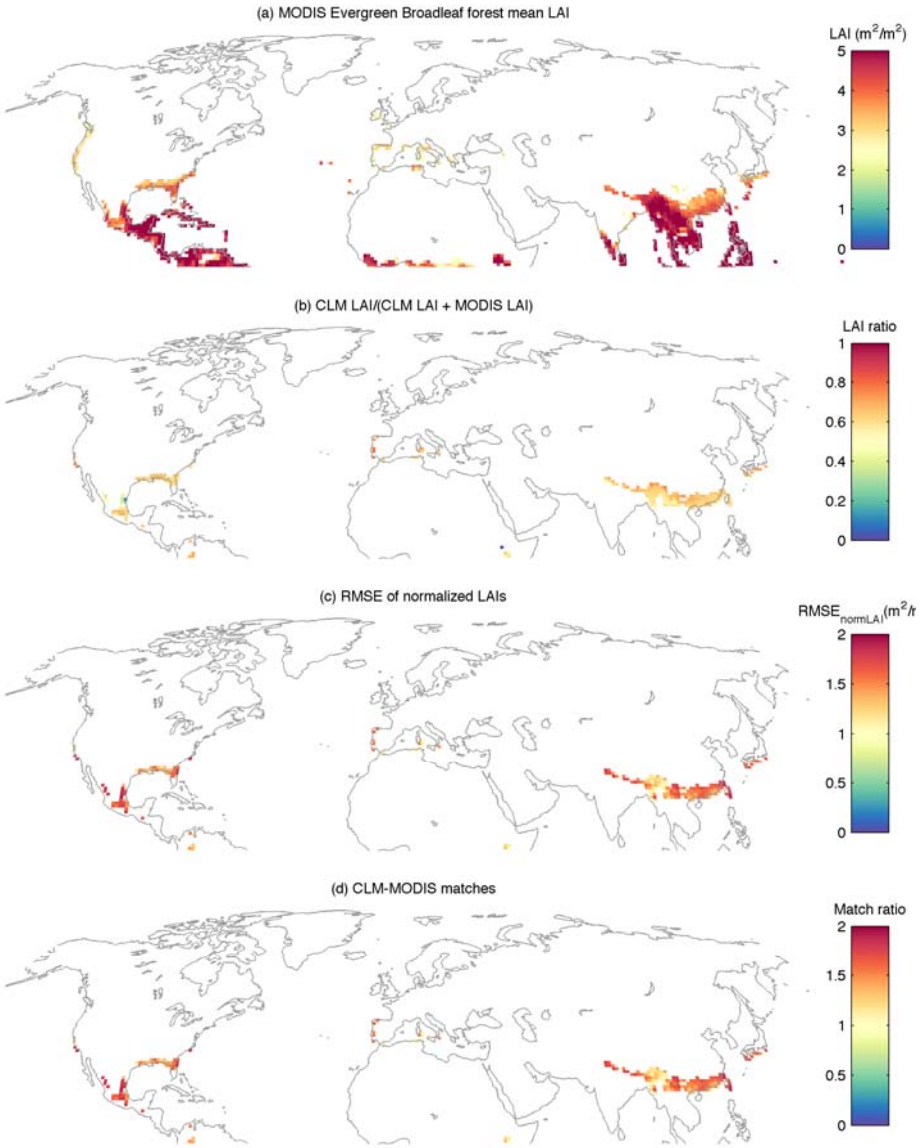

Figure 21. Maps showing agreement of LAI values and seasonal cycle between CLM5 with GSWP3 forcing and MODIS. (a): mean LAI for MODIS evergreen broadleaf forest averaged over 2003-2014. (b): summation of annual CLM evergreen broadleaf temperate tree LAI divided by summation of annual CLM evergreen broadleaf temperate tree LAI and annual MODIS evergreen broadleaf forest LAI, or the LAI ratio, averaged over 2003-2014. This ratio reflects how well CLM LAI values and seasonal amplitude match with MODIS. A LAI ratio close to 0.5 means good match. If LAI ratio is less than 0.5, then MODIS LAI is larger than CLM LAI over the course of a year, and vice versa. (c) RMSE between annually normalized LAIs in CLM and MODIS, averaged over 2003-2014. This ratio indicates agreement of LAI seasonal cycle between CLM and MODIS and smaller RMSE means better agreement. (d) overall match between CLM and MODIS LAI considering both LAI values and seasonal variation. Values closer to zero indicate larger agreement.

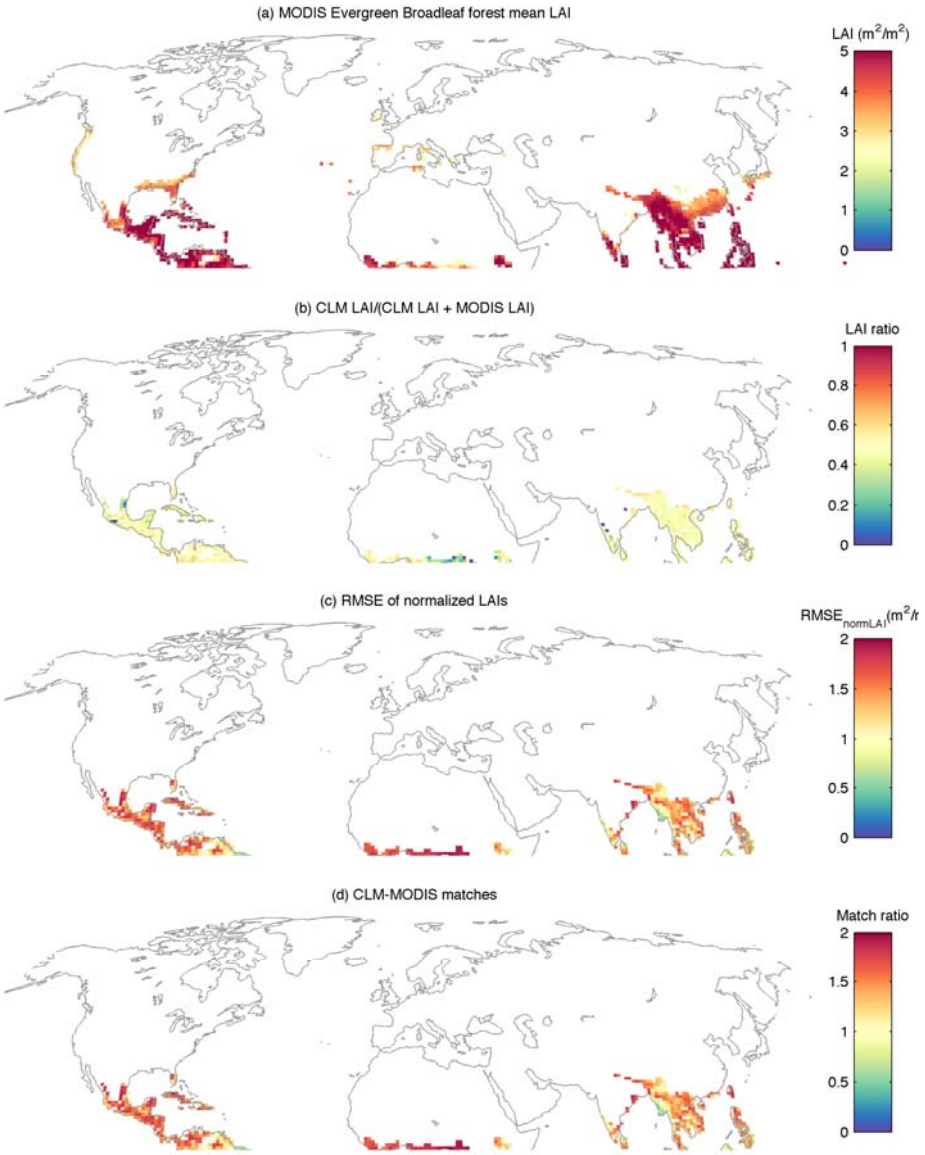

Figure 22. Maps showing agreement of LAI values and seasonal cycle between CLM5 with GSWP3 forcing and MODIS. (a): mean LAI for MODIS evergreen broadleaf forest averaged over 2003-2014. (b): summation of annual CLM evergreen broadleaf tropical tree LAI divided by summation of annual CLM evergreen broadleaf tropical tree LAI and annual MODIS evergreen broadleaf forest LAI, or the LAI ratio, averaged over 2003-2014. This ratio reflects how well CLM LAI values and seasonal amplitude match with MODIS. A LAI ratio close to 0.5 means good match. If LAI ratio is less than 0.5, then MODIS LAI is larger than CLM LAI over the course of a year, and vice versa. (c) RMSE between annually normalized LAIs in CLM and MODIS, averaged over 2003-2014. This ratio indicates agreement of LAI seasonal cycle between CLM and MODIS and smaller RMSE means better agreement. (d) overall match between CLM and MODIS LAI considering both LAI values and seasonal variation. Values closer to zero indicate larger agreement.

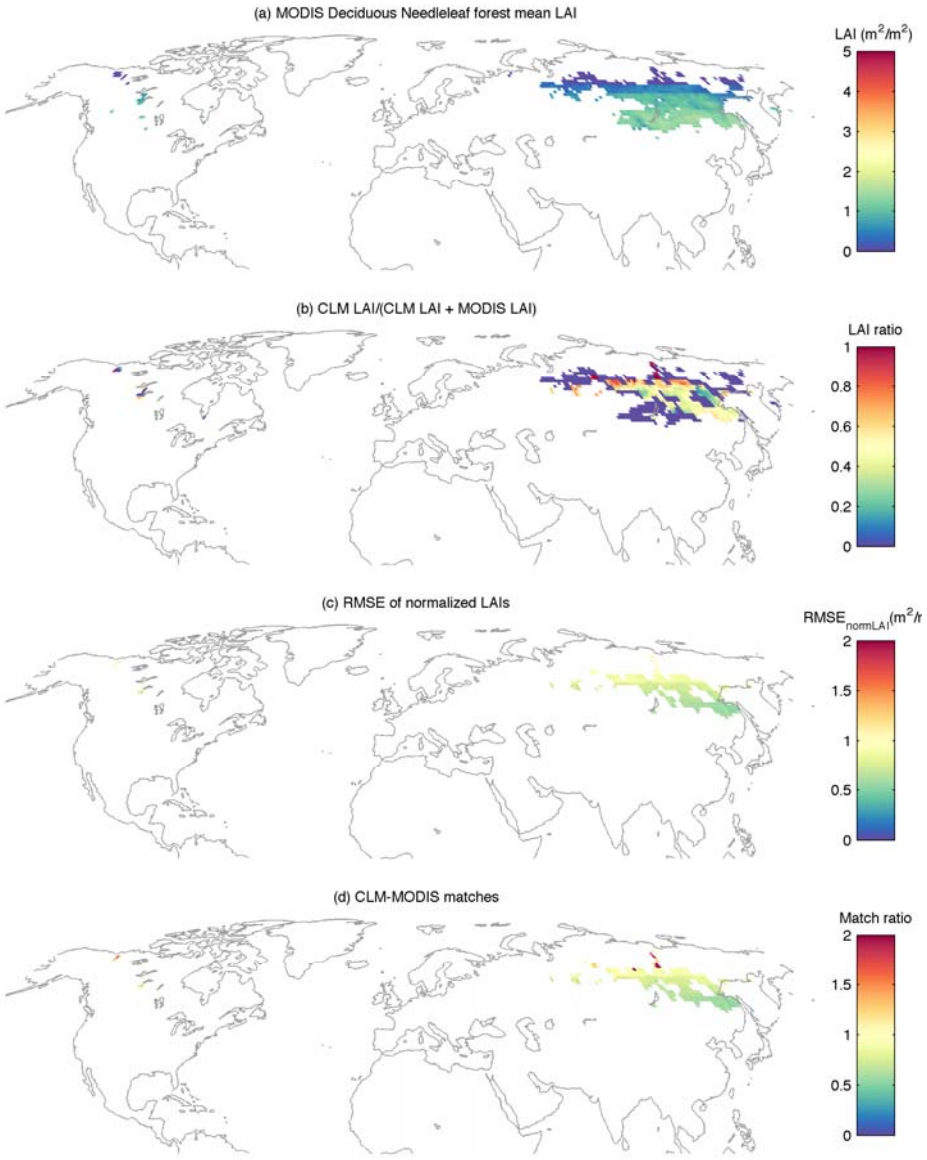

Figure 23. Maps showing agreement of LAI values and seasonal cycle between CLM5 with GSWP3 forcing and MODIS. (a): mean LAI for MODIS deciduous needleleaf forest averaged over 2003-2014. (b): summation of annual CLM deciduous needleleaf boreal tree LAI divided by summation of annual CLM deciduous needleleaf boreal tree LAI and annual MODIS deciduous needleleaf forest LAI, or the LAI ratio, averaged over 2003-2014. This ratio reflects how well CLM LAI values and seasonal amplitude match with MODIS. A LAI ratio close to 0.5 means good match. If LAI ratio is less than 0.5, then MODIS LAI is larger than CLM LAI over the course of a year, and vice versa. (c) RMSE between annually normalized LAIs in CLM and MODIS, averaged over 2003-2014. This ratio indicates agreement of LAI seasonal cycle between CLM and MODIS and smaller RMSE means better agreement. (d) overall match between CLM and MODIS LAI considering both LAI values and seasonal variation. Values closer to zero indicate larger agreement.

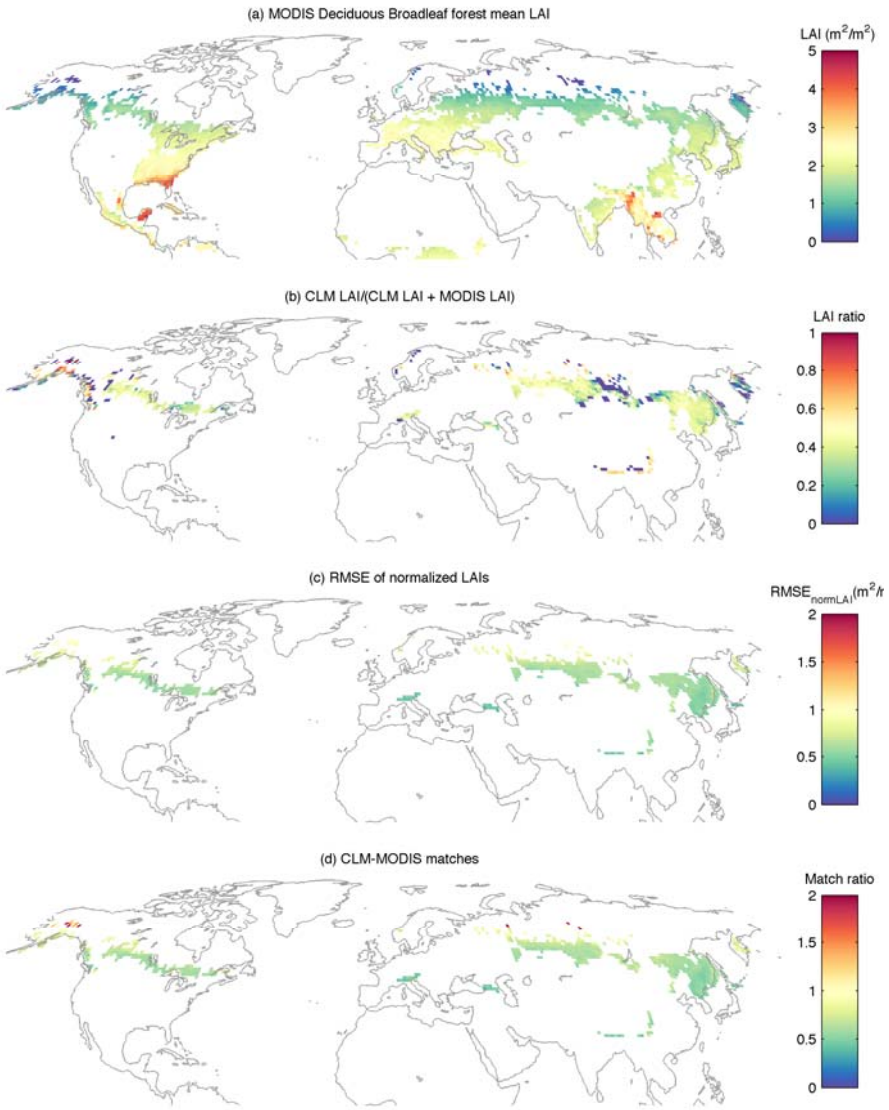

Figure 24. Maps showing agreement of LAI values and seasonal cycle between CLM5 with GSWP3 forcing and MODIS. (a): mean LAI for MODIS deciduous broadleaf forest averaged over 2003-2014. (b): summation of annual CLM deciduous broadleaf boreal tree LAI divided by summation of annual CLM deciduous broadleaf boreal tree LAI and annual MODIS deciduous broadleaf forest LAI, or the LAI ratio, averaged over 2003-2014. This ratio reflects how well CLM LAI values and seasonal amplitude match with MODIS. A LAI ratio close to 0.5 means good match. If LAI ratio is less than 0.5, then MODIS LAI is larger than CLM LAI over the course of a year, and vice versa. (c) RMSE between annually normalized LAIs in CLM and MODIS, averaged over 2003-2014. This ratio indicates agreement of LAI seasonal cycle between CLM and MODIS and smaller RMSE means better agreement. (d) overall match between CLM and MODIS LAI considering both LAI values and seasonal variation. Values closer to zero indicate larger agreement.

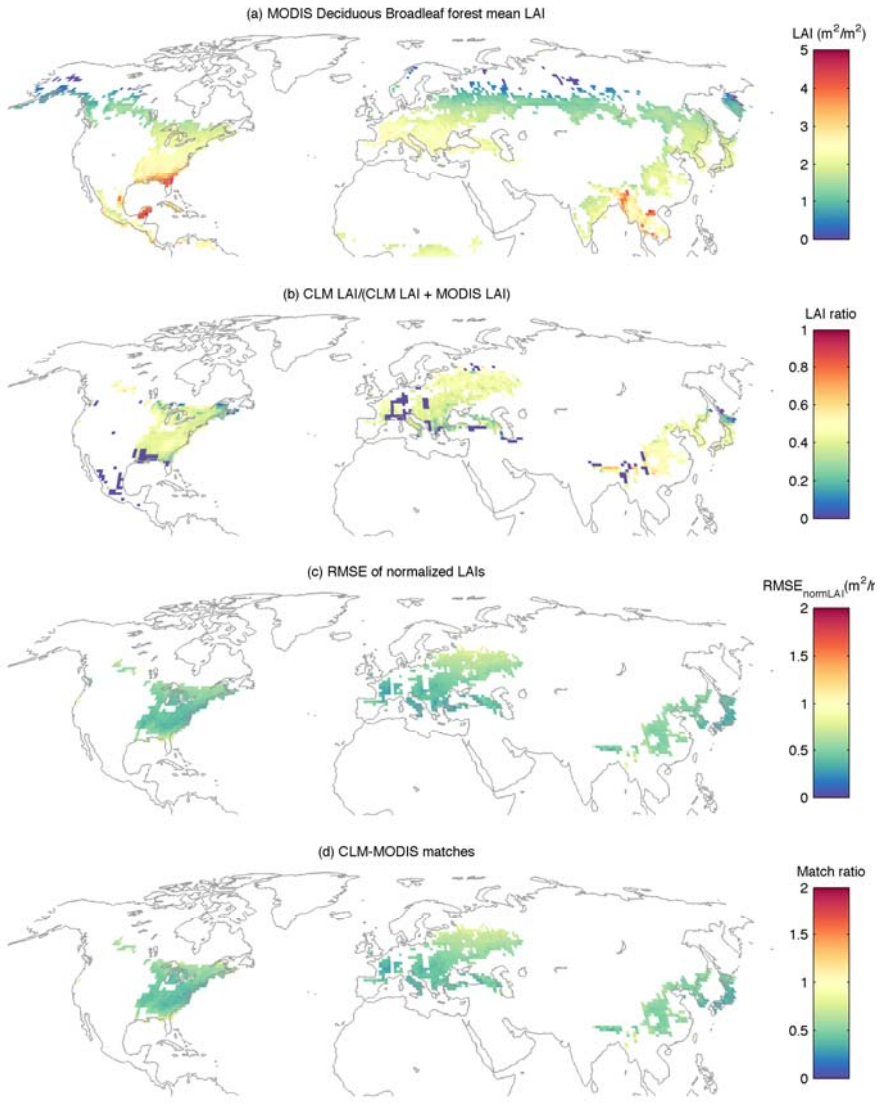

Figure 25. Maps showing agreement of LAI values and seasonal cycle between CLM5 with GSWP3 forcing and MODIS. (a): mean LAI for MODIS deciduous broadleaf forest averaged over 2003-2014. (b): summation of annual CLM deciduous broadleaf temperate tree LAI divided by summation of annual CLM deciduous broadleaf temperate tree LAI and annual MODIS deciduous broadleaf forest LAI, or the LAI ratio, averaged over 2003-2014. This ratio reflects how well CLM LAI values and seasonal amplitude match with MODIS. A LAI ratio close to 0.5 means good match. If LAI ratio is less than 0.5, then MODIS LAI is larger than CLM LAI over the course of a year, and vice versa. (c) RMSE between annually normalized LAIs in CLM and MODIS, averaged over 2003-2014. This ratio indicates agreement of LAI seasonal cycle between CLM and MODIS and smaller RMSE means better agreement. (d) overall match between CLM and MODIS LAI considering both LAI values and seasonal variation. Values closer to zero indicate larger agreement.

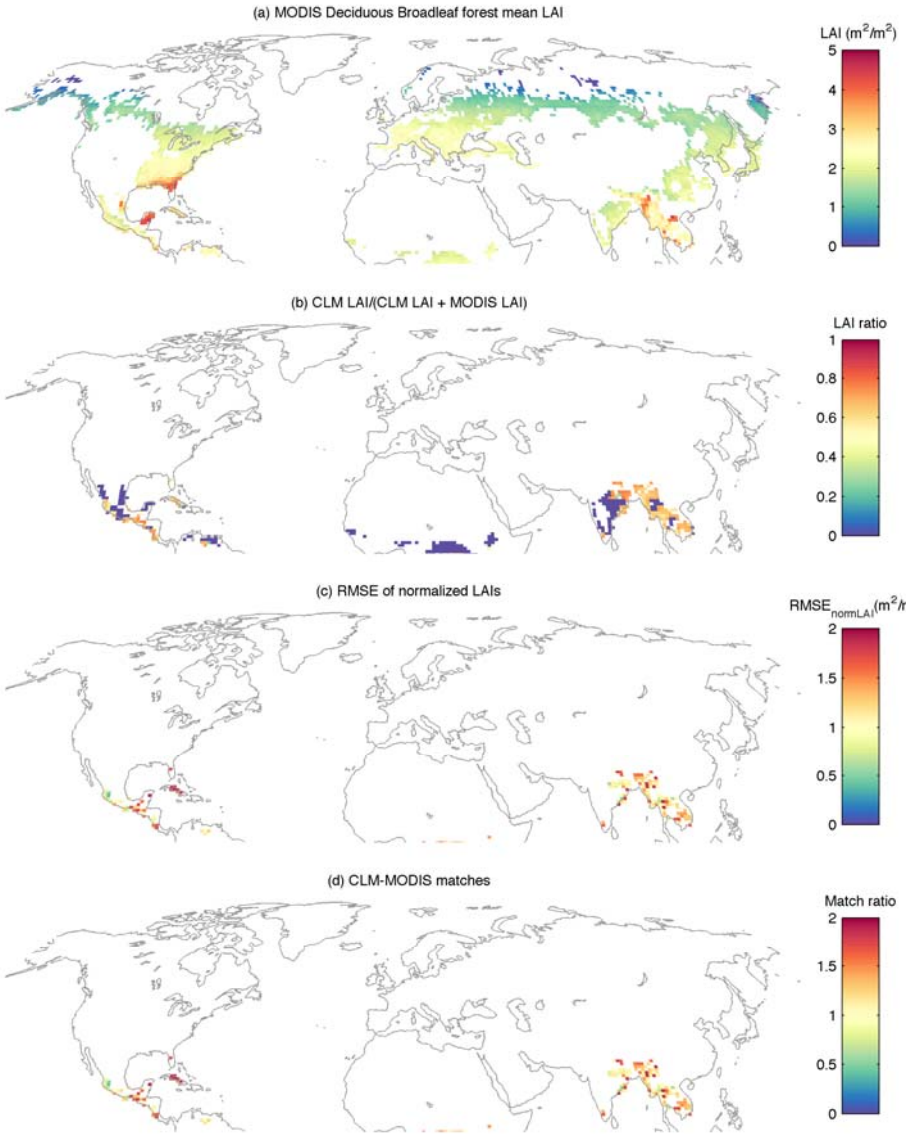

Figure 26. Maps showing agreement of LAI values and seasonal cycle between CLM5 with GSWP3 forcing and MODIS. (a): mean LAI for MODIS deciduous broadleaf forest averaged over 2003-2014. (b): summation of annual CLM deciduous broadleaf tropical tree LAI divided by summation of annual CLM deciduous broadleaf tropical tree LAI and annual MODIS deciduous broadleaf forest LAI, or the LAI ratio, averaged over 2003-2014. This ratio reflects how well CLM LAI values and seasonal amplitude match with MODIS. A LAI ratio close to 0.5 means good match. If LAI ratio is less than 0.5, then MODIS LAI is larger than CLM LAI over the course of a year, and vice versa. (c) RMSE between annually normalized LAIs in CLM and MODIS, averaged over 2003-2014. This ratio indicates agreement of LAI seasonal cycle between CLM and MODIS and smaller RMSE means better agreement. (d) overall match between CLM and MODIS LAI considering both LAI values and seasonal variation. Values closer to zero indicate larger agreement.

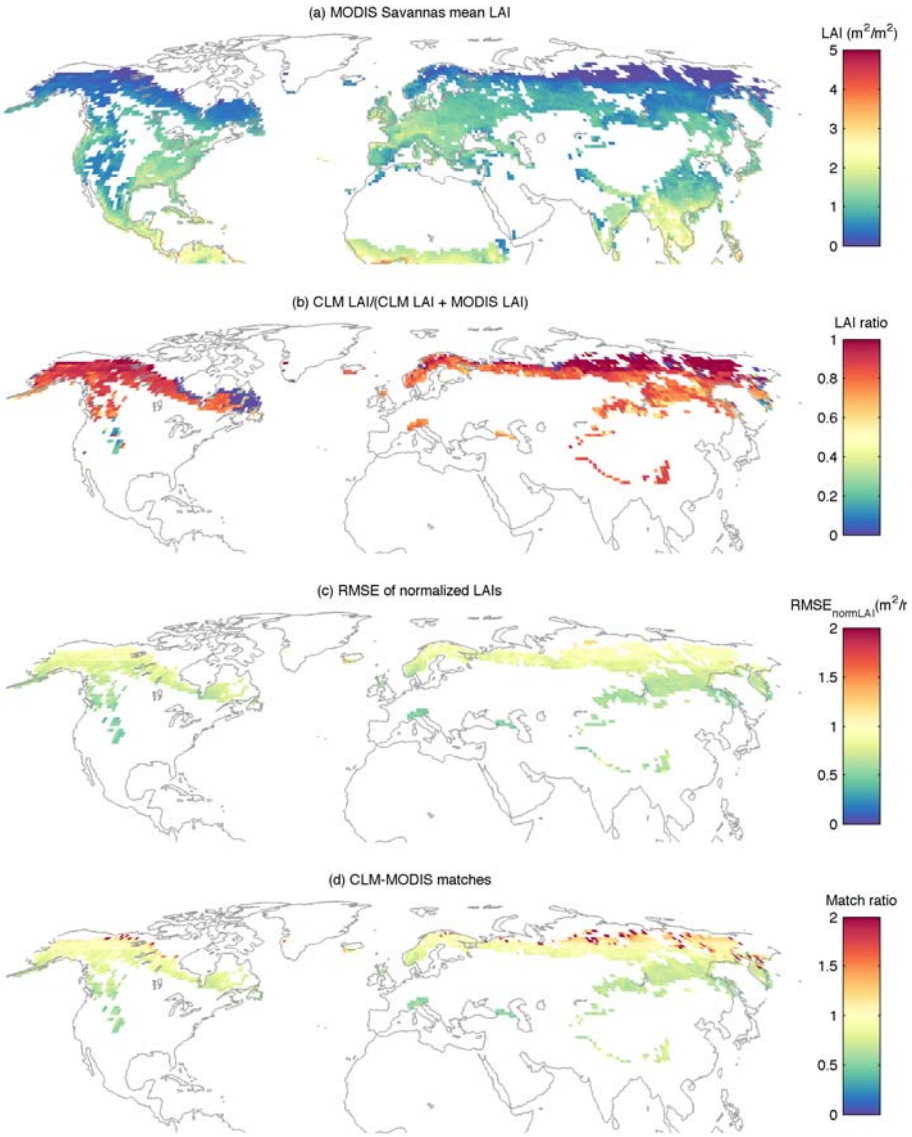

Figure 27. Maps showing agreement of LAI values and seasonal cycle between CLM5 with GSWP3 forcing and MODIS. (a): mean LAI for MODIS savannas averaged over 2003-2014. (b): summation of annual CLM C3 arctic grass LAI divided by summation of annual CLM C3 arctic grass LAI and annual MODIS savanna LAI, or the LAI ratio, averaged over 2003-2014. This ratio reflects how well CLM LAI values and seasonal amplitude match with MODIS. A LAI ratio close to 0.5 means good match. If LAI ratio is less than 0.5, then MODIS LAI is larger than CLM LAI over the course of a year, and vice versa. (c) RMSE between annually normalized LAIs in CLM and MODIS, averaged over 2003-2014. This ratio indicates agreement of LAI seasonal cycle between CLM and MODIS and smaller RMSE means better agreement. (d) overall match between CLM and MODIS LAI considering both LAI values and seasonal variation. Values closer to zero indicate larger agreement.

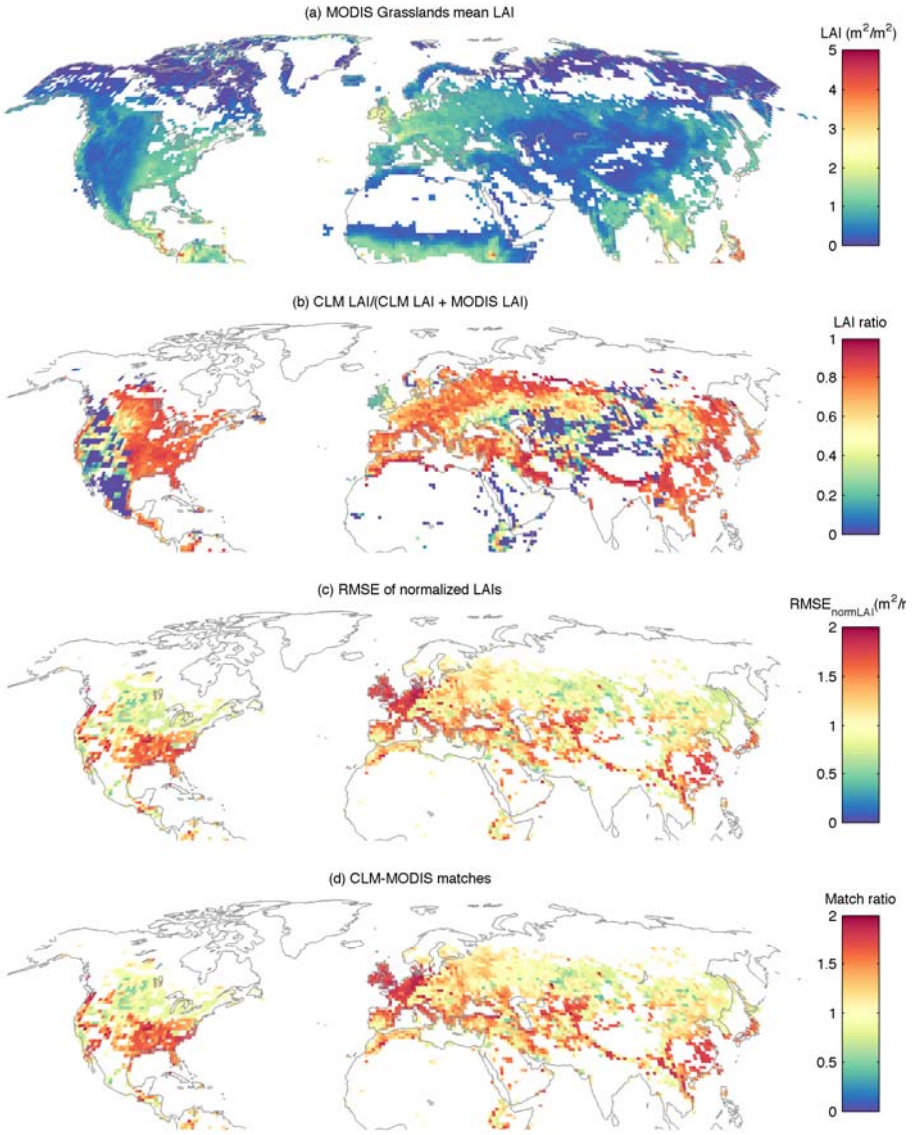

Figure 28. Maps showing agreement of LAI values and seasonal cycle between CLM5 with GSWP3 forcing and MODIS. (a): mean LAI for MODIS grassland averaged over 2003-2014. (b): summation of annual CLM C3 non-arctic grass LAI divided by summation of annual CLM C3 non-arctic grass LAI and annual MODIS grassland LAI, or the LAI ratio, averaged over 2003-2014. This ratio reflects how well CLM LAI values and seasonal amplitude match with MODIS. A LAI ratio close to 0.5 means good match. If LAI ratio is less than 0.5, then MODIS LAI is larger than CLM LAI over the course of a year, and vice versa. (c) RMSE between annually normalized LAIs in CLM and MODIS, averaged over 2003-2014. This ratio indicates agreement of LAI seasonal cycle between CLM and MODIS and smaller RMSE means better agreement. (d) overall match between CLM and MODIS LAI considering both LAI values and seasonal variation. Values closer to zero indicate larger agreement.

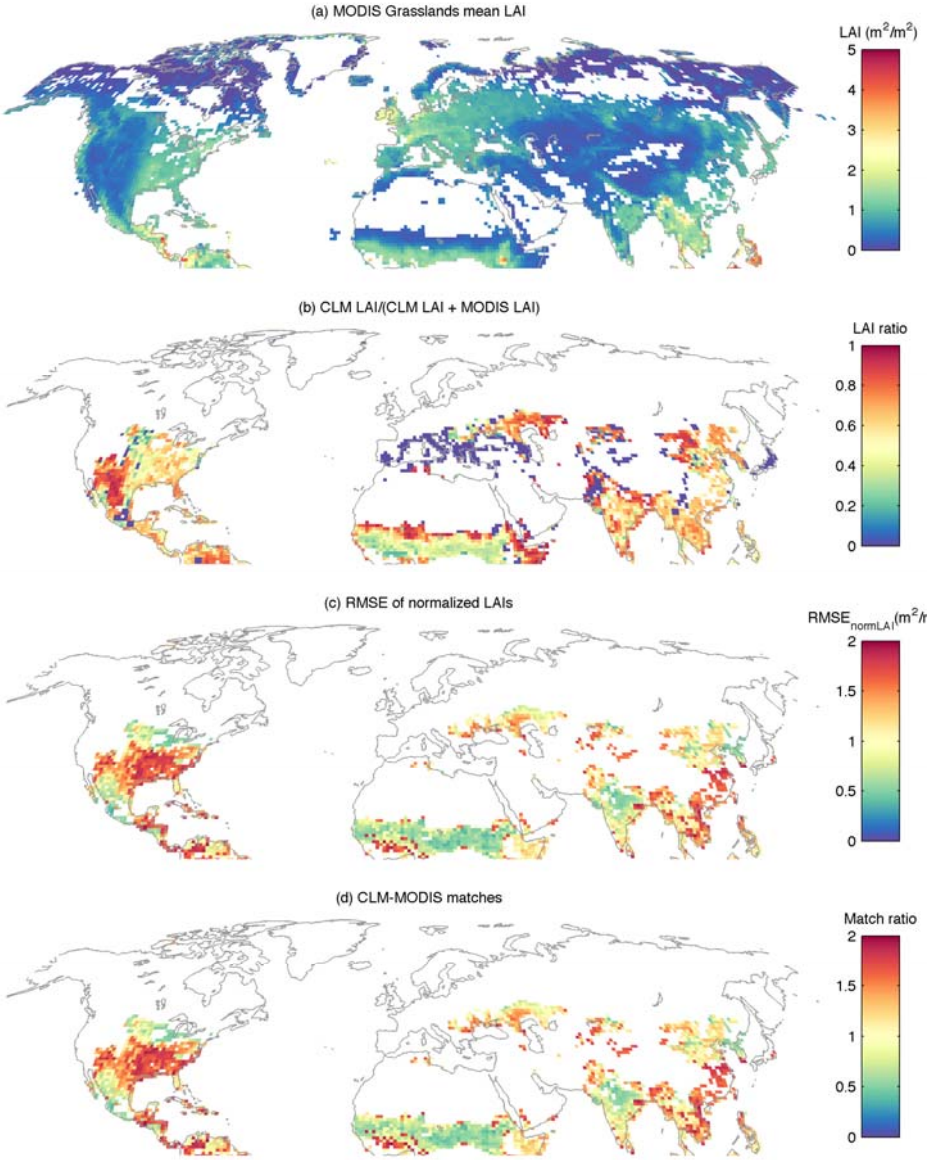

Figure 29. Maps showing agreement of LAI values and seasonal cycle between CLM5 with GSWP3 forcing and MODIS. (a): mean LAI for MODIS grassland averaged over 2003-2014. (b): summation of annual CLM C4 grass LAI divided by summation of annual CLM C4 grass LAI and annual MODIS grassland LAI, or the LAI ratio, averaged over 2003-2014. This ratio reflects how well CLM LAI values and seasonal amplitude match with MODIS. A LAI ratio close to 0.5 means good match. If LAI ratio is less than 0.5, then MODIS LAI is larger than CLM LAI over the course of a year, and vice versa. (c) RMSE between annually normalized LAIs in CLM and MODIS, averaged over 2003-2014. This ratio indicates agreement of LAI seasonal cycle between CLM and MODIS and smaller RMSE means better agreement. (d) overall match between CLM and MODIS LAI considering both LAI values and seasonal variation. Values closer to zero indicate larger agreement.

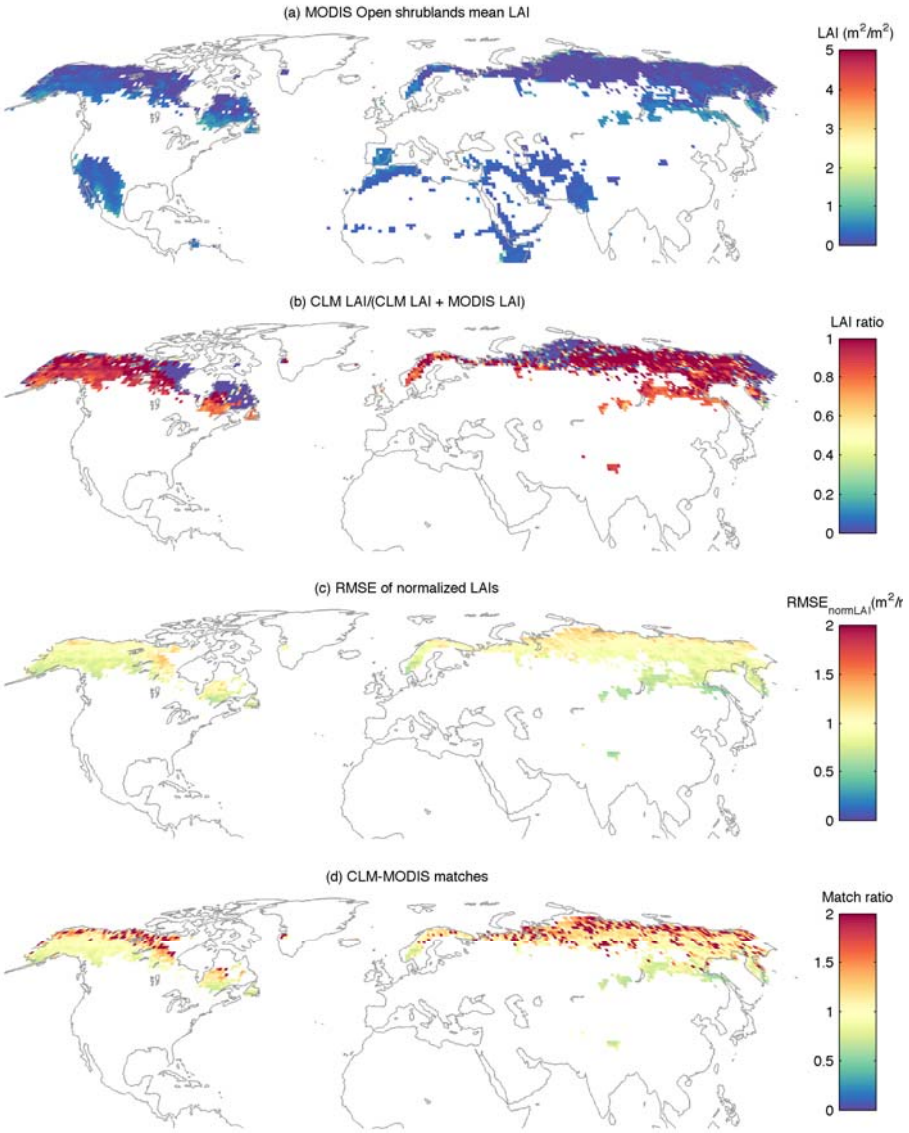

Figure 30. Maps showing agreement of LAI values and seasonal cycle between CLM5 with GSWP3 forcing and MODIS. (a): mean LAI for MODIS open shrubland averaged over 2003-2014. (b): summation of annual CLM broadleaf deciduous boreal shrub LAI divided by summation of annual CLM broadleaf deciduous boreal shrub LAI and annual MODIS open shrubland LAI, or the LAI ratio, averaged over 2003-2014. This ratio reflects how well CLM LAI values and seasonal amplitude match with MODIS. A LAI ratio close to 0.5 means good match. If LAI ratio is less than 0.5, then MODIS LAI is larger than CLM LAI over the course of a year, and vice versa. (c) RMSE between annually normalized LAIs in CLM and MODIS, averaged over 2003-2014. This ratio indicates agreement of LAI seasonal cycle between CLM and MODIS and smaller RMSE means better agreement. (d) overall match between CLM and MODIS LAI considering both LAI values and seasonal variation. Values closer to zero indicate larger agreement.

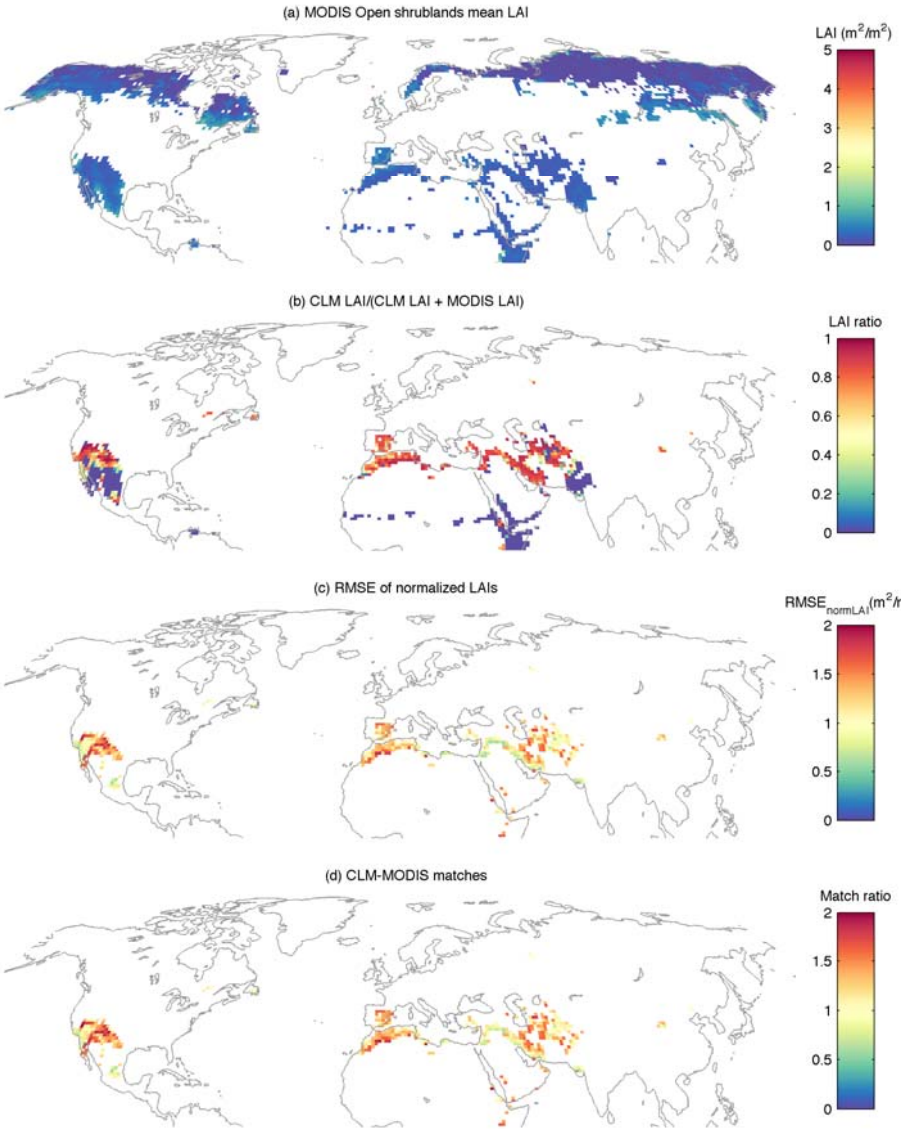

Figure 31. Maps showing agreement of LAI values and seasonal cycle between CLM5 with GSWP3 forcing and MODIS. (a): mean LAI for MODIS open shrubland averaged over 2003-2014. (b): summation of annual CLM broadleaf deciduous temperate shrub LAI divided by summation of annual CLM broadleaf deciduous temperate shrub LAI and annual MODIS open shrubland LAI, or the LAI ratio, averaged over 2003-2014. This ratio reflects how well CLM LAI values and seasonal amplitude match with MODIS. A LAI ratio close to 0.5 means good match. If LAI ratio is less than 0.5, then MODIS LAI is larger than CLM LAI over the course of a year, and vice versa. (c) RMSE between annually normalized LAIs in CLM and MODIS, averaged over 2003-2014. This ratio indicates agreement of LAI seasonal cycle between CLM and MODIS and smaller RMSE means better agreement. (d) overall match between CLM and MODIS LAI considering both LAI values and seasonal variation. Values closer to zero indicate larger agreement.

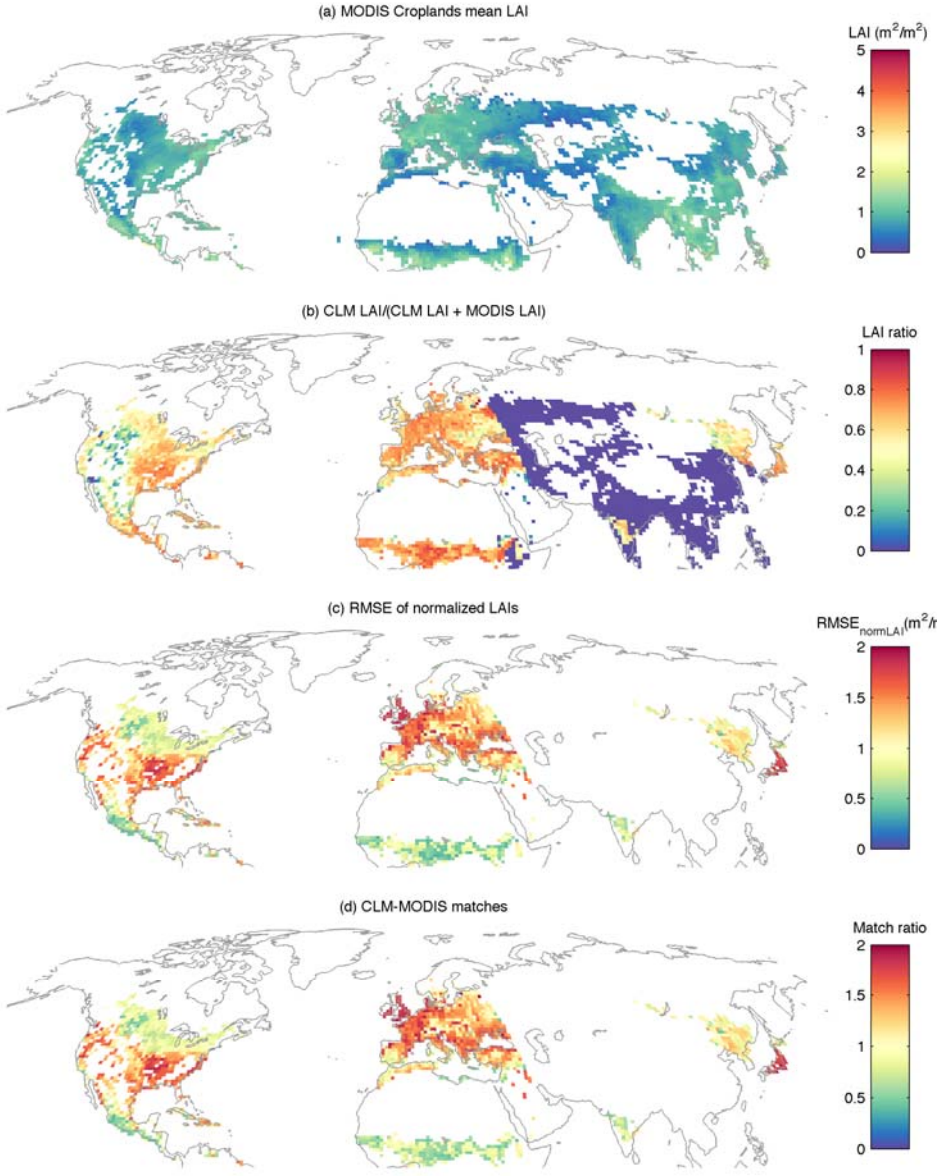

Figure 32. Maps showing agreement of LAI values and seasonal cycle between CLM5 with GSWP3 forcing and MODIS. (a): mean LAI for MODIS cropland averaged over 2003-2014. (b): summation of annual CLM C3 crop LAI divided by summation of annual CLM C3 crop LAI and annual MODIS cropland LAI, or the LAI ratio, averaged over 2003-2014. This ratio reflects how well CLM LAI values and seasonal amplitude match with MODIS. A LAI ratio close to 0.5 means good match. If LAI ratio is less than 0.5, then MODIS LAI is larger than CLM LAI over the course of a year, and vice versa. (c) RMSE between annually normalized LAIs in CLM and MODIS, averaged over 2003-2014. This ratio indicates agreement of LAI seasonal cycle between CLM and MODIS and smaller RMSE means better agreement. (d) overall match between CLM and MODIS LAI considering both LAI values and seasonal variation. Values closer to zero indicate larger agreement.

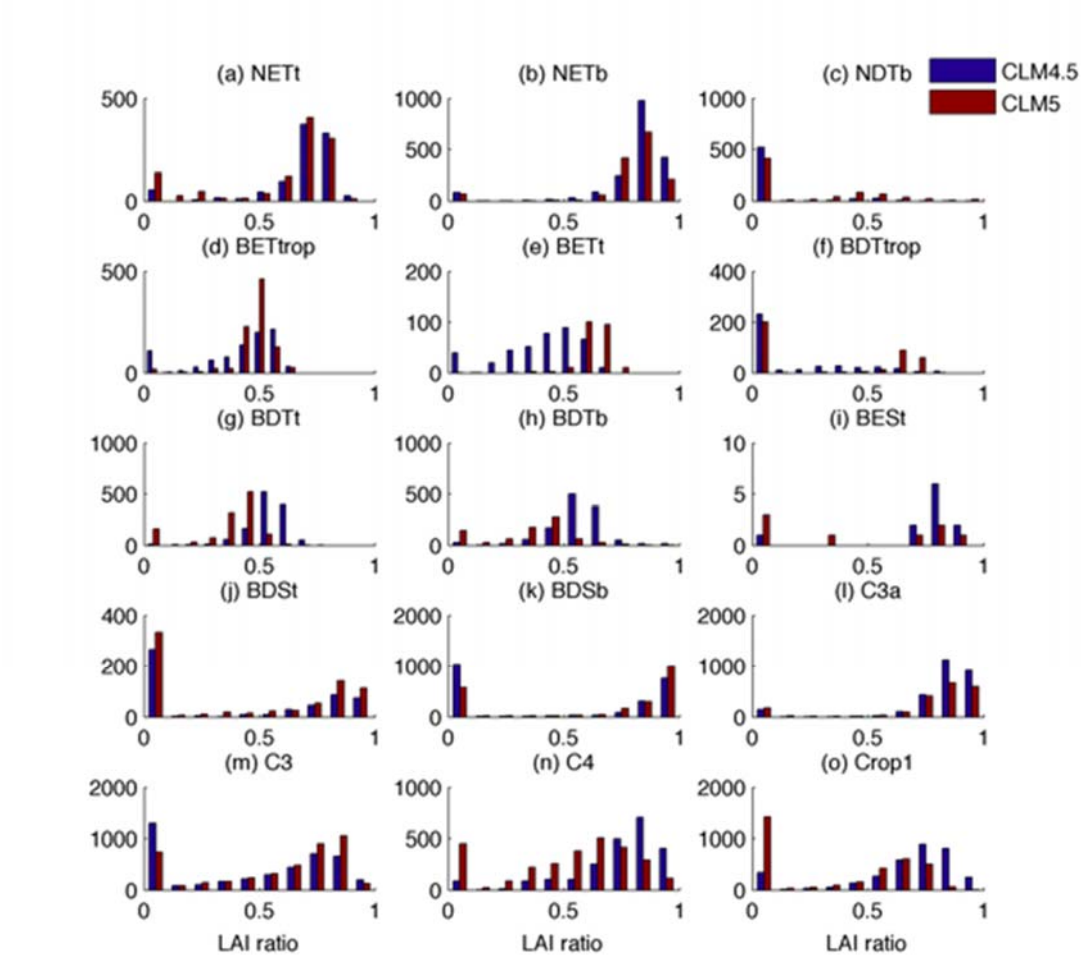

Figure 33. LAI ratios of different PFTs in CLM4.5 and CLM5, averaged over 2003-2014. Each value represents the meA LAI ratio of the PFT at one grid point. LAI ratio is defined as the summation of annual CLM LAI divided by summation of annual CLM LAI and annual MODIS LAI of corresponding land cover type. This ratio reflects how well CLM LAI values and seasonal amplitude match with MODIS. A LAI ratio close to 0.5 means good match. If LAI ratio is less than 0.5, then MODIS LAI is larger than CLM LAI over the course of a year, and vice versa. Plant functional types shown in this figure are: NETt: needleleaf evergreen temperate tree; NETb: needleleaf evergreen boreal tree; NDTb: needleleaf deciduous boreal tree; BETtrop: broadleaf evergreen tropical tree; BETt: broadleaf evergreen temperate tree; BDTtrop: broadleaf deciduous tropical tree; BDTt: broadleaf deciduous temperate tree; BDTb: broadleaf deciduous boreal tree; BES: broadleaf evergreen temperate shrub; BDSt: broadleaf deciduous temperate shrub; BDSb: broadleaf deciduous boreal shrub; C3a: C3 arctic grass; C3: C3 non-arctic grass; C4: C4 grass; Crop1: C3 generic crop.

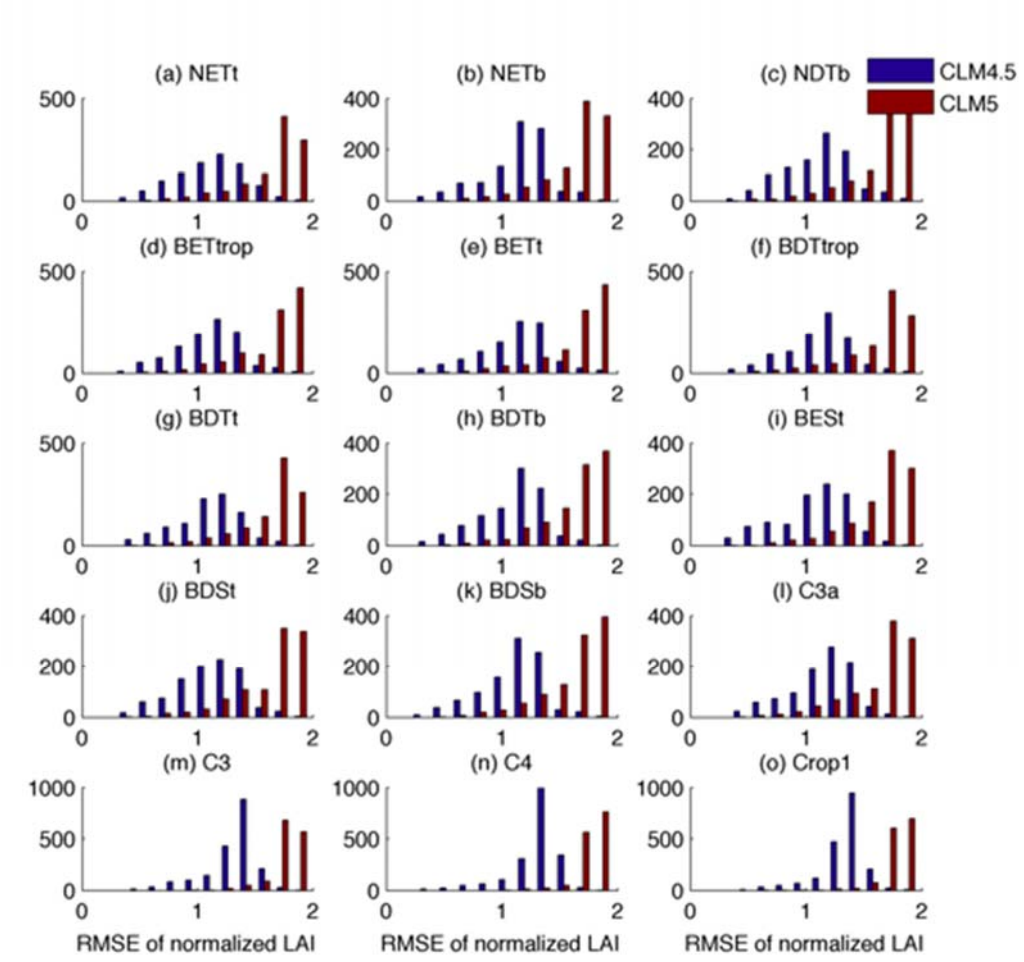

Figure 34. RMSE between normalized annual CLM and MODIS LAI for CLM4.5 and CLM5, respectively, averaged over 2003-2014. Each value represents the mean RMSE between normalized annual CLM and MODIS LAI at one grid point for the denoted PFT. Smaller RMSE indicates better agreement between CLM and MODIS LAI seasonal variation. Plant functional types shown in this figure are: NETt: needleleaf evergreen temperate tree; NETb: needleleaf evergreen boreal tree; NDTb: needleleaf deciduous boreal tree; BETtrop: broadleaf evergreen tropical tree; BETt: broadleaf evergreen temperate tree; BDTtrop: broadleaf deciduous tropical tree; BDTt: broadleaf deciduous temperate tree; BDTb: broadleaf deciduous boreal tree; BES: broadleaf evergreen temperate shrub; BDSt: broadleaf deciduous temperate shrub; BDSb: broadleaf deciduous boreal shrub; C3a: C3 arctic grass; C3: C3 non-arctic grass; C4: C4 grass; Crop1: C3 generic crop.

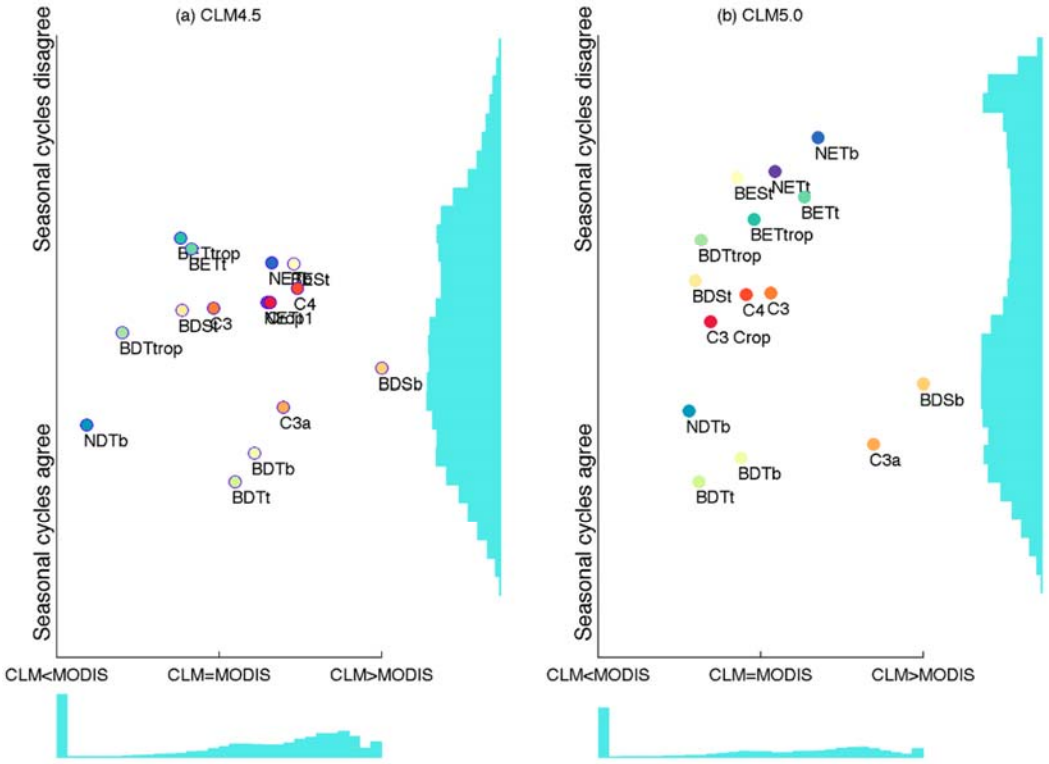

Figure 35. Plots showing LAI ratios and RMSE between normalized annual CLM and MODIS LAI for different PFTs in CLM4.5 and CLM5. Both LAI ratios and RMSE are averaged over 2003-2014 for each PFT. Lower and right panels of histograms show the distribution of LAI ratios and RMSEs from all grid points of all PFTs, respectively. Plant functional types shown in this figure are: NETt: needleleaf evergreen temperate tree; NETb: needleleaf evergreen boreal tree; NDTb: needleleaf deciduous boreal tree; BETtrop: broadleaf evergreen tropical tree; BETt: broadleaf evergreen temperate tree; BDTtrop: broadleaf deciduous tropical tree; BDTt: broadleaf deciduous temperate tree; BDTb: broadleaf deciduous boreal tree; BES: broadleaf evergreen temperate shrub; BDSt: broadleaf deciduous temperate shrub; BDSb: broadleaf deciduous boreal shrub; C3a: C3 arctic grass; C3: C3 non-arctic grass; C4: C4 grass; Crop1: C3 generic crop.

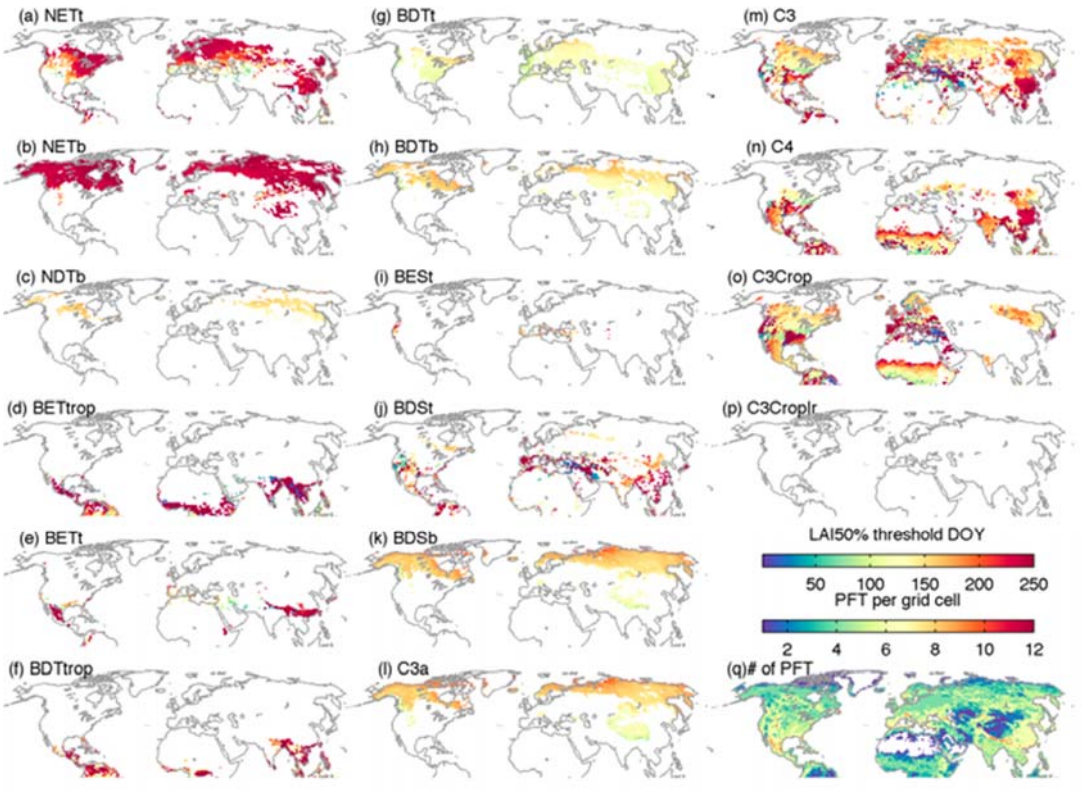

Figure 36. Maps showing day of the year when 50% threshold of LAI annual amplitude is reached within each PFT in CLM5. (a)-(p) mean DOY of LAI 50% threshold, averaged over 2003-2014. (q) number of PFTs coexist at each grid cell. Plant functional types shown in this figure are: NETt: needleleaf evergreen temperate tree; NETb: needleleaf evergreen boreal tree; NDTb: needleleaf deciduous boreal tree; BETtrop: broadleaf evergreen tropical tree; BETt: broadleaf evergreen temperate tree; BDTtrop: broadleaf deciduous tropical tree; BDTt: broadleaf deciduous temperate tree; BDTb: broadleaf deciduous boreal tree; BES: broadleaf evergreen temperate shrub; BDSt: broadleaf deciduous temperate shrub; BDSb: broadleaf deciduous boreal shrub; C3a: C3 arctic grass; C3: C3 non-arctic grass; C4: C4 grass; C3Crop: C3 generic Crop; C3CropIr: C3 generic crop with irrigation.

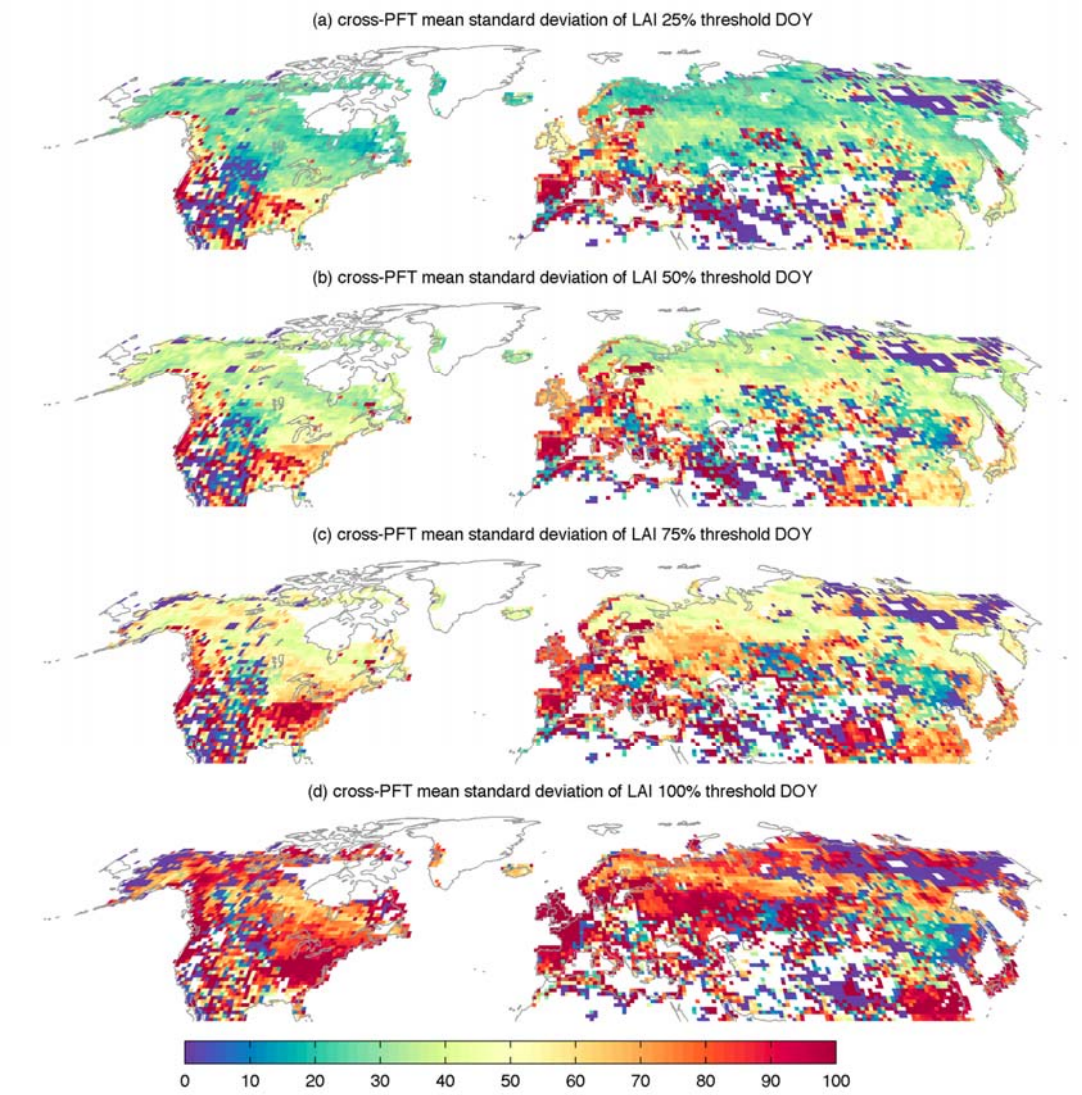

Figure 37. Maps showing cross-PFT standard deviation of the day of the year when each threshold of LAI annual amplitude is reached within each PFT in CLM5, average between 2003-2014. This value shows how different spring onset timing is between different PFTs coexisting in the same grid cell.

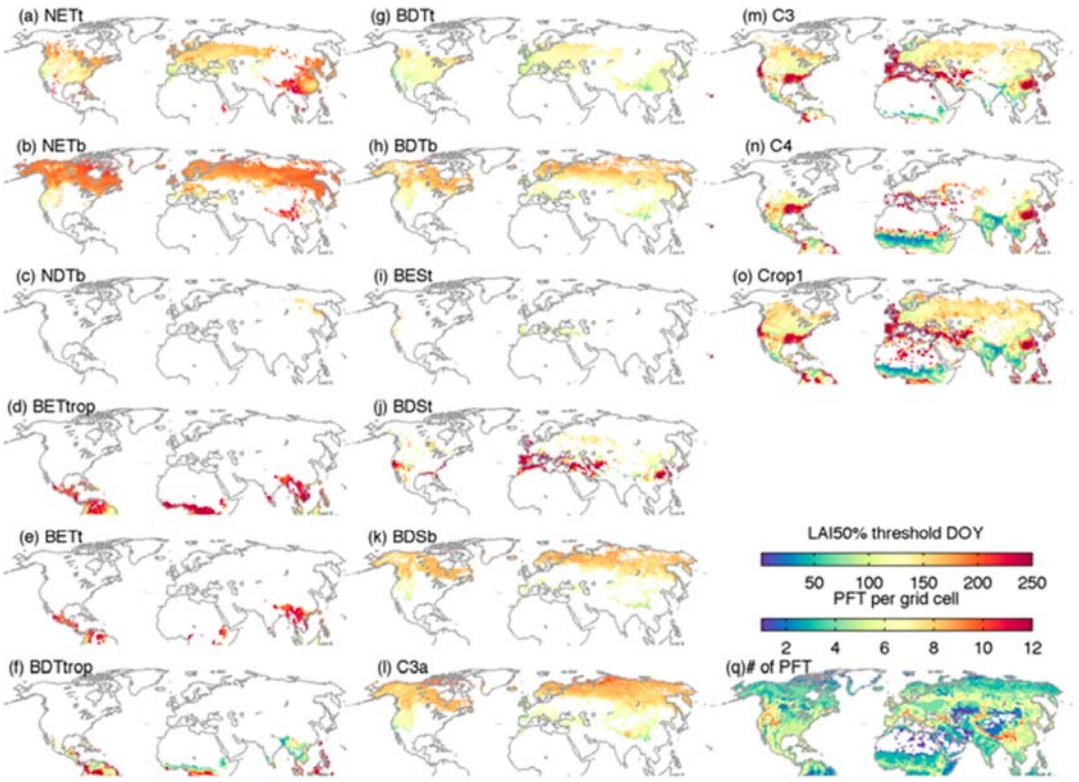

Figure 38. Maps showing day of the year when 50% threshold of LAI annual amplitude is reached within each PFT in CLM4.5. (a)-(p) mean DOY of LAI 50% threshold, averaged over 2003-2014. (q) number of PFTs coexist at each grid cell. Plant functional types shown in this figure are: NETt: needleleaf evergreen temperate tree; NETb: needleleaf evergreen boreal tree; NDTb: needleleaf deciduous boreal tree; BETtrop: broadleaf evergreen tropical tree; BETt: broadleaf evergreen temperate tree; BDTtrop: broadleaf deciduous tropical tree; BDTt: broadleaf deciduous temperate tree; BDTb: broadleaf deciduous boreal tree; BES: broadleaf evergreen temperate shrub; BDSt: broadleaf deciduous temperate shrub; BDSb: broadleaf deciduous boreal shrub; C3a: C3 arctic grass; C3: C3 non-arctic grass; C4: C4 grass; Crop1: C3 generic Crop.

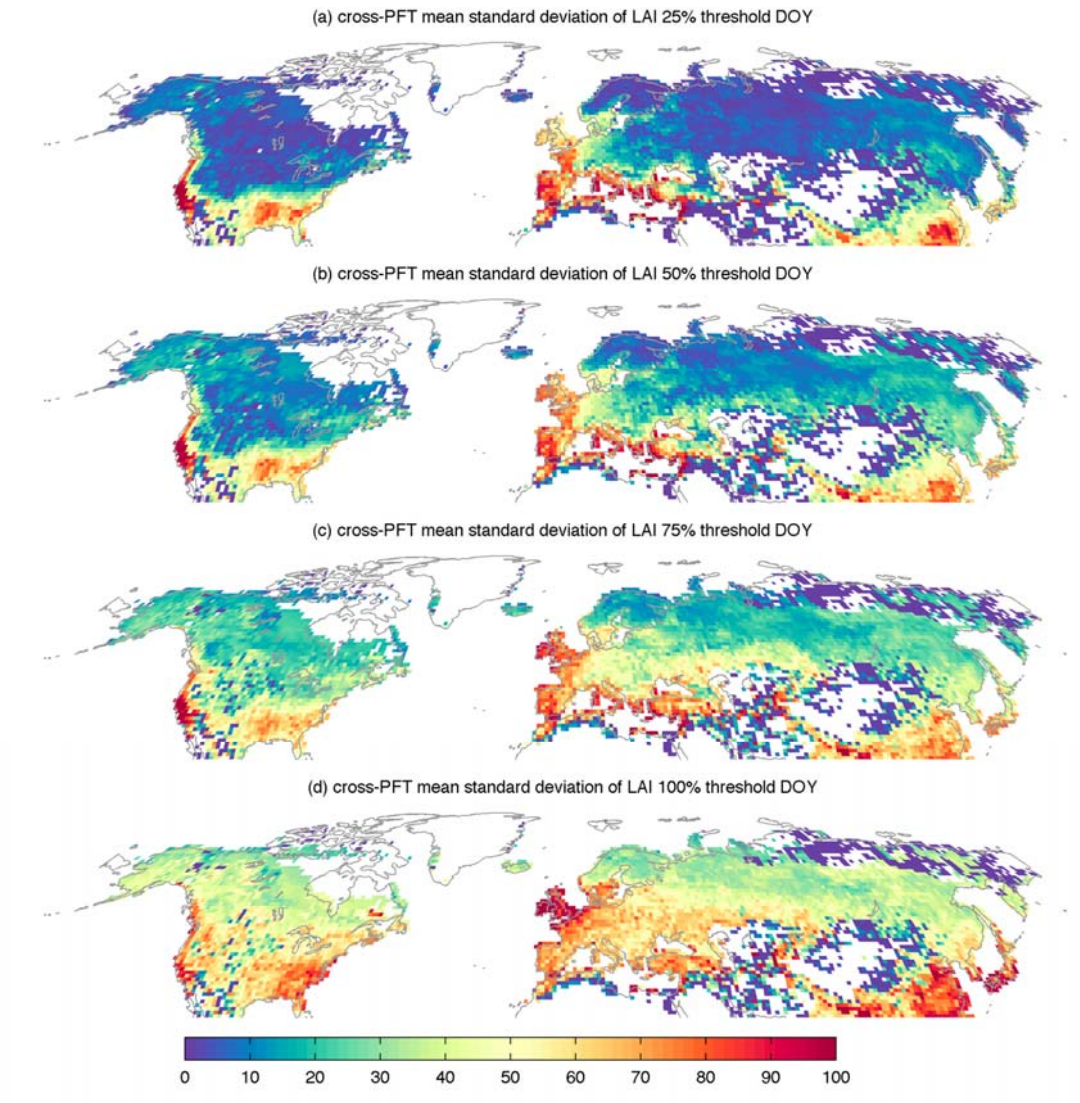

Figure 39. Maps showing cross-PFT standard deviation of the day of the year when each threshold of LAI annual amplitude is reached within each PFT in CLM4.5, average between 2003-2014. This value shows how different spring onset timing is between different PFTs coexisting in the same grid cell.

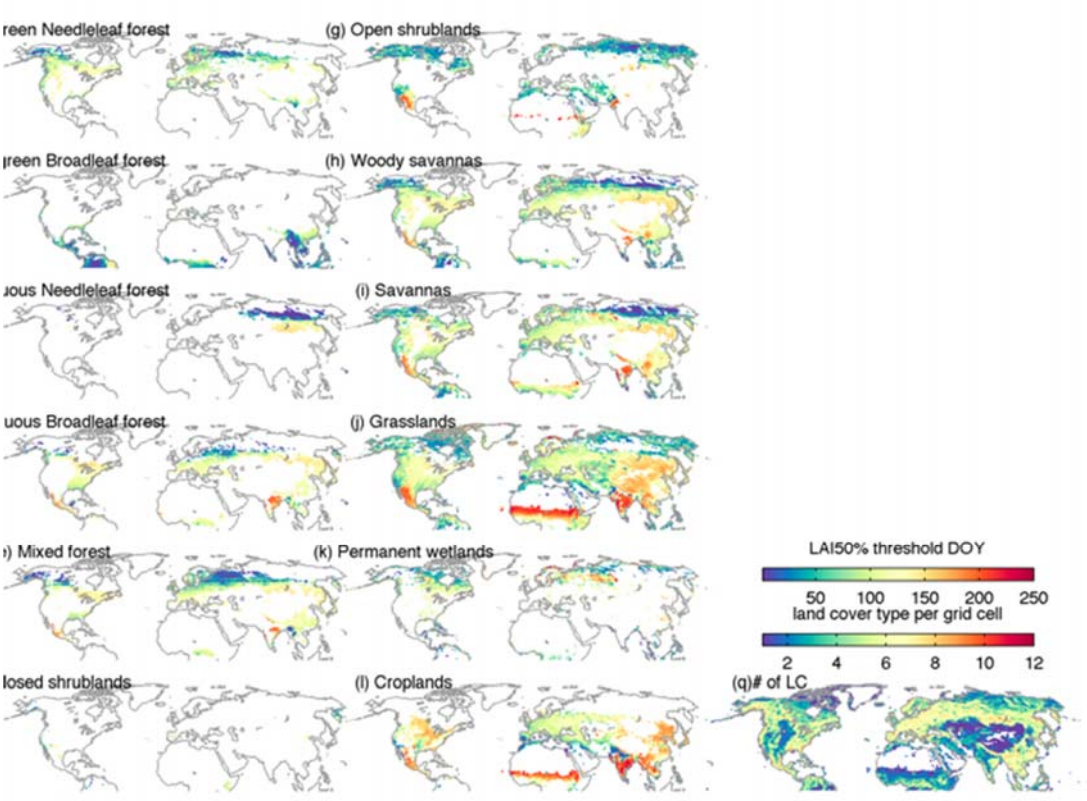

Figure 40. Maps showing day of the year when 50% threshold of LAI annual amplitude is reached within each land cover type in MODIS. (a)-(l) mean DOY of LAI 50% threshold, averaged over 2003-2014. (q) number of land cover types coexist at each grid cell.

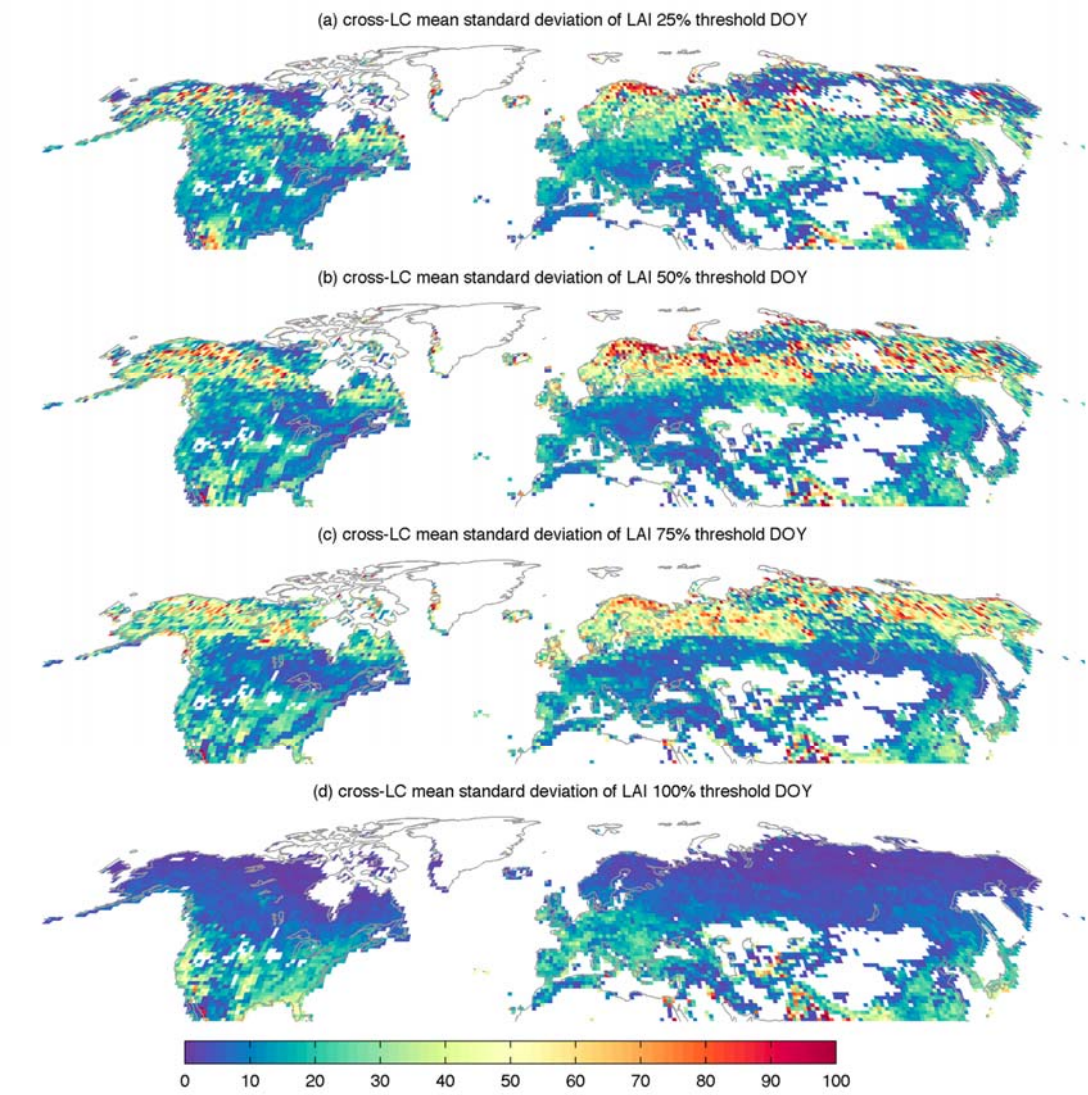

Figure 41. Maps showing cross land cover standard deviation of the day of the year when each threshold of LAI annual amplitude is reached in MODIS, average between 2003-2014. This value shows how different spring onset timing is between different land cover types coexisting in the same grid cell in MODIS.

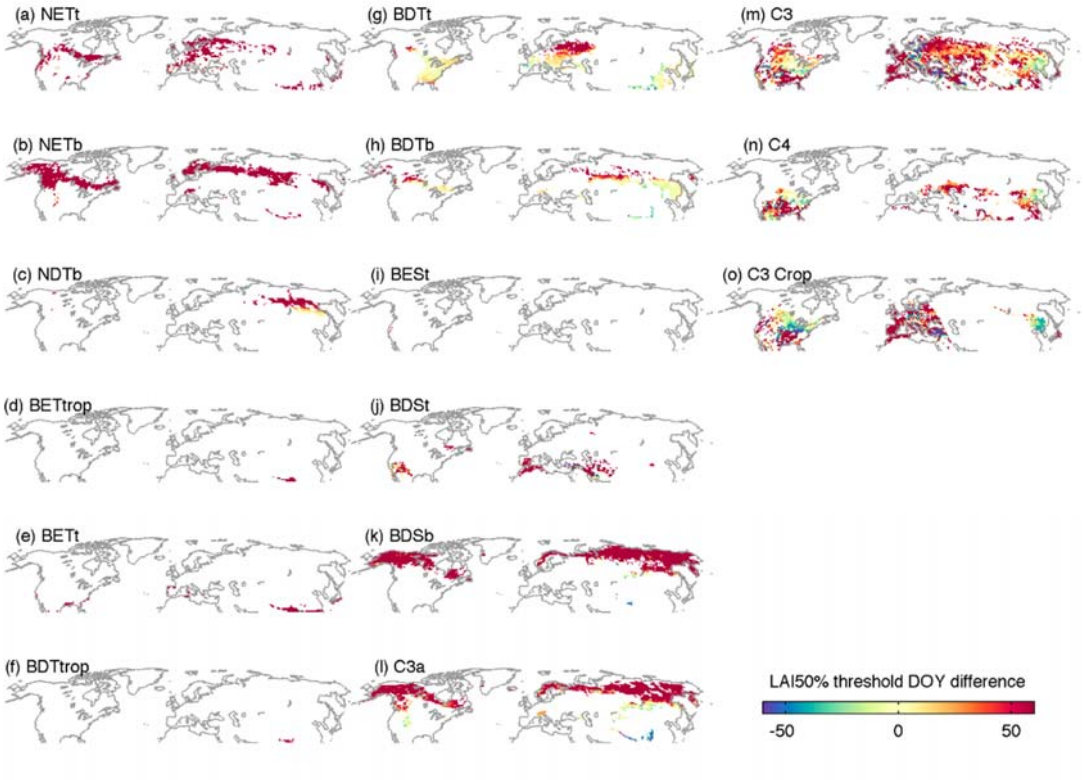

Figure 42. Maps showing difference between LAI 50% threshold dates in each CLM PFT-MODIS land cover type combination, averaged between 2003-2014. Positive difference means CLM LAI 50% threshold is reached later in CLM5 than in MODIS. Plant functional types shown in this figure are: NETt: needleleaf evergreen temperate tree; NETb: needleleaf evergreen boreal tree; NDTb: needleleaf deciduous boreal tree; BETtrop: broadleaf evergreen tropical tree; BETt: broadleaf evergreen temperate tree; BDTtrop: broadleaf deciduous tropical tree; BDTt: broadleaf deciduous temperate tree; BDTb: broadleaf deciduous boreal tree; BES: broadleaf evergreen temperate shrub; BDSt: broadleaf deciduous temperate shrub; BDSb: broadleaf deciduous boreal shrub; C3a: C3 arctic grass; C3: C3 non-arctic grass; C4: C4 grass; C3Crop: C3 generic Crop; C3CropIr: C3 generic crop with irrigation. Corresponding MODIS land cover type can be found in Table 1.

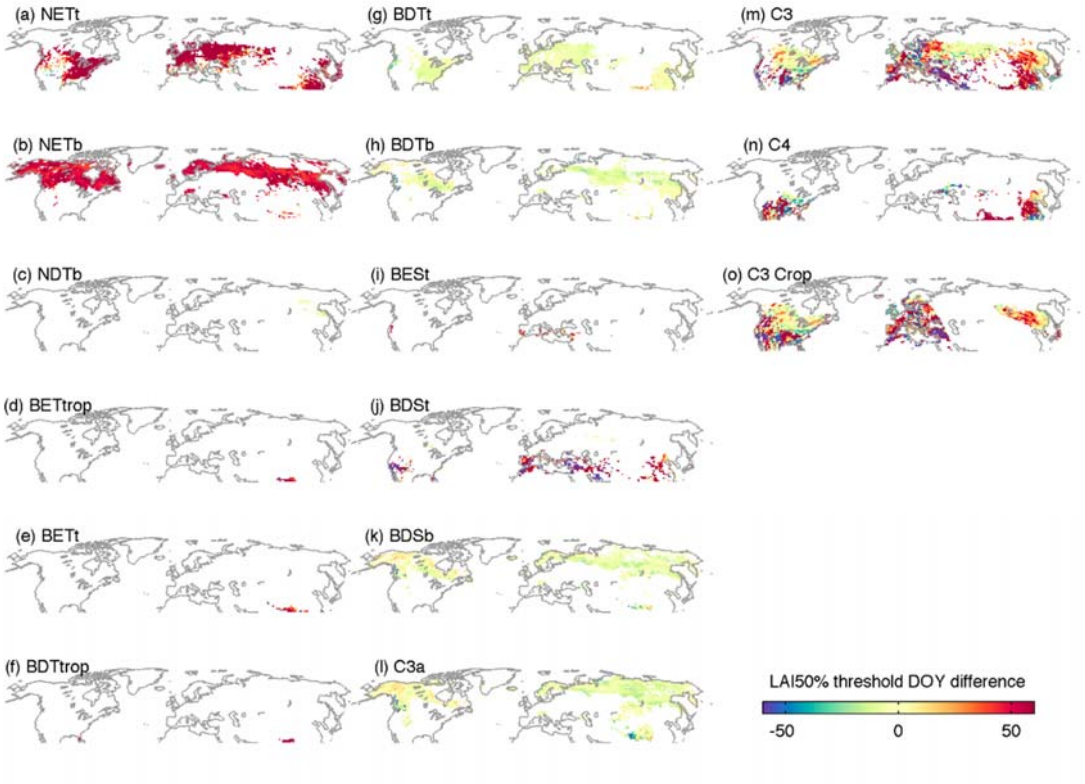

Figure 43. Maps showing difference between LAI 50% threshold dates between CLM5 and CLM4.5 for each CLM PFT, averaged between 2003-2014. Positive difference means LAI 50% threshold is reached later in CLM5 than in CLM4.5. Plant functional types shown in this figure are: NETt: needleleaf evergreen temperate tree; NETb: needleleaf evergreen boreal tree; NDTb: needleleaf deciduous boreal tree; BETtrop: broadleaf evergreen tropical tree; BETt: broadleaf evergreen temperate tree; BDTtrop: broadleaf deciduous tropical tree; BDTt: broadleaf deciduous temperate tree; BDTb: broadleaf deciduous boreal tree; BES: broadleaf evergreen temperate shrub; BDSt: broadleaf deciduous temperate shrub; BDSb: broadleaf deciduous boreal shrub; C3a: C3 arctic grass; C3: C3 non-arctic grass; C4: C4 grass; C3 Crop: C3 generic Crop.

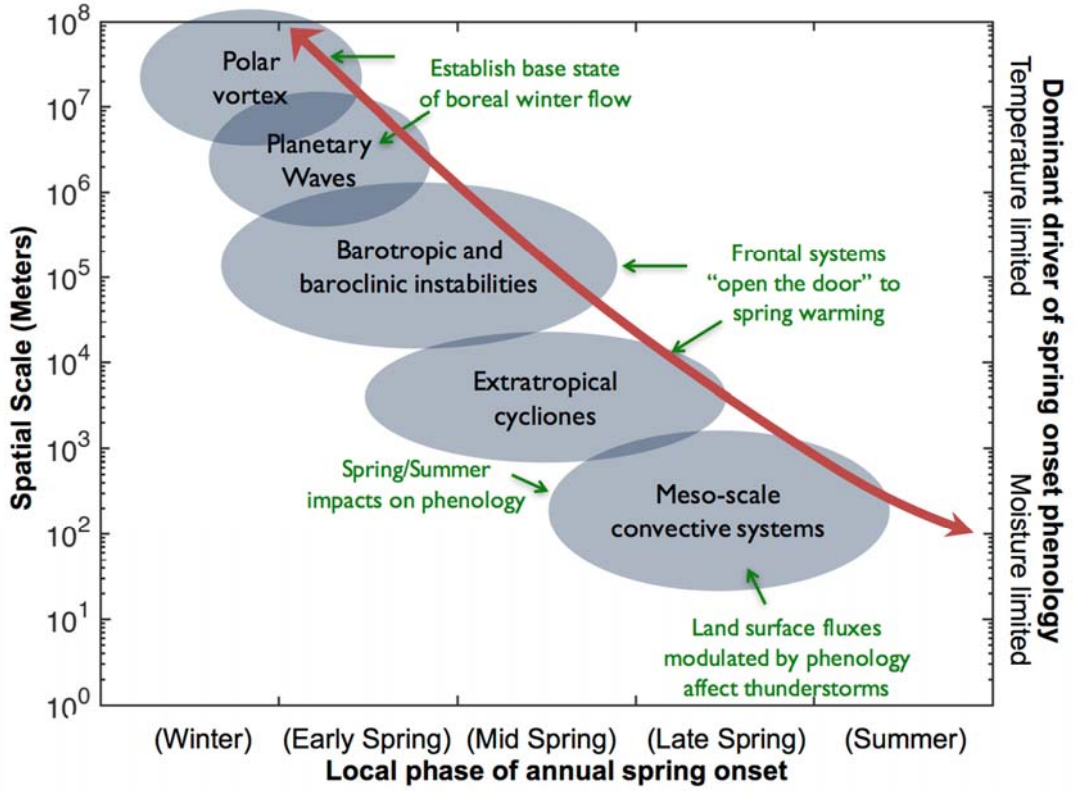

Figure 44. Schematic diagram of the hypothesized relationship between climate, spatial scale, and phenology. In winter, the spatial scales of atmospheric disturbances are large and govern surface temperature fluctuations that influence phenology in the terrestrial biosphere. During winter months, snow is often present at high latitudes, precipitation is relatively common, plants are dormant and evapotranspiration rates are slow due to the cooler temperatures. In summer, the spatial scales of atmospheric disturbances decrease and precipitation begins playing an increasingly dominant role in triggering spring phenology. Accordingly, PFTs that either (a) grow in high latitude cold-climates; or (b) respond to early spring warmth will tend to be responsive only to temperature because the available soil moisture will typically be high. Later in spring (right side), precipitation becomes more dominant for spring onset and the spatial scales of disturbances decrease, leading to phenological responses that are hypothesized to be more heterogeneous.